University of Alberta

Role of Colloidal Interactions in Bitumen Recovery from Oil Sands

by

Jianjun Liu

A thesis submitted to the Faculty of Graduate Studies and Research in partial fulfillment of the requirements for the degree of Doctor of Philosophy

in

Chemical Engineering

Department of Chemical and Materials Engineering

Edmonton, Alberta

Spring, 2004

Library and Archives Canada

Published Heritage Branch

395 Wellington Street
Ottawa ON K1A 0N4
Canada

Bibliothèque et Archives Canada

Direction du Patrimoine de l'édition

395, rue Wellington
Ottawa ON K1A 0N4
Canada

Your file Votre référence
ISBN: 0-612-96295-4
Our file Notre référence
ISBN: 0-612-96295-4

The author has granted a non-exclusive license allowing the Library and Archives Canada to reproduce, loan, distribute or sell copies of this thesis in microform, paper or electronic formats.

L'auteur a accordé une licence non exclusive permettant à la Bibliothèque et Archives Canada de reproduire, prêter, distribuer ou vendre des copies de cette thèse sous la forme de microfiche/film, de reproduction sur papier ou sur format électronique.

The author retains ownership of the copyright in this thesis. Neither the thesis nor substantial extracts from it may be printed or otherwise reproduced without the author's permission.

L'auteur conserve la propriété du droit d'auteur qui protège cette thèse. Ni la thèse ni des extraits substantiels de celle-ci ne doivent être imprimés ou aturement reproduits sans son autorisation.

In compliance with the Canadian Privacy Act some supporting forms may have been removed from this thesis.

Conformément à la loi canadienne sur la protection de la vie privée, quelques formulaires secondaires ont été enlevés de cette thèse.

While these forms may be included in the document page count, their removal does not represent any loss of content from the thesis.

Bien que ces formulaires aient inclus dans la pagination, il n'y aura aucun contenu manquant.

Canada

ABSTRACT

The colloidal interactions between oil sand components in model systems and a real system are investigated to understand the fundamental steps "liberation" and "aeration" in bitumen extraction processes.

A novel method of zeta potential distribution measurements by an electrophoremeter is developed to directly observe the hetero-coagulation between oil sand components. The interaction forces coupled with the adhesive forces measured by an atomic force microscope (AFM) are used to understand the colloidal interactions between oil sand components. The results show that solution pH and calcium addition are the main factors that significantly affect the colloidal interactions of various components in oil sand extraction systems. Between bitumen and silica, a higher solution pH corresponds to a good liberation/dispersion, however the presence of calcium triggers strong coagulation at pH above 10.5. For bitumen and bitumen, a lower pH results in a stronger coagulation and calcium has only a slight impact on their interactions. For bitumen and clays, montmorillonite shows a strong affinity to the bitumen surface only in the presence of calcium ions. In contrast, kaolinite clays show little affinity to the bitumen surface in the presence or absence of calcium. The fines collected from a poor processing ore attach more strongly to the bitumen surface than the fines from a good processing ore. The high content of divalent cations in the extraction system of poor processing ores leads to a slime coating and is responsible for low bitumen flotation recovery.

By fitting the measured force profiles with the classical DLVO or extended DLVO theory, it is found that the electrostatic double layer force controls the interactions between bitumen and silica, between bitumen and clays and between bitumen and fines

from good processing ores, while both the electrostatic double layer force and hydrophobic force dominate the interactions between bitumen and bitumen and between bitumen and fines from poor processing ores.

The current study demonstrates that the mega scale industrial process can be better understood from the results of micro scale experiments. These results provide fundamental insights into the mechanisms of bitumen extraction from oil sands and suggest approaches to improve the efficiency of bitumen extraction.

ACKNOWLEDGEMENTS

I would like to express my sincere gratitude and appreciation to:

- My supervisor Professor Zhenghe Xu, NSERC/EPCOR/AERI Industrial Research Chair in Advanced Coal Cleaning and Combustion Technology, for sharing his broad scientific knowledge and wisdom, invaluable guidance, support and encouragement during my study, and for many friendly moments during all these years. I really enjoyed the wonderful time of being his Ph. D student.

- Professor Jacob Masliyah, NSERC Industrial Research Chair in Oil sands and Canada Senior Research Chair, for his wonderful suggestions in oil sands research, critical and patient reading of the paper manuscripts, and his great and generous help in and out of the laboratory.

- Associate professor Anthony Yeung for his very useful discussions in oil sands research.

- Professor Hirotaka Ihara, Associate professor Makoto Takafuji and Mr. Yamada Taisuke for their support of my three month visit to Kumamoto University in Japan.

- Technicians Mr. James Skwarok, Mrs. Tina Barker, Mr. Walter Boddez and Secretaries Mrs. Leanne Swekla and Mrs. AnnMarie Brereton for their generous help. Drs. Zhiang Zhou, Liyan Zhang, Hahong Li, Mr. Chris Repka, Mrs. Nancy Su, Mr. Robert Lopetinsky and the oil sands group members for their assistance and friendship.

The financial support from COURSE with Syncrude Canada Ltd and Albian Sands as industrial partners, Natural Sciences and Engineering Research Council of Canada (NSERC), and Industrial Research and NSERC Chair in Oil Sands Engineering, the courtesy for providing oil sand samples by Syncrude Canada Ltd. is also acknowledged.

I would also like to thank my wife Juying Xiao, my mother and my daughters for their love and support.

TABLE OF CONTENTS

CHAPTER 1 INTRODUCTION *1*

1.1 Oil sand deposit **1**

1.2 Bitumen Extraction **2**

1.3 Objectives **3**

1.4 Organization of thesis **5**

1.5 List of papers pertinent to this thesis **6**

CHAPTER 2 LITERATURE REVIEW *8*

2.1 Characteristics of Athabasca oil sands **8**

2.2 Water-Based Extraction (WBE) process **9**

2.2.1 General description 9

2.2.2 Process parameters 13

2.3 Fundamental study on bitumen/sands/bubble interactions **15**

2.3.1 Bitumen surface properties 16

2.3.2 Subprocesses visualized 18

2.3.3 Current understanding/models 20

2.3.4 Interaction force 22

CHAPTER 3 SURFACE FORCE REVIEW *24*

3.1 DLVO theory **24**

3.1.1 Electrostatic double layer force 24

3.1.2 van der Waals forces 27

3.2 Extended DLVO theory **28**

3.2.1 Hydrophobic force 29

3.2.2 Hydration force 30

3.2.3 Steric force 30

3.3 Derjaguin approximation **31**

3.4 Adhesive force **32**

CHAPTER 4 MATERIALS AND EXPERIMENTAL TECHNIQUES..... 34

4.1 Materials 34

4.2 Preparation of fines, froth, and process water from flotation system..... 35

4.3 Zeta potential measurement..... 37

4.3.1 Emulsion or suspension preparation 37

4.3.2 Zeta potential measurement..... 38

4.4 Zeta potential distribution measurement 39

4.4.1 Principle of zeta potential distribution measurement..... 40

4.4.2 Technique of zeta potential distribution measurement 42

4.5 Surface force measurement (AFM technique) 43

4.5.1 Bitumen surface preparation (spin coating technique)..... 43

4.5.2 Probe particle preparation 44

4.5.3 Colloidal force measurement in a fluid..... 46

4.5.4 Reproducibility and measurement error 48

4.5.5 Data fitting and nature of long-range colloidal force 49

4.7 Other techniques 55

4.7.1 Film flotation..... 55

4.7.2 Contact angle measurement 55

4.7.3 Size distribution measurement 56

CHAPTER 5 ELECTROKINETICS OF OIL SAND COMPONENTS..... 58

5.1 Introduction..... 58

5.2 Bitumen..... 58

5.3 Silica 60

5.4 Clays..... 61

5.5 Fines from real oil sand ores..... 64

5.6 Implications 65

5.7 Summary of chapter 66

CHAPTER 6 INTERACTIONS BETWEEN BITUMEN AND SILICA ... 67

6.1 Introduction ... 67

6.2 Colloidal force measurement ... 68

6.2.1 System characteristics ... 68

6.2.2 Deformation of bitumen surface ... 69

6.2.3 Effect of pH ... 70

6.2.4 Effect of electrolyte (KCl) concentration ... 71

6.2.5 Effect of calcium ions ... 73

6.2.6 Effect of temperature ... 75

6.2.7 Data fitting and nature of colloidal force ... 77

6.2.8 Nature of adhesive force ... 82

6.3 Zeta potential distribution measurement ... 82

6.4 Relevance to the oil sands industry ... 84

6.5 Summary of chapter ... 86

CHAPTER 7 INTERACTIONS BETWEEN BITUMEN AND BITUMEN ... *88*

7.1 Introduction ... 88

7.2 Interactions in the absence of fines ... 89

7.2.1 General observation ... 89

7.2.2 Effect of solution pH ... 91

7.2.3 Effect of electrolyte concentration ... 93

7.2.4 Effect of calcium addition ... 94

7.3 Interactions in the presence of montmorillonite clay ... 95

7.3.1 In the absence of calcium ions ... 96

7.3.2 In the presence of calcium ions ... 98

7.4 Data fitting and nature of colloidal force ... 99

7.5 Nature of adhesive force ... 104

7.6 Relevance to the oil sands industry ... 105

7.7 Summary of chapter **105**

CHAPTER 8 INTERACTIONS BETWEEN BITUMEN AND CLAYS .. *107*

8.1 Introduction **107**

8.2 Surface properties of clay mineral **108**

8.3 Zeta potential distribution measurement **109**

8.3.1 Bitumen-montmorillonite clay 110

8.3.2 Bitumen-kaolinite clay 114

8.3.3 Practical implication 117

8.4 Colloidal force measurement **118**

8.4.1 Bitumen-montmorillonite clay 118

8.4.2 Bitumen-Kaolinite clay 120

8.4.3 Data fitting and implication 122

8.5 Summary of chapter **123**

CHAPTER 9 INTERACTIONS BETWEEN BITUMEN AND FINES .. *125*

9.1 Introduction **125**

9.2 Sample characterization **127**

9.2.1 Justification of samples 127

9.2.2 Surface properties of fines 128

9.3 Zeta potential distribution measurement **129**

9.3.1 Fines from good processing ore 129

9.3.2 Fines from poor processing ore 133

9.4 Surface force measurement **136**

9.4.1 Fines from good processing ore 137

9.4.2 Fines from poor processing ore 139

9.4.3 Data fitting and nature of colloidal force 142

9.5 Implication to bitumen flotation **143**

9.6 Summary of chapter **146**

CHAPTER 10 SUMMARY *148*

10.1 General conclusions **148**

10.2 Claim for original research **150**

10.3 Prospect of future work **151**

REFERENCES *152*

APPENDIX *165*

A: Fundamental principle of AFM **165**

B. AFM imaging technique **166**

C. AFM force profile and data analysis **167**

D: Numerical solution to DLVO theory-constant Stern potential as B.C. **172**

E: Numerical solution to DLVO theory-constant surface charge density as B.C. **178**

References **179**

LIST OF TABLES

Table 4.1 Composition of oil sand samples..... 33

Table 4.2 Cation content (A.A. analysis) in the process water..... 34

Table 4.3 Element wt% for probe particles with an energy dispersive x-ray analyzer (EDX) in a scanning electron microscope (SEM, K line)..... 45

Table 4.4 Hamaker Constants A (B for bitumen, C for clay, S for silica and W for water)..... 49

Table 9.1 Chemical element (C, H, N) analysis of fines obtained from oil sands..... 143

LIST OF FIGURES

Figure 1.1 A generalized scheme for oil sands processing using Water-based extraction processes..... 1

Figure 2.1 A typical bitumen extraction circuit (ore preparation, slurry conditioning, extraction and tailings treatment)..... 11

Figure 2.2 Conceptual stages for bitumen liberation and aeration..... 15

Figure 3.1 Schematics of Stern-Grahame electric double layer mode..... 24

Figure 4.1 Visual appearances of fines suspension from (a) a good processing ore and (b) a poor processing ore..... 35

Figure 4.2 Particle size distributions of the fines extracted from tailings and froth for a good processing ore and a poor processing ore..... 35

Figure 4.3 Particle size distributions of solvent extracted bitumen emulsion after various creaming time..... 36

Figure 4.4 Schematics of zeta potential measurement..... 38

Figure 4.5 Schematic zeta potential distributions for a binary particulate component system that can be interpreted for particle interactions..... 40

Figure 4.6 A typical AFM image of bitumen substrate with Tapping mode: three-dimensional and section analysis..... 43

Figure 4.7 Typical SEM micrographs of probing particles on tips of AFM cantilevers after force measurement..... 44

Figure 4.8 Schematics illustrating the principle of the atomic force microscope... 46

Figure 4.9 Schematics of the normalized long-range force as a function of separation distance for the classical DVLO theory..... 51

Figure 4.10 Schematic diagram of the normalized long-range force as a function of separation distance for the extended DVLO theory..... 52

Figure 4.11 Schematics of the interpreted particle coagulation behavior from the normalized repulsive barrier and adhesive force measured with AFM.. 53

Figure 4.12 Schematics of contact angle measurement..... 55

Figure 5.1 Average zeta potentials of bitumen emulsion as a function of solution pH in 1 mM KCl solutions..... 58

Figure 5.2 Average zeta potentials of bitumen emulsion as a function of solution pH in (a) KCl solutions; (b) 1 mM KCl solutions containing $CaCl_2$..... 59

Figure 5.3 Average zeta potentials of silica suspensions as a function of solution pH in (a) KCl solutions; (b) 1 mM KCl solutions containing $CaCl_2$..... 60

Figure 5.4 Schematic diagram of a clay plate..... 61

Figure 5.5 Average zeta potentials of montmorillonite suspensions as a function of solution pH in (a) KCl solutions; (b) 1 mM KCl solutions containing $CaCl_2$..... 62

Figure 5.6 Average zeta potentials of kaolinite suspensions as a function of solution pH in (a) KCl solutions; (b) 1 mM KCl solutions containing $CaCl_2$..... 63

Figure 5.7 Average zeta potentials of fines suspensions as a function of solution pH in (a) KCl solutions; and (b) 1 mM KCl solutions containing $CaCl_2$. Filled symbols: fines from a good processing ore; open symbols: fines from a poor processing ore..... 64

Figure 6.1 Raw data from a typical force measurement between the bitumen-silica and silica-silica in 1 mM KCl solutions at pH 8.2. Insert: interaction force barriers and adhesive forces measured at loading forces of 8~10 mN/m as a function of solution pH..... 68

Figure 6.2 Normalized interaction forces (F/R) between bitumen and silica as a function of separation distance in 1 mM KCl solutions at different solution pH..... 70

Figure 6.3 Normalized interaction forces (F/R) between bitumen and silica as a function of separation distance in KCl solutions at pH 8.2. Insert: interaction force barriers and adhesive forces measured at loading forces of 8~10 mN/m as a function of KCl concentration..... 71

Figure 6.4 Normalized interaction forces (F/R) between bitumen and silica as a function of separation distance in 1 mM KCl solutions containing $CaCl_2$ at pH 8.2. Insert: interaction force barriers and adhesive forces measured at loading forces of 8~10 mN/m as a function of calcium ion concentration..... 73

Figure 6.5 Normalized interaction forces (F/R) between bitumen and silica as a function of separation distance in 1 mM KCl solutions containing $CaCl_2$ at pH 10.5. Insert: interaction force barriers and adhesive forces measured at loading forces of 8~10 mN/m as a function of calcium ion concentration 74

Figure 6.6 Normalized interaction forces (F/R) between bitumen and silica as a function of separation distance in 1 mM KCl solution at pH 8.2 and different temperatures. Insert: interaction force barriers and adhesive forces measured at loading forces of 8~10 mN/m as a function of temperature..... 75

Figure 6.7 Normalized interaction forces (F/R) between bitumen and silica as a function of separation distance in a 1 mM KCl solution at pH 8.2..... 76

Figure 6.8 Comparison of best-fitted decay length from the measured force profiles with calculated decay length using Debye-Huckel theory from the actual electrolyte concentration used in the corresponding force measurement..... 78

Figure 6.9 Comparison of the best-fitted Stern potential from the measured force profiles with the classical DLVO theory and the measured corresponding zeta potentials of silica (open symbols) and bitumen droplets (filled symbols)..... 79

Figure 6.10 The best-fitted macromolecule "Tail Length L" for steric forces from the measured force profiles with the extended DLVO theory as a function of solution pH..... 80

Figure 6.11 Zeta potential distributions in 1 mM KCl solutions at pH 10.5 without calcium ion addition. (a) Individual bitumen emulsion and silica suspension; and (b) their mixture at a mass ratio of 1:1..... 82

Figure 6.12 Zeta potential distributions in 1 mM KCl solutions containing 1 mM $CaCl_2$ at pH 10.5. (a) Individual bitumen emulsion and silica suspension; and (b) their mixture at a mass ratio of 1:1..... 83

Figure 7.1 Normalized interaction forces (F/R) between bitumen and silica as a function of separation distance in 1 mM KCl solution at pH 8.2. (a) Open circle: pair of bitumen coated on silica wafer - silica sphere; and (b) filled star: pair of silica wafer - bitumen coated on the silica sphere surface..... 89

Figure 7.2 Normalized interaction force (F/R) profiles as a function of incubation time in a 1 mM KCl solution at pH 5.7..... 90

Figure 7.3 Normalized interaction forces (F/R) between bitumen surfaces as a function of separation distance in 1 mM KCl solutions at different solution pH. Insert: interaction force barriers and adhesive forces measured at loading forces of 8~10 mN/m as a function of solution pH..... 91

Figure 7.4 Normalized interaction forces (F/R) between bitumen surfaces as a function of separation distance in KCl solutions at pH 8.2. Insert: interaction force barriers and adhesive forces measured at loading forces of 8~10 mN/m as a function of KCl concentration..... 92

Figure 7.5 Normalized interaction forces (F/R) between bitumen surfaces as a function of separation distance in 1 mM KCl solutions containing $CaCl_2$ at pH 8.2. Insert: normalized adhesive forces (F_{ad}/R) measured at loading forces of 8~10 mN/m as a function of calcium ion concentration. Inner insert: distribution of normalized adhesive forces (F_{ad}/R) in a 1 mM KCl solution at pH8.2..... 94

Figure 7.6 Normalized interaction forces (F/R) between bitumen surfaces as a function of separation distance in 1 mM KCl solutions at pH 5.7. Insert: distribution of normalized adhesive forces (F_{ad}/R) measured at loading forces of 8~10 mN/m..... 95

Figure 7.7 Schematics of possible interactions between bitumen surfaces after conditioning with 0.1 % montmorillonite suspension containing 1 mM KCl at pH 8.2 in AFM. (a) Approaching with sparse montmorillonite particles attached weakly on the bitumen surface; (b) initial contact; and (c) "jump-in" when "squeezing-out" of montmorillonite particle under threshold forces..... 97

Figure 7.8 Normalized interaction forces (F/R) between bitumen surfaces as a function of separation distance in 1 mM KCl solution containing 1 mM $CaCl_2$ at pH 8.2. Insert: distribution of normalized adhesive forces (F_{ad}/R) measured at loading forces of 8~10 mN/m..... 98

Figure 7.9 Normalized interaction forces (F/R) between bitumen and bitumen as a function of separation distance in a 1 mM KCl solution at pH 5.7..... 99

Figure 7.10 Comparison of the best-fitted Stern potentials from the measured force profiles with the extended DLVO theory and the measured corresponding zeta potentials of bitumen droplets..... 100

Figure 7.11 Comparison of the values of best-fitted hydrophobic force constant K from the measured force profiles with the extended DLVO theory and the measured corresponding contact angle values of air bubble on the bitumen surface in water..... 101

Figure 7.12 The best-fitted macromolecule "Tail Length L" for steric force from the measured force profiles with the extended DLVO theory as a function of solution pH..... 102

Figure 8.1 Calcium adsorption on clay minerals as a function of time in solutions containing initially 1 mM $CaCl_2$ at a solid to liquid ratio of 1g/L..... 108

Figure 8.2 Zeta potential distributions in 1 mM KCl solutions at pH 8.2. (a) Individual bitumen emulsion and montmorillonite clay suspension; and (b) their mixture at a mass ratio of 1:1..... 110

Figure 8.3 Zeta potential distributions in 1 mM KCl solutions containing 1 mM $CaCl_2$ at pH 8.2. (a) Individual bitumen emulsion and montmorillonite clay suspension; (b) their mixture at a mass ratio of 1:1..... 111

Figure 8.4 Effect of ratio of montmorillonite clays to bitumen on zeta potential distributions measured in 1 mM KCl solutions containing 1 mM $CaCl_2$ at pH 8.2..... 112

Figure 8.5 Peak position of single modal zeta potential distribution measured with a mixture of montmorillonite clay suspension and bitumen emulsion at different ratios. The measurement was conducted in 1 mM KCl solutions containing 1 mM $CaCl_2$ at pH 8.2..... 113

Figure 8.6 Zeta potential distributions in 1 mM KCl solutions at pH 8.2. (a) Individual bitumen emulsion and kaolinite clay suspension; and (b) their mixture at a mass ratio of 1:1..... 114

Figure 8.7 Effect of kaolinite clays to bitumen ratio on zeta potential distributions measured in 1 mM KCl solutions containing 1 mM $CaCl_2$ at pH 8.2..... 115

Figure 8.8 Schematics of calcium as a binder for the interaction between bitumen and clay fines..... 117

Figure 8.9 Normalized interaction forces (F/R) between bitumen and montmorillonite as a function of separation distance at pH 8.2. (a) In 1 mM KCl solutions; (b) in 1 mM KCl solutions containing 1 mM $CaCl_2$..... 118

Figure 8.10 Distribution of normalized adhesive forces (F_{ad} / R) between bitumen and montmorillonite, at loading forces of 8~10 mN/m. (a) In 1 mM KCl solutions; (b) in 1 mM KCl solutions containing 1 mM $CaCl_2$..... 119

Figure 8.11 Normalized interaction forces (F/R) between bitumen and kaolinite as a function of separation distance at pH 8.2. (a) in 1 mM KCl solutions; (b) in 1 mM KCl solutions containing 1 mM $CaCl_2$..... 120

Figure 8.12 Distribution of normalized adhesive forces (F_{ad} / R) between bitumen and kaolinite at loading forces of 8~10 mN/m. (a) In 1 mM KCl solutions; (b) in 1 mM KCl solutions containing 1mM $CaCl_2$..... 120

Figure 8.13 Comparison of the best-fitted Stern potentials from the measured force profiles with the classical theory and the measured corresponding zeta potentials of bitumen droplets (square symbols), montmorillonite (circle symbols) and kaolinite (star symbols)..... 121

Figure 9.1 X-ray diffraction patterns of fines from oil sand ores. CuKα radiation (with graphite monochrometer), scanned at 0.05 °2θ step and 4 s per step..... 127

Figure 9.2 Partition of the fines at air-aqueous methanol solution interface. Filled circles: fines from a poor processing ore; open circles: fines from a poor processing ore washed with toluene; and filled triangles: fines from a good processing ore..... 128

Figure 9.3 Zeta potential distributions in 1 mM KCl solutions at pH 8. (a) Emulsified bitumen and fines suspension measured separately; (b) their mixture at a mass ratio of 1:1; and (c) emulsified froth from a good processing ore..... 129

Figure 9.4 Zeta potential distributions in 1 mM KCl solutions containing 1 mM $CaCl_2$ at pH 8. (a) Emulsified bitumen and fines suspension measured separately; (b) their mixture at a mass ratio of 1:1; and (c) emulsified froth from a good processing ore..... 130

Figure 9.5 Zeta potential distributions in its corresponding process water. (a) Emulsified bitumen and fines suspension measured separately; (b) their mixture at a mass ratio of 1:1; and (c) emulsified corresponding froth from a good processing ore..... 131

Figure 9.6 Zeta potential distributions in 1 mM KCl solutions at pH 8. (a) Emulsified bitumen and fines suspension measured separately; (b) their mixture at a mass ratio of 1:1; and (c) emulsified froth from a poor processing ore..... 133

Figure 9.7 Zeta potential distributions in 1 mM KCl solutions containing 1 mM $CaCl_2$ at pH 8. (a) Emulsified bitumen and fines suspension measured separately; (b) their mixture at a mass ratio of 1:1; and (c) emulsified froth from a poor processing ore..... 134

Figure 9.8 Zeta potential distributions in its corresponding process water. (a), Emulsified bitumen and fines suspension measured separately; (b) their mixture at a mass ratio of 1:1; and (c) emulsified froth from a poor processing ore..... 135

Figure 9.9 Normalized interaction forces (F/R) between bitumen and fines from a good processing ore as a function of separation distance in 1 mM KCl solutions at pH 8. Insert: distribution of normalized adhesive forces (F_{ad}/R) measured at loading forces of 8~10 mN/m..... 136

Figure 9.10 Normalized interaction forces (F/R) between bitumen and fines from a good processing ore as a function of separation distance in 1 mM KCl solutions containing 1 mM $CaCl_2$ at pH 8. Insert: distribution of normalized adhesive forces (F_{ad}/R) measured at loading forces of 8~10 mN/m 137

Figure 9.11 Normalized interaction forces (F/R) between bitumen and fines from a good processing ore as a function of separation distance in its corresponding process water. Insert: distribution of normalized adhesive forces (F_{ad}/R) measured at loading forces of 8~10 mN/m..... 138

Figure 9.12 Normalized interaction forces (F/R) between bitumen and fines from a poor processing ore as a function of separation distance in 1 mM KCl solutions at pH 8. Insert: distribution of normalized adhesive forces (F_{ad}/R) measured at loading forces of 8~10 mN/m..... 139

Figure 9.13 Normalized interaction forces (F/R) between bitumen and fines from a poor processing ore as a function of separation distance in 1 mM KCl solution containing 1 mM $CaCl_2$ at pH 8. Insert: distribution of normalized adhesive forces (F_{ad}/R) measured at loading forces of 8~10 mN/m..... 140

Figure 9.14 Normalized interaction forces (F/R) between bitumen and fines from a poor processing ore as a function of separation distance in its corresponding process water. Insert: distribution of normalized adhesive forces (F_{ad}/R) measured at loading forces of 8~10 mN/m..... 141

Figure 9.15 Schematics of interactions between bitumen and fines. (a) Active sites (cations and surfactants) on the surface of fines; and (b) surfactants and cations as binders for interactions between bitumen and fines..... 144

NOMENCLATURE

A	Hamaker constant, J
A_{131}	Hamaker constant of two identical phases 1 through a medium 3, J
A_{132}	Hamaker constant of phase 1 and phase 2 through a medium 3, J
a	spherical particle radius, m
C	electrolyte concentration, M
C_0,C_1,C_2	a constant for evaluation of hydrophobic force, N m^{-1}
D	separation distance between two surfaces, m
D_0,D_1,D_2	a constant for evaluation of hydrophobic force, m
e	elementary electron charge, 1.602×10^{-19} C
f	density factor of macromolecules in Equation (4-2), N nm K^{-1} m^{-4}
F_{ad}	adhesive force, N
$F_{C\text{-}C}$	interaction force between cylinder and cylinder, N
F_{total}	sum of all interaction force, N
F_E	electrostatic double layer force, N
F_{HB}	hydrophobic force, N
F_S	steric force, N
$F_{S\text{-}P}$	interaction force between sphere and plane, N
$F_{S\text{-}S}$	interaction force between sphere and sphere, N
F_V	van der Waals forces, N
h	separation distance between two surfaces, m

k	Boltzmann constant, 1.381×10^{-23} J K^{-1}
K	hydrophobic force constant, J
L	length of polymer tail, m
N_B	number of monomer units per polymer chain, dimesionless
m	coefficient for adhesive forces, dimesionless
n_j	number density of ions j in the solution, m^{-3}
$n_{j\infty}$	number density of ions j in the bulk solution, m^{-3}
r	radial coordinate, m
P	pressure, N m^{-2} or Pa
R	radius of a spherical particle, m
R_A	radius of spherical particle A, m
R_B	radius of spherical particle B, m
R_1	radius of spherical particle 1, m
R_2	radius of spherical particle 2, m
s	average spacing between two grafted points of polymer molecules
T	absolute temperature, K
U_E	electrophoretic mobility, (m s^{-1})/(V m^{-1})
$U_{p\text{-}p}$	interaction energy per unit area between two planar plates, J m^{-2}
U_V	interaction energy from van der Waals force, J
x	coordinate or a distance, m
z	absolute value of valence for a (z:z) electrolyte solution
z_j	valence of ion j in solution

ψ	potential in an electric double layer, V
ψ_d	Stern potential at Stern plane in an electric double layer, V
ψ_0	surface potential at solid surface in an electric double layer, V
ψ_B	Stern potential of bitumen, mV
ψ_S	Stern potential of silica, mV
ψ_M	Stern potential of montmorillonite, mV
ψ_K	Stern potential of kaolinite, mV
ψ_F	Stern potential of fines, mV
ρ_f	electric charge density, C m^{-3}
ρ	gravity density, g m^{-3}
κ	inverse Debye length, m^{-1}
κ^{-1}	Debye length, m
ζ	zeta potential at shear plane in an electric double layer, V
ε	relative permitivity of the medium (dielectric constant), dimensionless
ε_0	permitivity of vacuum, 8.854×10^{-12} C V^{-1} m^{-1}
∇^2	Laplacian operator, m^{-2}
η	fluid viscosity, Pa s
θ	contact angle, degree
γ	interfacial energy, J m^{-2}
γ_{BW}	interfacial energy at bitumen/water interface, J m^{-2}

CHAPTER 1 INTRODUCTION

1.1 Oil sand deposit

Oil sands are also known as tar sands or bituminous sands. Oil sand deposit is one of the world largest petroleum resources. A large proportion of oil sand deposit is located in Alberta, Canada (Camp, 1976, 1977; Masliyah, 2000, 2003). The oil sands in Alberta typically contain 10 % bitumen, 85 % quartz, 4 % water and some fine clays. To date, the oil sand deposits in Alberta have already been found to reach 3 trillion barrels of oil in reserve (Outrim and Evans, 1977; Masliyah, 2003; Masliyah et al., 2003). This amount of oil represents half of all hydrocarbon oil reserves in the world. The exploration of Alberta's oil sand deposits can potentially secure the energy supply for Canada for the next 200-300 years.

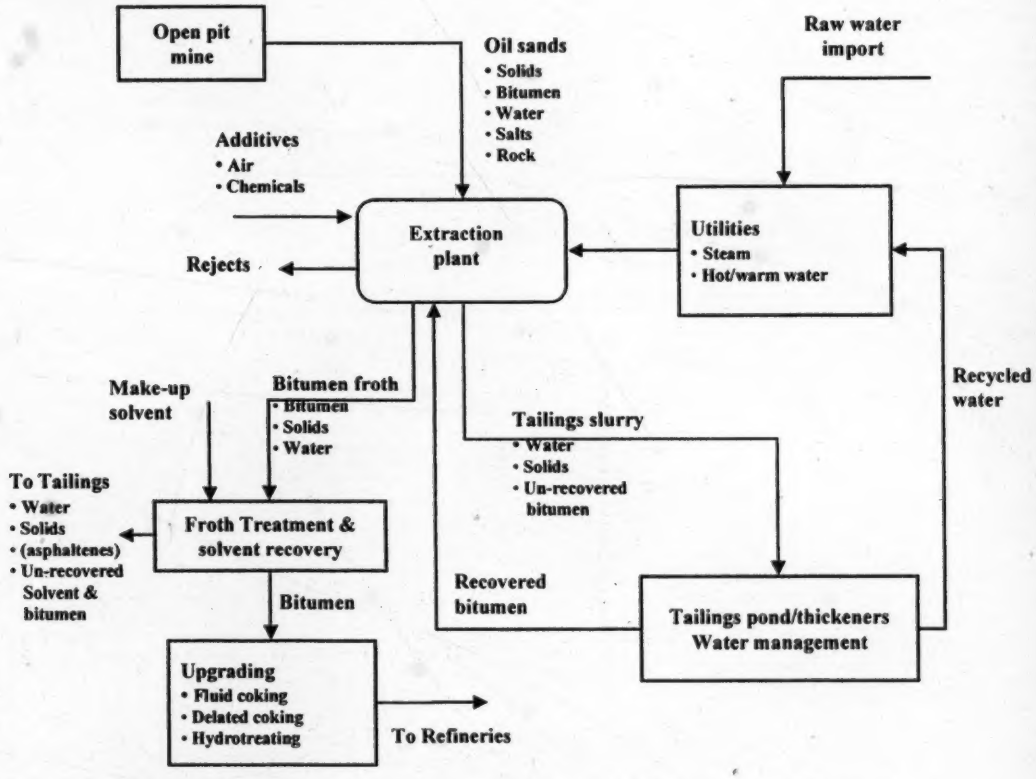

Figure 1.1 A generalized scheme for oil sands processing using Water-Based Extraction processes (Masliyah et al., 2003).

In recent years, high crude oil prices have attracted many industrial ventures to invest in the oil sands processing industry. This industry has become one of the fastest growing industries in Canada. Bitumen extraction from oil sand ores represents a mega scale operation, mining and processing at a rate of more than 1000 tons of ore per minute. The processing of oil sand ores includes mining oil sands, extracting bitumen from the mined oil sands, and upgrading the extracted bitumen by coking to produce "Synthetic Crude Oil". A generic process diagram of oil sand mining to bitumen upgrading is shown in Figure 1.1 (Adaptation from FTFC, 1995; Masliyah et al., 2003). Currently, more than 1 million barrels of crude oil, an oil supply for more than 30 % of overall Canadian oil demand, are produced daily through mining, extraction and upgrading operations from the Athabasca oil sand deposit at Syncrude Canada Ltd., Suncor Energy Inc. and other oil sands companies. Moreover, a number of new oil sands companies will be in full operation in the near future.

1.2 Bitumen Extraction

Considerable research efforts over the last several decades have led to the commercial application of Water-Based Extraction (WBE) process for recovering bitumen from oil sands (Hepler and Hsi, 1989; Hepler and Smith, 1994; Masliyah et al., 2003). The most successful commercial bitumen extraction method is the Hot Water Extraction (HWE) process, which was pioneered by Clark in the 1920's (Hepler and Hsi, 1989; Hepler and Smith, 1994). Recently, low or warm temperature bitumen extraction process was proposed to reduce energy consumption (Sury, 1990, 1992; Spence et al., 1996; Mankowski et al., 1996). A typical bitumen extraction process involves the following fundamental steps: liberation (separation) of bitumen from sand grains; aeration (attachment or engulfment, depending on the temperature) of the liberated bitumen to air bubbles; and flotation of bitumen-air bubble aggregates to the top of the slurry to form a bitumen-rich froth. The collected froth product is diluted with naphtha, and then centrifuged to remove the contained solids and water. The final bitumen after removal of diluents is further upgraded by thermal cracking and/or catalytic hydrocracking to obtain synthetic crude oils.

Bitumen extraction from good processing ores with HWE process has been very successful in a number of commercial operations and the bitumen recovery can easily exceed 93 %. However, there are many technological challenges faced when extracting bitumen from poor processing ores. For example, low bitumen recovery of less than 70 % and/or poor froth quality is often experienced when processing poor processing ores. From operation point of view, 1 % recovery loss is equivalent to 100, 000 US$ loss daily at current operation scale. Therefore, fully understanding the subprocesses of the bitumen extraction system is essential to improve bitumen extraction efficiency. In WBE process, the liberation of bitumen from sand grains and the subsequent stabilization against hetero-coagulation of the liberated bitumen with sand grains is a prerequisite for bitumen recovery. The aeration of bitumen with air bubbles is critical for the liberated bitumen droplets to float. The size of bitumen droplets plays an important role in the attachment of bitumen droplets with air bubbles. Bitumen "liberation" from the sand grains is controlled by the colloidal interactions between the bitumen and sand grains. Bitumen "aeration", on the other hand, is dependent on the hydrophobicity of the bitumen surface and size of bitumen droplets, which are controlled by water chemistry and the colloidal interactions between bitumen and fine solids. Therefore, understanding the colloidal interactions between various components (bitumen/sands/bubbles) in the bitumen extraction system is of great interest to researchers and of great importance to controlling and optimizing commercial bitumen extraction process.

Fundamentals involved in bitumen extraction have been studied extensively. Many experimental methods were developed to study the colloidal interactions between oil sand components. A number of hypotheses were proposed to explain the mechanisms behind the observations. Although it has been recognized that the physicochemical properties of the constituents in the oil sands and water chemistry dominate the bitumen extraction process, the real mechanism remains to be further investigated.

1.3 Objectives

The objectives of this thesis are to study the fundamentals involved in Water-Based Extraction process directly and/or quantitatively. The colloidal interactions between oil sand components in both model and real systems are investigated to understand the two

fundamental steps "liberation" and "aeration" in the bitumen extraction process. More specific objectives are:

- To characterize the surface electric properties of oil sand components to provide the basis for further studies on the colloidal interactions between the components in oil sands extraction system.
- To measure directly the colloidal forces between oil sand components using an atomic force microscope in attempt to predict their interaction behavior and explore the essence of their interactions.
- To investigate the effect of the industrial operation parameters such as solution pH, salinity, and divalent ions on the colloidal interactions between oil sand components.
- To observe directly or quantitatively hetero-coagulation between oil sand components using a novel method of zeta potential distribution measurement developed in this thesis.
- To study the slime coating phenomenon, i.e., the interactions between bitumen and fines.
- To identify the cause for the poor processibility of poor processing ores and suggest avenues to improve bitumen recovery from poor processing ores.
- To determine the origin of the interaction forces between oil sand components and provide guidance to control their interactions.

To accomplish these objectives, the bitumen extraction system is studied from two aspects: tracking the change of surface electric properties, resulted from hetero-coagulation, of oil sands components and measuring the interaction force, resulting in colloidal interactions, between oil sand components. The findings through these studies are expected to provide an overall understanding and insight into the bitumen extraction

fundamentals for Water-Based Extraction technology, thereby advancing the current knowledge to a more direct and/or quantitative level.

1.4 Organization of thesis

The thesis is a summary of the results collected during the Ph. D program. These results are published in 11 technical papers, which are listed at the end of this chapter.

In Chapter 1, a brief introduction to bitumen extraction, the objectives, and the organization of the thesis are given.

Chapter 2 reviews the literature of bitumen extraction including characteristics of oil sands, Water-Based Extraction process, and up-to-date fundamental studies of bitumen extraction systems.

Chapter 3 summarizes the theories of colloidal forces, including the classical DLVO and the extended DLVO theories. The origin and quantitative or empirical expressions of colloidal forces (such as electrostatic double layer force, van der Waals forces, hydrophobic force, steric force and so on) are described. The topics related to adhesive forces are also included.

In Chapter 4, the main experimental techniques used in this thesis research are described. Introduced are the principles of zeta potential distribution measurement for hetero-coagulation and surface force measurement using an atomic force microscope (AFM). Other techniques described include contact angle measurement and particle size distribution measurement.

Chapter 5 concerns the surface eletric properties of oil sand components including bitumen, silica, clays and fines, on which the colloidal interactions between the oil sand components are dependent to a large extent.

Chapter 6 presents the results of colloidal force measurement between bitumen and silica. The effect of solution pH, monovalent and divalent electrolyte concentration, and temperature on both long-range forces and adhesive forces is reported. The colloidal

force profiles are fitted with an extended DLVO theory and the interpreted interaction behavior is confirmed with zeta potential distribution measurements.

Chapter 7 demonstrates how AFM force measurement can be applied to study the colloidal interactions between bitumen and bitumen. The effect of solution pH, salinity, calcium ions and montmorillonite clay addition on both long-range forces and adhesive forces is investigated. The colloidal force profiles are fitted with an extended DLVO theory.

Chapter 8 focuses on bitumen-clay interactions using the novel method of zeta potential distribution measurement. The hetero-coagulation behaviors between bitumen-kaolinite and bitumen-montmorillonite are compared in the presence and absence of calcium addition. Through this investigation, the developed novel method of zeta potential distribution measurement is proved to be a powerful tool to study hetero-coagulation of colloidal particles. The interpreted conclusion is validated with AFM force measurements.

Chapter 9 expands the studies from model systems to the real flotation system of oil sands. The colloidal interactions between bitumen and fines collected from oil sand ores are studied with zeta potential distribution measurements and AFM force measurements. The coagulative behaviors between bitumen and the fines from a good processing ore and a poor processing ore are compared. A model accounting for poor processibility of poor processing ores and potential approaches of improving its processibility are proposed.

The general conclusions are given in Chapter 10.

1.5 List of papers pertinent to this thesis

1. J. Liu, Z. Xu and J. Masliyah, "Colloids Science in Bitumen Extraction from Oil Sands", submitted to ***J Colloid Interface Sci*** (Sept. 2003).

2. J. Liu, Z. Xu and J. Masliyah, "Interaction between Bitumen and Fines in Oil Sands Extraction System: Implication to Bitumen Recovery", submitted to ***Can J Chem Eng***, (Aug. 2003).

3. J. Liu, Z. Xu and J. Masliyah, "Role of Clay Fines in the Bitumen Extraction from Oil Sands", accepted by ***AIChE Journal***, (Dec. 2003).

4. J. Liu, Z. Xu and J. Masliyah, "Studies on Bitumen-Silica Interaction in Aqueous Solutions by Atomic Force Microscopy", ***Langmuir***, Vol.19 (9), 3911-3920, 2003.

5. Z. Xu, J. Liu, J. Choung and Z. Zhou, "Electrokinetic Study of Clay Interactions with Coal in Flotation", ***Inter J Miner Proc***, Vol.68, 183-196, 2003.

6. J. Liu, Z. Zhou, Z. Xu, J. Masliyah, J. Choung and T. Kasongo, "Study of Slime Coatings in Flotation by Electrophoretic Mobility Distribution Measurement", in: ***34# Canadian Mineral Processing Operators Conference*** (ed. by J. Nesset), CIM, Ottawa, Canada, 403-416, 2002.

7. J. Liu, Z. Zhou, Z. Xu and J. Masliyah, "Interactions between Clays and Bitumen in Aqueous Media from the Measurement of Zeta Potential Distributions", ***J Colloid Interface Sci***, Vol.252, 409-418, 2002.

8. J. Liu, Z. Zhou and Z. Xu, "Electrokinetic Study of Hexane Droplets in Surfactant Solutions and Process Water of Bitumen Extraction Systems" ***Ind Eng Chem Res***, Vol.41, 52-57, 2002.

9. J. Liu, Z. Zhou and Z. Xu, "Electrokinetic Study of Hexane Droplets in Surfactant Aqueous Solutions", in: ***Interactions in Mineral Processing*** (ed. by J.A. Finch, S.R. Rao and L. Huang), CIM, Montreal, 375-384, 2001.

10. J. Liu, Z. Zhou and Z. Xu, "Fundamental Study of Reactive Oily-Bubble Flotation", ***Miner Eng***, Vol.15, 667-676, 2002.

11. Z. Xu, J. Liu and C. Kenny, "Fundamental Study of Reactive Oily Bubbles in Sulphide Floatation", in: ***35# Annual meeting of the Canadian Mineral Processors*** (ed. by S. Wilson), Ottawa, Canada, 607-620, 2003.

CHAPTER 2 LITERATURE REVIEW

2.1 Characteristics of Athabasca oil sands

The oil sand ore in Athabasca, Alberta, is a mixture of bitumen, sand grains (quartz and clay minerals), water and electrolytes. The connate water contains various amounts of water-soluble organics and inorganic ions such as –COOH, $-OSO_3$, $-NH_2$, Na^+, K^+, Ca^{2+} and Mg^{2+}. The bitumen content in oil sands ranges from 0~16 % by weight. According to the bitumen content, oil sand ore is classified as: low-grade (poor) ore (6~8 % bitumen), average-grade (medium) ore (8~10 % bitumen) and high-grade (good) ore (>10 % bitumen). Although the bitumen content varies in oil sands, the total content of bitumen and its connate water is fairly constant at 16 %, balanced with 84 % of mineral solids. It is commonly recognized that the fines (fines are defined as the solids less then 44 micron in size), water and inorganic content is a function of ore grade, with higher content corresponding to lower-grade ore. The mineral composition of the sands is over 90 % quartz with minor amount of potash, feldspar, chert and muscovite (Boon, 1978). Clay minerals, which are predominantly kaolinite, illite and a small amount of montmorillonite, only appear in the fines fractions. In Athabasca area, the sands in oil sand ores are water-wettable and packed with about 35 % porosity. The sand grain is surrounded with a thin water film (about 10 nm) and then the continuum bitumen. Only a small portion of total water is contained in this film. The remaining water forms pendular rings at the grain-to-grain contact points. Clay minerals are suspended in the water phase (Cottrell, 1963; Mossop, 1980; Takamura, 1982).

Two important characteristics of oil sands in Athabasca have been identified. The most distinguished feature of Alberta oil sands is the water-wettable characteristics of the associated sand grains in the oil sand ore. The water-wettability of sand grains is the cornerstone for bitumen extraction with water-based technology. This feature distinguishes these oil sands from other oil sand deposit. For instance, sand grains in Utah's oil sand ore are oil-wettable and therefore a solvent-based extraction technology is needed. Water-wettable nature of the associated sands makes the extraction of bitumen from oil sand ores in Alberta economically attractive. The second feature is the

dependence of bitumen content on particle size distribution of the associated solids. This is a primary reason why low-grade ore is of "poor processing" characteristics.

A wealth of physical data related to oil sands is provided in a number of AOSTRA publications (Helper and Hsi, 1989; Helper and Smith, 1994; Masliyah, 2000, 2003).

2.2 Water-Based Extraction (WBE) process

2.2.1 General description

In the 1920's, Dr. Clark developed and patented the Hot Water Extraction (HWE) process for bitumen extraction from oil sands in Canada. In the 1930's, he patented his HWE process and the related apparatus in the USA. Since then, considerable research efforts have led to the commercial application of Hot Water Extraction process for recovering bitumen from oil sands in Athabasca area (Hepler and Hsi, 1989; Hepler and Smith, 1994). The oil sands are slurried with water and caustic (such as sodium hydroxide) at slurry pH 8~8.5 and temperature 80°C (by injecting steam). To reduce the energy consumption and associated operating cost in the oil sands extraction, a Low Temperature Extraction (LTE) process was proposed and patented in 1990 (Sury, 1990, 1992). In this process, the oil sands are slurried and digested in a hydrotransport pipeline at slurry temperature of 2 to 15°C by taking advantage of the shear action during the transportation of the slurry from mining site to extraction plant. In the pipeline, air and floatation aids (100-800 ppm kerosene and 50-400 ppm MIBC) are introduced to facilitate bubble generation and bitumen aeration. Since 1994, two novel technologies including Warm Slurry Extraction (WSE) process operating at 50°C and Low Energy Extraction (LEE) process operating at 25°C have been developed in Syncrude (Spence, 1996; Mankowski, 1996). Those two novel technologies are based on hydrotransport technology for oil sand slurry preparation and transportation. Process aids such as collector, frother and air are added to the slurry pipeline feed. With the development of novel technologies, recent efforts in bitumen extraction have been aimed at process optimization.

A typical bitumen extraction circuit is shown in Figure 2.1 (Masliyah et al., 2003). In such commercial operations, the oil sands is mined in the prepared open-pit mine using

trucks and shovels. The oil sand lumps are crushed and then mixed with recycled process water in mixing boxes, stirred tanks, cyclo-feeders or rotary breakers. The prepared oil sands slurry is introduced to conditioning hydrotransport pipelines or to tumblers, where the oil sand lumps are sheared and size reduction takes place. Within the tumblers or the hydrotransport pipelines bitumen is released, or "liberated", from the sand grains. Chemical additives can be included at this stage. Entrained or introduced air attaches to bitumen in the tumblers and hydrotransport pipelines. The aerated bitumen is then separated and recovered as it floats to the top of the slurry. This is accomplished in large gravity separation vessels, normally referred to as primary separation vessels (PSV), separation cell or primary separation cell (PSC). Small amount of small bitumen droplets (usually un-aerated bitumen) present within the gravity separation vessel is further recovered using induced air flotation in mechanical flotation cells. The operating slurry temperature ranges from about 75°C in tumblers to as low as 3 °C in Syncrude's Aurora hydrotransport based operation. Typically, a 40-55°C slurry temperature is used. A typical overall bitumen recovery in commercial operations is about 90-95 %. The recovered bitumen froth normally contains 60 % bitumen, 30 % water and 10 % solids. The froth product is then de-aerated, and diluted with solvents to provide a density difference between water and bitumen and to reduce the bitumen viscosity with subsequent removal of the solids and water from the bitumen froth using inclined plate settlers, cyclones and/or centrifuges. At both Syncrude and Suncor operations, naphtha is used as solvent while at Albian's froth treatment plant, a paraffinic diluent (mainly hexane) is used. The diluted froth is centrifuged to remove the remaining solids and water. After removing the diluents, the bitumen is upgraded by thermal cracking and/or catalytic hydrocracking to obtain synthetic crude oils. The tailings stream from the extraction plant goes to the tailings pond for solid-liquid separation and recycling of the water to the extraction plant. To accelerate tailings handling, Suncor and Syncrude employ consolidated (composite) tailings (CT) process by adding gypsum together with mature fine tails to consolidate the fines and the coarse sands into a non-segregating mixture that can be disposed off with accelerated dewatering characteristics. At Albian, the tailings from the extraction plant are cycloned, with the overflow (fine tailings) pumped to thickeners and the cyclone underflow (coarse tailings) pumped to the tailings

pond. Fine tailings are treated with flocculants, then thickened and pumped to a tailings pond. The three oil sand operators are planning to use paste technology, consolidated (composite) tailings, or a combination of the two (i.e., CT and paste technology) for immediate water release and recycle for bitumen processing.

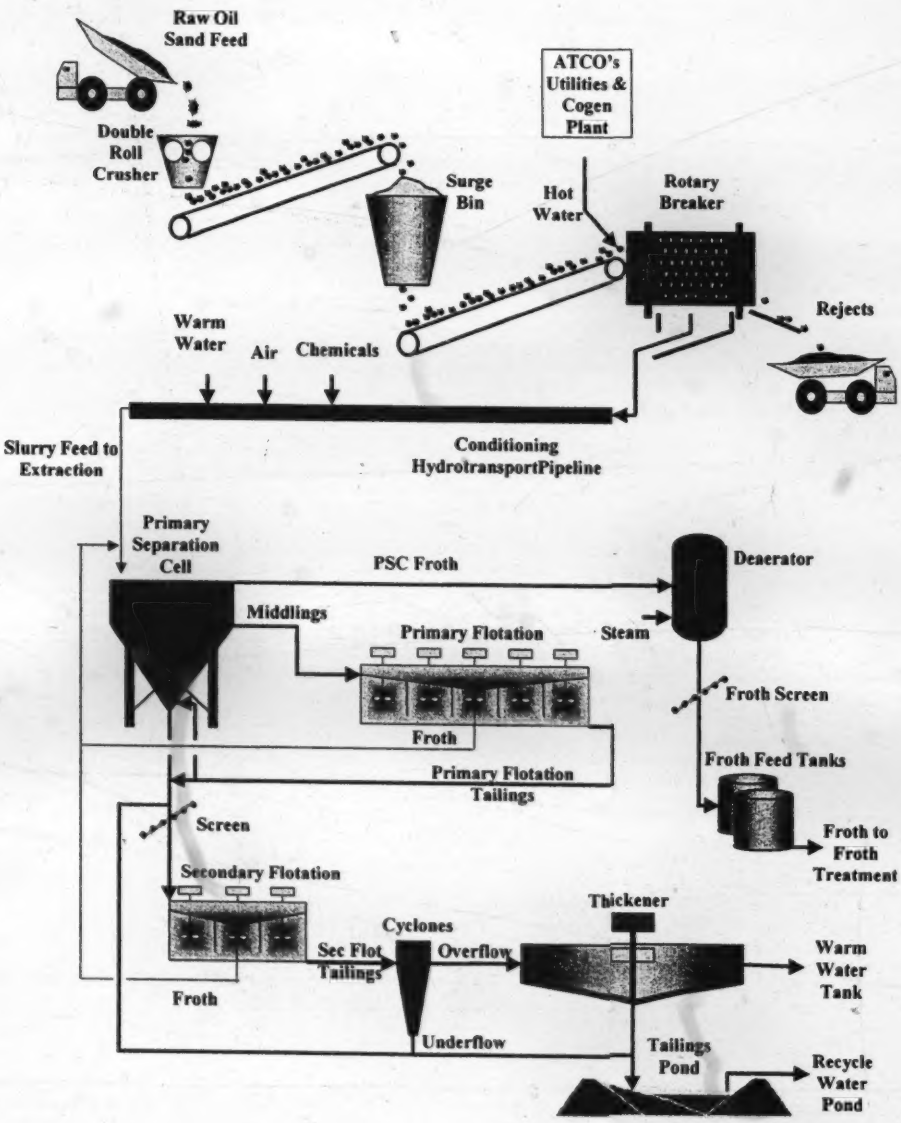

Figure 2.1 A typical bitumen extraction circuit (ore preparation, slurry conditioning, extraction and tailings treatment). Courtesy of Dr. Robert Tipman, Shell Canada Ltd. (Masliyah et al., 2003).

2.2.2 Process parameters

The importance of the slurry-conditioning environment on bitumen extraction has been recognized, and studied extensively. The main effect of process parameters on bitumen recovery is summarized below.

Caustic addition In early1932, Clark et al. (1932) reported the necessity of sufficient amount of alkaline additive to maximize bitumen recovery. In 1979, Sanford and Seyer (1979) developed a laboratory-scale Batch Extraction Unit (BEU) to standardize bitumen flotation tests. With BEU tests, the roles of NaOH were identified: neutralization of organic acids in bitumen and generation of natural surfactants that are believed to facilitate bitumen flotation. In 1983, Sanford (1983) reported that the maximum NaOH required to achieve a desired level of bitumen recovery was a function of fine solid content. In 1992, Smith and Schramm (1992) showed that only a small fraction of added NaOH is required to produce the needed natural surfactants, and the bulk of NaOH reacted with multivalent metal ions and minerals. Using a model oil sand ore, Dai and Chung (1996) studied the effect of NaOH addition on bitumen liberation from sands and on bitumen emulsification. They identified a critical NaOH dosage needed to achieve an optimal effect. Over-dose of NaOH was found to cause bitumen to emulsify, forming small size bitumen droplets and resulting in a low flotation recovery.

Role of surfactants In 1944, Clark (1944) noted, by listing dissolved species in water, the importance of surfactants that displace the oil from sand grains in the HWE process. Later, it was proven that surfactants were not always beneficial, and excess surfactants might induce the floatability of the associated mineral solids (Bapt sta and Bowman, 1969). An optimal free surfactant concentration for bitumen recovery was observed (Sanford and Seyer, 1979; Sanford, 1983; Schramm et al., 1984a, b, 1987), which corresponded well to the establishment of surface charges (Schramm et al., 1985). Recently, the application of novel surfactants in Low Temperature Extraction process and improvement of the processibility of poor processing ores has been emphasized.

Role of cations Using a modified BEU, Kasongo et al. (2000) conducted doping tests by adding a given amount of calcium and/or clays into a rich estuarine oil sand ore. They

found that the addition of calcium (up to 40 ppm) or clay (kaolinite, illite or montmorillonite) at 1 wt% of the oil sand ore processed had a marginal effect on bitumen recovery. However, a sharp depression of bitumen recovery was observed when montmorillonite clays at about 1 wt% of oil sand ore were co-added with greater than 30 ppm calcium ions in solution, hereby suggesting a detrimental synergetic effect of calcium ions with montmorillonite clay. Such a depression was *not* observed with calcium ions and kaolinite or illite.

Air addition Considering the comparable densities of bitumen and water, the introduction of air bubbles is another important process parameter. Insufficient air was found to drpress bitumen flotation rate (Flynn et al., 2001), while too much air could result in the entrainment of mineral fines in the froth (Camp, 1976). Moran et al. (2000) examined the aeration of bitumen droplets by visual observations and surface energy determination. They concluded that a positive spreading coefficient of bitumen on the air bubble does not always lead to the aeration of bitumen droplets. Drelich et al. (1995) studied the effect of aeration on bitumen recovery from Whiterock oil sands. They proposed that the air bubble attaches to bitumen first, and then the aerated bitumen detaches from sand grains. The effect of bubble size on the bitumen-air bubble attachment was investigated recently (Gu et al., 2003; Wang et al., 2003a, b, c). The gas nuclei or tiny bubble present in water can enhance the attachment of air bubbles on the bitumen (Gu et al., 2003).

Other parameters It was also found by many researchers (Boon, 1978; Sanford, 1983) that a shear action is of vital importance. Without sufficient mechanical energy, it would be impossible to liberate bitumen from sands to get high bitumen recovery, even with process aids. Studies on other operating parameters such as temperature, sand grain size, oil sand grade, and salinity of process water were also reported in literature (Dai and Chung, 1995, 1996).

2.3 Fundamental study on bitumen/sands/bubble interactions

The fundamentals involved in bitumen extraction have been studied extensively using both the oil sand ores and model oil sand systems with different techniques. A bitumen extraction system involves the following sub-processes (Eskin, 2002; Masliyah, 2003;

Masliyah et al., 2003). Oil sand lumps, either in a tumbler or a hydrotransport pipeline, are subjected to shear action in the presence of added water and process aids. The shear action, compounded with the heating of the outer layer of an oil sand lump, ablates away the outer layer of the oil sand lump, and exposes fresh surfaces to be further heated and sheared away. The sheared layers contain sand grains covered with bitumen. The bitumen further ***liberates*** from sand grains. As shown in Figure 2.2a, bitumen "liberation" can be described in three steps: I) bitumen thins to form a pinhole; II) the pinhole expands for bitumen to recess from the sand surface until an equilibrium contact angle is achieved among the sand, bitumen and water; III) the bitumen in the form of droplets on the sand grain detaches from sand grains under hydrodynamic actions. The liberated bitumen droplets might be ***aerated*** with air bubbles. The "aeration" of bitumen droplets with air bubbles in oil sands slurry is schematically shown in Figure 2.2b. Under favorable slurry conditions, the fines present in the system do not attach to the surfaces of bitumen droplets. Therefore, the bitumen droplets might first coalesce (I) to form larger bitumen droplets and then attach to air bubbles (II), or directly attach to air bubbles (III). In this case, the bitumen droplets can further engulf air bubbles. If the temperature is sufficiently high, the resultant buoyant force causes the aerated bitumen to float. In this case, a high bitumen recovery and a good froth quality would be observed. In the case that the fines readily attach to the surfaces of bitumen droplets and/or air bubbles (IV), forming less hydrophobic aggregates, the fines attached on the surfaces will hinder the attachment of bitumen to air bubbles. If these aggregates can still attach with air bubbles, a poor froth quality would be observed. If these aggregates cannot attach with air bubbles anymore, a low bitumen recovery would be observed.

It is obvious that the essence of the "liberation" and "aeration" processes is the colloidal interactions between bitumen/sands/bubbles, which depend on their surface properties and solution conditions.

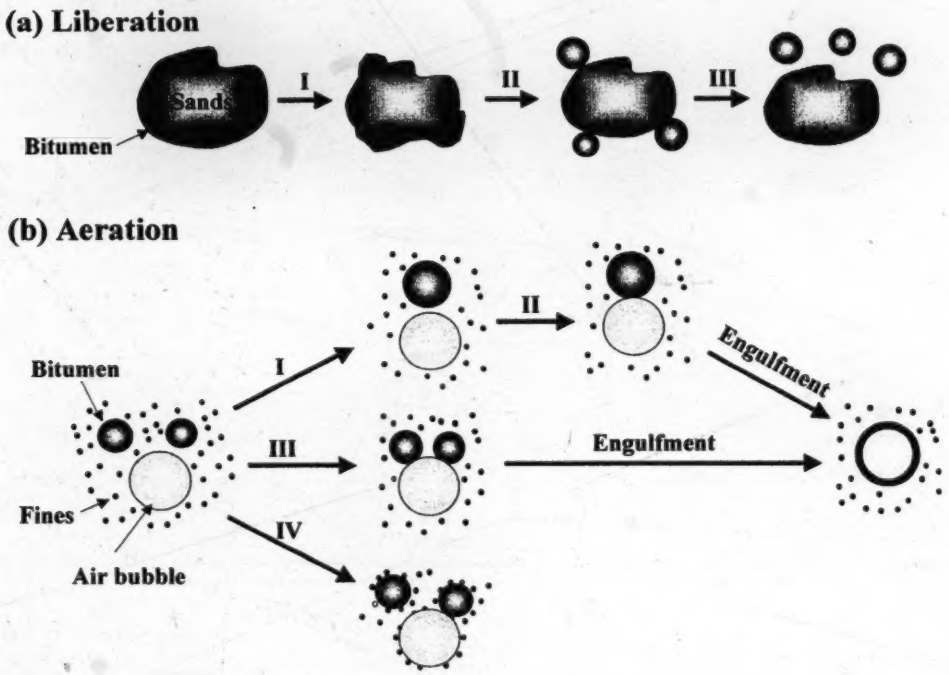

Figure 2.2 Conceptual stages for bitumen liberation and aeration (Modified from Masliyah, 2003).

2.3.1 Bitumen surface properties

Knowledge on surface properties of bitumen is critical to understand colloidal interactions between oil sands components. The principal surface properties pertinent to bitumen extraction are summarized below.

Surface composition The components of bitumen surface not only determine bitumen/water interfacial properties (such as zeta potential, interfacial tension and wettability), but also readily releases into solution to further modify solids/bitumen/liquid/air interfacial properties and hence their interactions. It is well documented that bitumen consists of 15~20 % asphaltene balanced by a mixture of resins, saturated and aromatic molecules (Boukir et al., 2001; Zhang et al., 2003a, b). Extensive studies have been made to understand the role of various components in the bitumen extraction. Some researchers (Mackay et al., 1973; Borve et al., 1992; Yoon et al., 1995, 1999; Gu et al., 2002) believe that the asphaltenic layer at water/oil interface

stabilizes the water in oil emulsion, indicating that asphaltene dominates the characteristics of bitumen surfaces. Salou et al. (1998a, b, 2001) indicated that the resin to asphaltene molar ratio controls water/bitumen interfacial properties, with a higher resin content facilitating the migration and dissociation of asphaltene molecules at the bitumen surface to stabilize the bitumen droplets. From a molecule point of view, the type of *molecules* exposed at the bitumen/water interface is critical. It is generally accepted that oil sand process streams contain various forms of organic acids mainly with carboxylic groups (Clark, 1944; Bowman, 1967; Baptista and Bowman, 1969; Sanford and Seyer, 1979; Sanford, 1983; Scharmm et al., 1984). Schramm et al. (1984, 1987) also identified the presence of sulfate/sulfonate type of surfactants. More recently, the presence of amine-bearing surfactants was postulated by some researchers (Drelich and Miller, 1994; Zhou et al., 1999; Liu et al., 2002).

Electrokinetics The zeta potential of bitumen was found to be a function of solution pH, salinity and temperature (Takamura and Chow, 1983; Masliyah, 1994; Dai and Chung, 1995; Zhou et al., 1999). An iso-electric point (iep) of a bitumen emulsion was found to occure at pH 3. More negative zeta potential values of bitumen emulsion were observed at higher solution pH and lower salinity. By assuming that the charge at the bitumen/water interface was derived from the ionization of carboxyl groups, Takamura and Chow (1985, 1988) applied the surface ionization model to describe the electrokinetic properties of bitumen/water interfaces as a function of solution pH. They further correlated the measured bitumen electrokinetics with bitumen recovery.

Interfacial tension The interfacial tension of bitumen was found to be a function of pH and temperature (Bowman, 1967; Drelich et al., 1994, 1995; Moran et al., 2000; Schramm et al., 2003). A temperature change from 20°C to 60°C, for example, caused a substantial reduction of surface tension from 23.6 mN/m to 20.5 mN/m for a bitumen sample from Whiterock tar sands. The maximum interfacial tension of bitumen was observed in the pH range of 5~9. A similar observation was made for toluene-extracted bitumen from Utah oil sands as determined by Welhelmy plate and contact angle technique (Drelich et al., 1994).

Wettability The hydrophobicity of bitumen surfaces, measured by contact angle, is another important surface characteristics. It is recognized that bitumen recovery and receding contact angle are qualitatively correlated. The contact angle of air bubbles on bitumen surfaces in water varies between 50 and 100 degrees, depending on the contact angle measurement methods used. The contact angle of bitumen exhibits a strong dependence on solution pH, fines content and multivalent metal ions (Kasongo et al., 2000).

2.3.2 Subprocesses visualized

Since the late 1980's, with the development of advanced optical microscopes and digital video systems, visualization methods were developed to observe directly the colloidal interactions between bitumen/sands/bubbles in model systems. The visualization devices allowed us to observe the impact of various individual process variables on the subprocesses of bitumen extraction processes. For instance, Buckley et al. (1989) carried out adhesion tests and found that the adhesion of crude oil on glass surface was a strong function of pH and ionic strength. The results were explained by electrostatic double layer force calculations in combination with the surface ionization model. Dai and Chung (1995) performed visual pick up tests, and found that the interactions between bitumen and silica were highly dependent of pH, particle size, temperature and solvent addition.

Using a model system of bitumen on a glass slide, Basu et al. (1996, 1997, 1998a, b) investigated the effect of pH, temperature, chemical additives (such as NaCl, MIBC and kerosene), and clay addition on bitumen film pinning and recession, film rupture and formation of contact angle. To validate the observations made in a model system, Basu et al. (1998c) later reported a visual observation of the disintegration process of bitumen in a real oil sand ore under the optical microscope. Bitumen recession on the sand grain was compared with that on a microscope glass slide. They concluded that the static contact angle of bitumen droplets on a sand grain is similar to that observed on a glass slide in an aqueous solution at pH 9. To further investigate the bitumen displacement, Basu et al. (2000) investigated the displacement of a rectangular strip of bitumen coated on a glass slide in aqueous solutions at different pH and temperature. It was found that the rectangular strip experiences the growth of ridge and modulated structures at the

bitumen/water interface and bitumen/water/glass contact line. With increasing the contact time, the modulated contact line and ridge-like structure at the interface evolved further and eventually led to the formation of daughter droplets.

Drelich et al. (1996) studied spreading characteristics of bitumen on air bubble surfaces in a model system. By placing air bubbles on bitumen-coated glass slides, they found that the positive spreading coefficient favors bitumen spreading at the air bubble surface. Alexander and Li (1996) investigated the effect of bitumen films over air bubble surfaces on bitumen-bubble attachment by measuring the time and temperature dependence of bubble surface tension and contact angle. The experimental data obtained for the apparent surface tension showed that a thin bitumen film weakens the strength of the bitumen-bubble attachment by 1-10 %, depending on the size of the bitumen droplets and the air bubbles. A comparable size of air bubbles with bitumen droplets enhances the bitumen-bubble attachment.

Malysa et al. (1999a, b) designed a device with a "Luba Tube". By inserting the device into a separation cell, rising bitumen-air aggregates were sampled into the tube and images were recorded. The size, shape, mass, rising velocity and the number of aggregates were determined. Ng et al. (2000a, 2000b) and Zhou et al. (2000b) used this method to observe the bubble loading of bitumen in flotation. It was found that with good processing ores, the bubbles are fully loaded with bitumen. In contrast, little bitumen was attached to air bubbles in poor processing ore slurry.

Moran et al. (2000) examined the factors affecting the aeration of small bitumen droplets from a surface energy perspective and compared the results with direct observations. They concluded that a positive spreading coefficient does not always guarantee the aeration of bitumen droplets, and that such a process may best be described from a statistical point of view.

The bitumen-bubble attachment in the presence of montmorillonite clays and 1 mM calcium (~40 ppm) was also studied with impinging jet tests (Yang et al, 2000a, b; Masliyah et al., 2003). It was found that only co-addition of montmorillonite clay and calcium significantly decreased the flux of gas bubbles attaching to the bitumen surface.

In contrast, the presence of clay and calcium alone or the combination of calcium with kaolinite showed little effect on the gas bubble flux attaching to the bitumen surface. An induction time device (Gu et al., 2003) was also developed to observe directly the attachment between bitumen and air bubbles. A similar conclusion for bitumen and air bubble attachment in the presence of montmorillonite and calcium was derived from the induction time study.

With a high speed CCD camera to record images of slurry on-line, an on-line image analysis technique was developed (Luthra, 2001; Wallwork, 2003) to evaluate the degree of bitumen liberation from oil sands slurry either in a loop or in a Couette device. By determining the "darkness" level of recorded images, the kinetics of bitumen displacement from the sand grains and flotation can be assessed. This on-line visualization device made it possible to distinguish bitumen liberation and aeration kinetics.

As seen above, the colloidal interactions between bitumen/silica/bubble were extensively studied by visualization methods. These studies advance our knowledge on bitumen/silica/bubble interactions from various aspects. However, these research efforts were of phenomena observation and did not explore the essence of their interactions. To date, there has been no direct observation of bitumen/clays and bitumen/fines interactions.

2.3.3 Current understanding/models

To understand the mechanism of bitumen extraction from oil sands, a few phenomenological models have been proposed.

In 1967, Bowman (1967) assumed that the surface charge of bitumen was dictated by natural surfactants with carboxylic groups while the surface charge of sands was affected by divalent ions in the process media. The dissociation of the carboxylic groups on bitumen and the form of divalent ions on sand surface at different pH level determined the heterocoagulation/separation of bitumen and sands. From the measured zeta potentials of bitumen and sands and the application of the classical DLVO theory, it was proposed that the presence of calcium ions in solution would cause the attachment of

bitumen to sands, thereby deteriorating the bitumen-sand separation and bitumen attachment to air bubbles (Takamura and Chow, 1983). Brown and Neustadter (1990) speculated that the presence of surfactants in crude oils in the form of protonated nitrogenous species might be responsible for the coagulation of fine silica with the oil over an acidic pH range. Based on observations from settling tests and zeta potential measurements in a model system with the addition of various surfactants and calcium ions, Zhou et al. (1999) postulated that electrostatic double layer forces play a critical role in the coagulation between bitumen and sands. For a sheared colloidal system such as in a bitumen extraction process, the DLVO theory might under- or over-estimate the coagulation behavior due to existence of non-DLVO forces. Since the particles possess hydrodynamic (kinetic) energy, both long-range and adhesive forces are critical in considering colloidal stability.

From calcium ion analysis of flotation test water, the detrimental impact of calcium ions and montmorillonite clay on bitumen flotation recovery was found to be associated with preferential up-take of calcium ions by montmorillonite than by kaolinite or illite clays (Kasongo et al., 2000). It was speculated that the calcium ions up-taken by montmorillonite clay activated the interactions between montmorillonite clay and bitumen, resulting in a layer of montmorillonite clay particles coated on the bitumen surface. This layer of hydrophilic or much less hydrophobic montmorillonite clay particles on bitumen droplets acted as a barrier for bitumen-air bubble attachment, leading to a low attachment efficiency and hence low bitumen flotation rate. Although zeta potentials of the three different clays tested did not show any correlation with the bitumen recovery, a qualitative correlation between bitumen recovery and receding contact angle was established. Zhou et al. (2000a) reported the results of air holdup measurement to study the effect of natural surfactants released from the oil sands on air holdup in a water column. From their results, it was suggested that the higher air holdup and lower recovery of poor processing ores could be due to the release of a larger amount of surface active species during conditioning and the presence of more fines in the ores. Although these hypothesis/models can reasonably account for the observations in bitumen extraction, they are speculative and/or qualitative in nature and do not provide the essence of the observations.

2.3.4 Interaction force

With recent development of state-of-the-art instruments such as AFM and SFA (Surface Force Apparatus), quantitative investigation on colloidal particle interactions in oil sands extraction systems became possible. The direct measurement of interaction forces allows us to explore the essence (origin) of the colloidal interactions between the various components in a bitumen extraction system. The interaction forces between solid and model oil droplets with AFM have been measured in a number of cases (Mulvaney et al., 1996; Synder et al., 1997; Aston and Berg, 1998; Hartley et al., 1999; Rabinovich et al., 2002). In contrast, there were only a few reports on quantitative investigation of surface forces in bitumen-related systems. Using SFA, AFM and L-B deposition techniques, Yoon et al. (1995, 1999) investigated the effect of solution pH and temperature on the interaction forces between bitumen surfaces. They detected a strong repulsive force (believed to be of steric origin) resulting from protruding tails of asphaltene molecules. These asphaltene "tails" on bitumen surfaces stabilize bitumen emulsions. Wu et al. (2000), on the other hand, determined the colloidal forces between bitumen droplets by analyzing the droplet-droplet collision trajectories (Wu et al., 1999a) and the hydrodynamic forces required to breakup a bitumen doublet (Wu et al., 1999b). Later, they (Laroche et al., 2002) applied similar methods to study the effect of solution pH and asphaltene content on the dynamic and static forces between bitumen droplets. They found that in addition to an electrostatic double layer repulsive force, heterogeneous protrusion of asphaltene on bitumen surface further increased the repulsive force. The repulsion between the bitumen droplets under a static condition was much weaker than in a dynamic system. These investigations provided some basis to better understanding bitumen/bitumen interactions in the sequential process (flotation stage) of the Water-Based Extraction system. Basu and Sharma (1996) have applied AFM and oil dip-coating techniques to investigate the interactions between oil (octadecane and crude oil) and mineral (glass and mica) surfaces, with an aim of better understanding the wettability alternation in oil reserves.

To our best knowledge, little work has been reported on the quantitative investigation of the colloidal interactions between bitumen/silica, bitumen/clays and bitumen/bubbles to understand the role of colloidal interactions in bitumen extraction systems. The effect of

various process parameters such as water chemistry and clay addition on bitumen/bitumen and bitumen/solid interactions remains to be further studied.

CHAPTER 3 SURFACE FORCE REVIEW

It is well known that the adhesive force (pull-off force) corresponds to the strength at which the two surfaces are attached to each other, while long-range colloidal force (or called non-contact force in literature) controls the ease at which two surfaces approach each other. Therefore, understanding the surface colloidal forces between oil sand components in oil sands extraction systems is of great importance. The related theories or descriptions of colloidal forces are summarized as follows.

3.1 DLVO theory

The long-range colloidal force is generally described by DLVO (Derjaguin and Landau of the USSR, Verwey and Overbeek of the Netherland) theory. The DLVO theory takes into account two components: van der Waals forces F_V and electrostatic double layer force F_E (Israelachvili, 1991; Masliyah, 1994). The DLVO theory is generally expressed as:

$$F_{total} = F_V + F_E \tag{3-1}$$

3.1.1 Electrostatic double layer force

A surface immersed in an electrolyte solution is usually charged. The charging mechanism could be specific adsorption of ions from solution, dissociation of surface species or crystal lattice defects, just to name a few.

The surface charges are balanced by oppositely charged counterions in solution. This kind of charge distribution forms an electric double layer. The structure of the electric double layer was first described with Helmbotz (1879) model of a parallel plate capacitor. In the 1910s, Gouy (1910) and Chapman (1913) proposed a diffuse double layer model by assuming that ions have no volume. With this model, the Poisson-Boltzmann equation was derived. Later, Stern (1924) and Grahame (1947) proposed a modern electric double layer model, known as Stern-Grahame model. In the Stern-Grahame model, counterions bound to the surface form the *Stern layer*, while the remaining counterions form a cloud in rapid thermal motion, extending out from the surface, as shown in Figure 3.1. The

potential at the shear plane is called the "zeta potential", which could be determined with electrophoresis or electrical osmosis measurement.

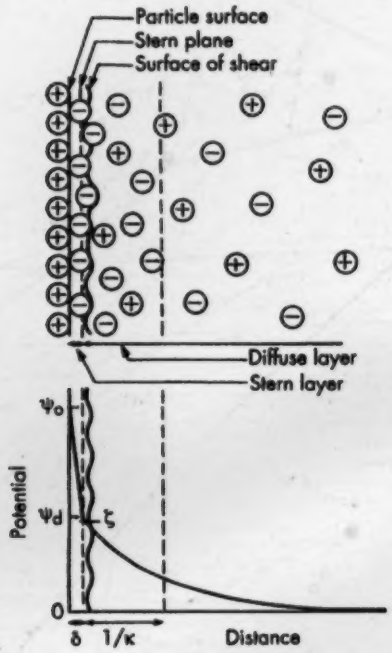

Figure 3.1 Schematics of Stern-Grahame electric double layer model. ψ_0 is surface potential at the particle surface, ψ_d is Stern potential at the Stern plane and ζ is zeta potential at the shear plane.

The electrolyte ions in the diffuse double layer are known to obey the Boltzmann distribution (Israelachvili, 1991; Masliyah, 1994):

$$n_j = n_{j\infty} e^{-\frac{z_j e \psi}{kT}} \tag{3-2}$$

where n_j is the number density of ion j with valence z_j, $n_{j\infty}$ is the number density of ion j in the bulk, ψ is the potential in the electric double layer, e is the electron charge, k is Boltzmann constant and T is the absolute temperature.

According to Maxwell's equation, we can obtain the well-known non-linear Poisson-Boltzmann equation

$$\varepsilon\varepsilon_0\nabla^2\psi = -e\sum_j z_j n_{j\infty} e^{-\frac{z_j e\psi}{kT}} \tag{3-3}$$

where ε and ε_0 are the relative permittivity of the medium and the permittivity of vacuum, respectively.

If the surface potential is small (e.g. ψ less than 26mV at 25°C or $\frac{ze\psi}{kT}$ <<1), the Debye-Huckel approximation becomes applicable (Israelachvili, 1991), and equation (3-3) can be linearlized to the form of

$$\nabla^2\psi = \kappa^2\psi \tag{3-4}$$

$$\text{where } \kappa^{-1} = \left(\frac{\varepsilon\varepsilon_0 kT}{\sum_j n_{j\infty} e^2 z_j^2}\right)^{1/2} \tag{3-5}$$

The κ^{-1} in equation (3-5) is known as the Debye length. Debye length is a characteristic parameter describing the double layer thickness or the decay of the electric potential and hence the interaction between the two neighboring surfaces.

When two charged surfaces approach each other, the electric double layer surrounding each particle starts to overlap, resulting in a repulsion or attraction of osmotic pressure origin. The interaction force $F_E(D)$ and energy $U_E(D)$ between two parallel planes at separation D can be expressed by equation (3-6) and (3-7), respectively (Chan et al., 1976; Israelachvili, 1991; Masliyah, 1994).

$$F_E(D) = kT\sum_j (n_j - n_{j\infty}) - \frac{\varepsilon\varepsilon_0}{2}\left(\frac{d\psi}{dx}\right)^2 \quad \text{per unit area} \tag{3-6}$$

$$U_E(D) = -\int_\infty^D F_E(h)dh \quad \text{per unit area} \tag{3-7}$$

Only with some approximations, can surface potential distribution ψ(x), interaction force $F_E(D)$ and energy $U_E(D)$ be algebraically solved (Israelachvili, 1991; Masliyah, 1994). In general, surface potential distribution ψ(x), interaction force $F_E(D)$ and energy $U_E(D)$ can only be obtained by numerical solutions of equations (3-3), (3-6) and (3-7) with proper boundary conditions (B.C.). If the surface charge arises from irreversible adsorption of charged species or dissociation of surface strong acid/base groups or lattice imperfections, the surface charge density is independent of the surface potential and the separation between the two interacting surfaces. In this case, the constant surface charge density (σ) boundary condition is appropriate since the potential-determining ions have insufficient time to re-arrange during the approach of the two surfaces during force measurement (Hunter, 1993). In this case, the surface charge density can be obtained by either simplifying equation (3-3) or using the surface charge regulation model (site binding model) (Grabbe and Horn, 1993). If the surface charge arises from reversible ion adsorption, the potential-determining ions are flexible to re-arrange quickly to suit every configuration of interacting surfaces and the surface potentials would remain constant when the two surfaces approach each other at a slow rate (Warszynski et al., 1997). In this case, the constant surface potential (ψ) boundary condition is more applicable.

In reality, the surface charge density of ionizable surfaces is a function of separation distance as the two interacting surfaces approach each other. The assumption of constant surface charge density and constant surface potential constitutes the upper and lower limits of interaction forces, respectively. Therefore, a realistic description of the interaction would fall in - between these two limits.

3.1.2 van der Waals forces

van der Waals forces exist between any surfaces in any medium. Generally, they dominate over a separation range of 0.2-10 nm. The van der Waals forces have three distinct origins: a) *Kessom or orientation* force between two dipoles; b) *Debye or induction* force between a dipole and an induced dipole; and c) *London or dispersion* force between two induced dipoles created by fluctuation of electronic charges. It should be noted that the van der Waals forces are dependent on properties of the materials, and are less sensitive to environmental changes. More detailed description of the van der

Waals forces can be found in textbooks by Israelachvili (1991) and Masliyah (1994). As an example, the van der Waals energy between two parallel surfaces at separation D can be calculated by equation (3-8):

$$U_V = -\frac{A}{12\pi D^2} \text{ per unit area} \tag{3-8}$$

The characteristic constant A in equation (3-8) is known as *Hamaker constant*. The Hamaker constant can be calculated based on the Lifshitz (1956) approach or surface energy measurement (Vanoss et al., 1988; Israelachvili, 1991).

For the interaction of phase 1 and phase 2 through media 3, the combined Hamaker constant A_{132} can be calculated through the Lifshitz approach, or the combining law by equation (3-9) (Israelachvili, 1991; Masliyah, 1994).

$$A_{132} = (\sqrt{A_{11}} - \sqrt{A_{33}})(\sqrt{A_{22}} - \sqrt{A_{33}}) \tag{3-9}$$

where A_{ii} is the known Hamaker constant of material i.

3.2 Extended DLVO theory

Over the past several decades, numerous force profiles measured with AFM (atomic force microscope) or SFA (surface force apparatus) cannot be explained with the classical DLVO theory. Considerable evidence suggested the existence of additional forces, which usually result in the deviation from the DLVO theory. These forces include repulsive hydration force for hydrophilic surfaces at a separation range of 2~3 nm (Pashley, 1981a, b), attractive hydrophobic force for hydrophobic surfaces at a longer separation range (Israelachvili and Pashley, 1982), and repulsive steric force or attractive bridge force for polymer-bearing surfaces (Ingersent et al., 1990). Although the nature of these non-DLVO forces remains to be understood, some empirical expressions have been derived. The total force can be written as equation (3-10):

$$F_{total} = F_E + F_V + F_{HB} + F_S + F_{HD} \bullet\bullet\bullet \tag{3-10}$$

where F_{T_E} is the electrostatic double layer force; F_{T_V} is the van der Waals forces; $F_{T_{HB}}$ is the hydrophobic force; F_S is the steric force; and F_{HD} is the hydration force. Equation (3-10) is known as the so-called extended DLVO (or EDLVO) theory

3.2.1 Hydrophobic force

Hydrophobic attraction has been found to exist between hydrophobic surfaces immersed in aqueous solutions (Ben-Nain, 1980; Ralston, 2001). Hydrophobic (i.e. water-hating) surfaces prefer to be in contact with each other rather than with water. The hydrophobicity of surfaces is arisen from the reorientation of water molecules near the surface to attain the best configuration of the maximized number of H-bonds, i.e. increase in parallel orientation of water molecule dipole moment (Israelachvili, 1991 p129). Both theoretical and experimental studies indicated that the reorientation of water molecules around a non-polar surface is entropically unfavorable. Therefore, once two hydrophobic surfaces approach each other, the rearrangements of H-bond configurations in the overlapping salvation zones would result in their attraction to reduce the entropy. From the direct force measurement, the hydrophobic force is found to operate over longer surface separation ranges than the van der Waals forces. Although the mechanisms of the hydrophobic force has not been fully understood, several empirical relationships have been proposed over the years (Israelachvili and Pashley, 1984; Claesson et al., 1986, Rabinovich and Yoon, 1994; Ravishankar and Yoon, 1997; Graig et al., 1999), mainly based on the information from direct force measurements (Parker and Claesson, 1994; Yoon et al., 1997). The commonly used empirical equations for calculating hydrophobic force F_{HB} of a plate-sphere configuration include:

$$\frac{F_{HB}}{R} = -C_0 \exp(-\frac{D}{D_0}) \tag{3-11}$$

$$\frac{F_{HB}}{R} = -C_1 \exp(-\frac{D}{D_1}) - C_2 \exp(-\frac{D}{D_2}) \tag{3-12}$$

$$\frac{F_{HB}}{R} = -\frac{K}{6D^2} \tag{3-13}$$

where D is the separation distance between two surfaces, R is the radius of the spherical particle, and C_0, C_1, C_2, D_0, D_1, D_2 and K are empirical constants which depend on the hydrophobicity of the surfaces.

3.2.2 Hydration force

In contrast to the hydrophobic force, the hydration force has been identified experimentally as a strong, short-range repulsive force between hydrophilic surfaces. Hydrophilic (i.e. water-loving) surfaces prefer to be in contact with water rather than with each other. The hydrophilicity of surfaces arises from the strongly binding nature of water molecules with surfaces. When the two surfaces approach each other, an additional force is needed to remove water molecules from surface regions, showing as a repulsive hydration force. The hydration force was first observed in swelling of clays. Later, it was measured with the surface force apparatus (SFA) (Israelachvili and Adams, 1978). This kind of short-range repulsive force has also been observed in silica, lipid, and surfactant systems (Meagher, 1992; Grabbe and Horn, 1993; Ducker et al., 1991, 1994; Nishimura, 1998). Empirically the hydration force was described by an exponential force law with decay lengths of 0.4~4.0 nm. Recently, numerical methods based on the statistical thermodynamics theory (Besseling, 1997), boundary element method (Wang et al., 1997) and Monte Carlo simulation (Forsman et al., 1997) have been used to evaluate the hydration force.

3.2.3 Steric force

Steric forces are often found in systems involving brush-like surfaces, such as polymer- or surfactant-bearing surfaces. From direct surface force measurements (Klein, 1980; Klein and Luckham, 1984; Israelachvili et al., 1984; Aimog and Klein, 1985; Marra and Hair, 1988; Butt et al., 1999), at least three types of steric interactions have been identified: the osmotic repulsion in good solvent, the osmotic attraction in poor solvent (also known as depletion force), and the attractive bridging effect due to polymer chains simultaneously adsorbed on both surfaces. Based on the theoretical consideration of scaling concept and experimental data, a number of equations have been derived for calculating these various types of steric forces (Israelachvili, 1991; de Gennes, 1987 and O'Shea et al., 1993).

- For uncharged polymeric surfaces, *de Gennes* (1987) assumed an brush-model and derived an expression of the steric force as a function of the separation distance D for a plate-sphere configuration:

$$\frac{F_S}{R} = \frac{16\pi kTL}{35s^3}\left[7\left(\frac{D}{2L}\right)^{-5/4} + 5\left(\frac{D}{2L}\right)^{7/4} - 12\right] \quad \text{for D<2L} \qquad (3\text{-}14)$$

where L is the thickness of polymeric layer, and s is the average spacing between two grafted points of polymer molecules.

- For charged polymeric surfaces, Pincus (1991) developed an expression of steric force as a function of the separation distance for a plate-sphere configuration:

$$\frac{F_S}{R} = \frac{4\pi kTN_B^2}{Cs^4}\left[\frac{1}{D} - \frac{1}{2L}\right] \quad \text{for D<2L} \qquad (3\text{-}15)$$

where C is the added salt concentration, and N_B is the number of monomer units per chain.

3.3 Derjaguin approximation

Theoretically, it is easier to evaluate the interaction between two parallel plates in terms of interaction energy per unit area. Experimentally, the actual force measurement is conveniently carried out with geometry other than two parallel plates. Derjaguin (Israelachvili, 1991) and White (1983) derived a relationship between the interaction force F for a given geometry and the interaction energy U_{p-p} of two parallel plates:

$$F = 2\pi\sqrt{R_A R_B}U_{p-p} \qquad (3\text{-}16)$$

- For sphere (R_1)-sphere (R_2): $R_A = R_B = \dfrac{R_1 R_2}{R_1 + R_2}$, $F_{s-s} = 2\pi\dfrac{R_1 R_2}{R_1 + R_2}U_{p-p}$

- For sphere (R)-plane: $R_A = R_B = R$, $F_{s-p} = 2\pi RU_{p-p}$

- For cylinder (R_1)-cylinder (R_2) crossed: $R_A = R_1$ and $R_B = R_2$

$$F_{c-c} = 2\pi\sqrt{R_1 R_2}U_{p-p}$$

3.4 Adhesive force

Adhesive forces between two surfaces mainly originate from the molecular/atomic interactions in the contact area. Electrostatic interactions, chemical bonds and hydrogen bonding can all contribute to the adhesion between the two surfaces. The long-range forces outside of the contact area also contribute to the adhesive force, but to a much less extent. It is clear that the adhesive force is highly sensitive to surface composition.

Contact mechanics provides the link necessary for the adhesion hysteresis to be quantified with respect to material properties. Several theories such as JKR (1971), DTM (1975) and BCP (1999) have emerged from the pioneering work by Hertz (Meyer et al., 1998; Burnham et al., 1999). The expression of the adhesive force for a plate-sphere configuration is summarized in equation (3-17)

$$\frac{F_{ad}}{R} = m\gamma \tag{3-17}$$

where γ is the interfacial energy per contact area ($\gamma = \gamma_1 + \gamma_2 - \gamma_{12}$), and m is the coefficient with a value between π and 2π, depending on the theory involved.

According to these theories, the adhesive force between bitumen and a substrate can be expressed as a function of the bitumen/water interfacial tension γ_{BW} and the contact angle θ of a bitumen droplet on the substrate.

$$\frac{F_{ad}}{R} = m\gamma_{BW}\ (1\text{-}\cos\theta) \tag{3-18}$$

It should be noted that all these theories were established on the basis of equilibrium. However, in the AFM force measurement the contact time between two surfaces is very short (80~ 100ms), which could result in a significant deviation of the m value obtained from the prediction with theories. In this case, the m value could be much lower.

Although many other detailed theories describing long-range and adhesive forces are available in literature, theories described above are pertinent to the current work and will be referred to in later chapters when quantitatively describing the measured force profiles and adhesive forces.

CHAPTER 4 MATERIALS AND EXPERIMENTAL TECHNIQUES

4.1 Materials

Three types of bitumen samples (coker feed bitumen, solvent extracted bitumen and oxidized bitumen) and two types of oil sand samples (a good processing ore and a poor processing ore) were provided by Syncrude Canada Ltd.. Coker feed bitumen and solvent-extracted bitumen were used in the study for the model system and real system, respectively. Oxidized bitumen was used for the purpose of comparison. A comparison of some pertinent properties between these two oil sand samples was shown in Table 4.1.

Table 4.1 Composition of oil sand samples.

Oil sands	Bitumen (%)	Water (%)	Solids (%)	Fines (-44μm, %)
Good processing ore	14.3-14.5	0.5-0.8	85.3-85.5	4
Poor processing ore	7.3-7.5	7.3-7.8	85.3-86	40

Silica microspheres (~8 μm) purchased from Duke Scientific Co. (USA) was used to model sand grains for colloidal force measurement. Silica sands (-40 μm), provided by Pacific, MO (USA), were ground to -5 μm size and used in the zeta potential distribution measurements. Clays including montmorillonite and kaolinite from Wards's Minerals (USA) were used for zeta potential measurement and for colloidal force measurements without further purification or treatment by chemicals.

Silicon wafers of 100 crystal planes were purchased from MEMC Electronic Materials (Italy) and used as the substrate for supporting bitumen by the spin coating technique. Reagent grade HCl and NaOH (Fisher) were used as pH modifiers. Ultrahigh purity KCl (>99.999 %, Aldrich) was used as the supporting electrolyte while reagent grade $CaCl_2$ (99.9965 %, Fisher) was used as the source of calcium ions. Reagent grade toluene (Fisher) and in-house distilled absolute ethanol were used as the dilution and cleaning solvents, respectively. De-ionized water with a resistivity of 18.2MΩ cm, prepared with an Elix 5 followed by a Millipore-UV plus ultra water purification system (Millipore Inc.,

Canada), was used throughout all the experiments. All the experiments were conducted at the room temperature (22±0.1°C), unless otherwise specified.

4.2 Preparation of fines, froth, and process water from flotation system

To obtain fines, froth, and process water samples, bitumen flotation tests for a good processing ore and a poor processing ore were carried out in de-ionized water using a modified batch extraction procedure described in the literature (Kasongo et al., 2000). The flotation tests result in two products: a froth and a tailings sample. The mass ratio of bitumen to solids in the froth is about 42:1 and 0.3:1 for the good processing ore and the poor processing ore, respectively. The bitumen recovery is about 95% and 70% for the good processing ore and the poor processing ore, respectively. The obtained froth was directly emulsified to prepare suspensions for zeta potential distribution measurements. The obtained tailings sample was allowed to settle for 30 minutes to remove the coarse sand grains. The supernatant collected after 30 minutes of settling was transferred to a centrifuge tube and centrifuged at 15,000 g-force for 30 minutes. The sediments in the centrifuge tube, referred to as fines, were collected for further analysis, zeta potential distribution measurement and surface force measurement. To estimate the concentration of the fines in the sediment, to prepare the probe particle for surface force measurement, and to characterize the fines, part of the sediment was dried in a desiccator under vacuum. The upper clear water in the centrifuge tube, on the other hand, was further filtered. The filtrate, referred to as the process water, was kept for chemical analysis and was used as probing medium in zeta potential distribution and surface force measurements.

Table 4.2 Cation content (A.A. analysis) in the process water.

Process water from	Good processing ore	Poor processing ore
pH	7.65	7.89
Ca^{2+} (ppm)	0.16	8.8
Mg^{2+} (ppm)	0.51	4.8
Electrolyte* (mM)	3.72	4.33

* equivalent monovalent electrolyte

The pH of the process water obtained varied between 7.5 and 8. The calcium and magnesium concentration in the process water from the good processing ore was much lower than that from the poor processing ore, as shown in Table 4.2. The obtained suspension of fines from the good and poor processing ores has a brown and a dark appearance, respectively, as shown in Figure 4.1. X-ray microanalysis indicates that they were mainly aluminosilicate minerals. The particle size distributions of the fines from tailings were measured with a Mastersizer (Malvern Instruments Inc. USA). As shown in Figure 4.2, the fines from the good processing ore and the poor processing ore exhibited very similar bimodal particle size distribution characteristics.

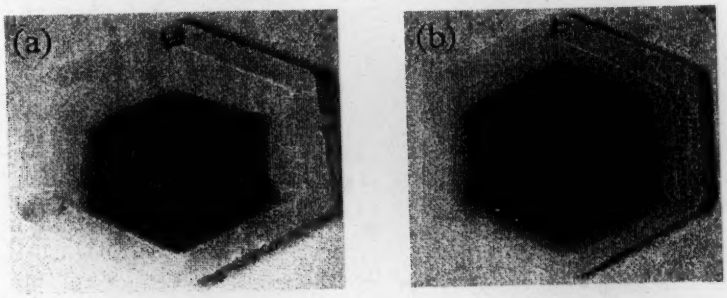

Figure 4.1 Visual appearances of fines suspension from (a) a good processing ore and (b) a poor processing ore.

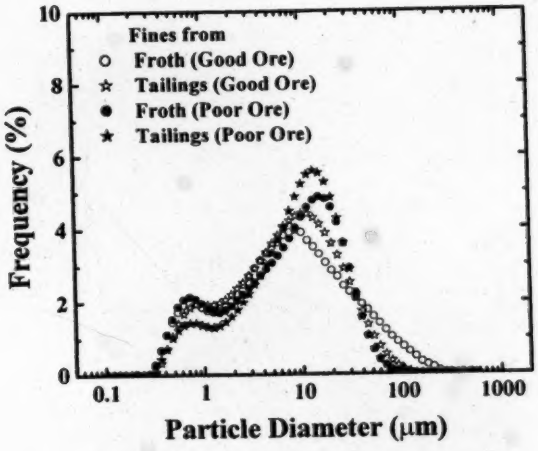

Figure 4.2 Particle size distributions of the fines extracted from tailings and froth for a good processing ore and a poor processing ore.

4.3 Zeta potential measurement

4.3.1 Emulsion or suspension preparation

The bitumen/water emulsion was prepared using an ultrasonic method. Approximately 1 g of bitumen was placed in 100 ml of 1mM KCl solution and emulsified using a 550 Sonic dismembrator (Fisher) for about 15 minutes. The emulsified suspension was allowed to cream for 30 minutes. Its particle size distribution was measured with a Master[illegible] (Malvern Instruments Inc., USA). The peak was centred at approximately 12 μm, as shown in Figure 4.3. It should be noted that the emulsion size distribution changed only marginally when creaming time was increased up to 6 hours, suggesting minimal effect of emulsion size variation with creaming time on the measured zeta potential. For zeta potential measurement, a sample of emu[illegible]sion was transferred to a testing solution of the same chemical composition. This dilution was necessary to obtain a suspension containing about 0.01~0.1 wt% of bitumen, suitable for zeta potential measurement with an electrophoresis technique. The bitumen flotation froth was emulsified for zeta potential measurement using a similar procedure.

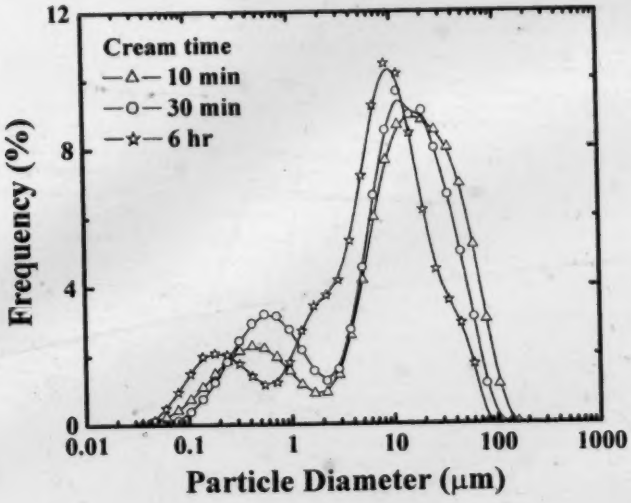

Figure 4.3 Particle size distribution of solvent extracted bitumen emulsion after various creaming time.

Clay or silica suspension was prepared in an ultrasonic bath. The sample was first manually ground in a mortar to about 2~5 μm. The suspension with a 0.01~0.1 wt% concentration was made in an ultrasonic bath by conditioning for about 10 minutes. After settling for about 0.5 hr, the upper portion of the suspension was taken as the clay or silica suspension for zeta potential measurement. Fines suspensions for zeta potential measurement was prepared by diluting the fines sediments obtained from flotation tests to a concentration of about 0.01~0.1 wt%.

4.3.2 Zeta potential measurement

Zeta potential was measured with a Zetaphoremeter III (SEPHY/CAD), as shown in Figure 4.4. This zeta-meter consists of a rectangular electrophoresis cell, a pair of hydrogenated Palladium electrodes, a laser-illuminator, an optical microscope and a digital video image capture (CCD camera)/viewing system. The computerized operating system allows for accurate positioning of the optical microscope view field at a stationary layer for accurate measurement of electrophoretic mobility. About 40 ml of the prepared particle suspension or oil/bitumen emulsion was used to fill the electrophoresis quartz cell. Great care was taken to avoid trapping air bubbles. Through the laser-illuminating and video-viewing system, the movement of the droplets or particles under the applied electric field in the stationary layer was traced, 5 times for each direction by alternating positive/negative electrode potentials. The captured images were then analyzed by the built-in image processing software. A unique feature of this instrument was that it can trace 50-100 particles simultaneously each time, and a distribution histogram of electrophoretic mobility or zeta potential for these particles was provided. The distribution histogram of electrophoretic mobility V_E and corresponding average value were converted to zeta potential value ζ using Henry's equation (4-1).

$$\zeta = \frac{3\eta}{2\varepsilon\varepsilon_0 f(\kappa a)} V_E \tag{4-1}$$

$$f(\kappa a) = \begin{cases} 1 \text{ for large spheres } (\kappa a \to \infty), \text{ Smoluchowski's equation} \\ 1.5 \text{ for small spheres } (\kappa a \to 0) \end{cases}$$

With this instrument, the conductivity and pH of the suspension were continuously monitored during the measurement. The environmental temperature was maintained at 22±0.1°C. Each test was repeated for 4 times and the average value was reported. The measurement error was generally less than 5 %, except at high electrolyte concentrations above 10^{-2} M, in which case the error could be as high as 10 %.

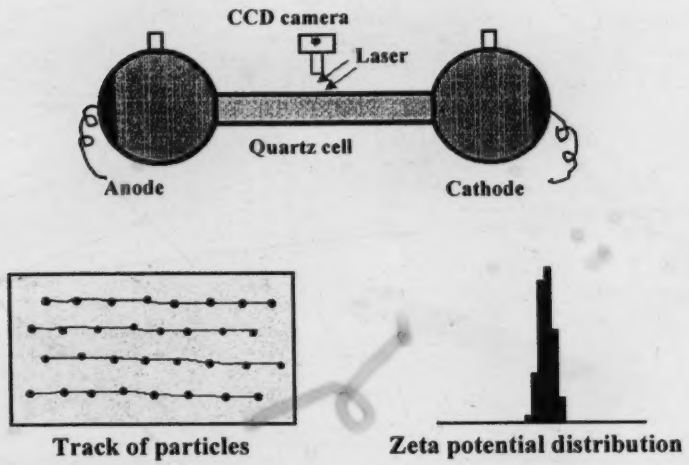

Figure 4.4 Schematics of zeta potential measurement.

4.4 Zeta potential distribution measurement

In conventional zeta potential measurements (as described above), only the average electrophoretic mobility or zeta potential value is reported. In the case of a binary mixture, the measured average zeta potentials of two components often over- or under-estimates the electrokinetic behavior of the system. This can give rise to misleading information for the interpretation of interactions between the two components.

In this thesis, zeta potential distribution measurement was developed into a technique to study the colloidal interactions between oil sand components and slime coating of the fines on the bitumen surface. It has been proven that the zeta potential distribution measurement is a simple, yet powerful tool to study hetero-coagulation for a complex colloidal system by a few case studies (Xu et al., 2003). Such a method is of great importance to the oil sands industry.

4.4.1 Principle of zeta potential distribution measurement

It is recognized that different particles should possess different surface properties. Therefore, tracing the change of surface properties could provide us with an important avenue to study hetero-coagulation. Zeta potential is one of the most important surface properties in a colloidal system. Based on this idea, it is possible to identify the deposition condition of one component on the other in a binary suspension. This surface properties-based technique does not suffer from the limitations of particle density and geometry. It should be noted that this technique is particularly useful for the systems where the atomic force microscope or surface force apparatus is not applicable due to the complex nature of the system. The concept for this application is described below.

When zeta potential distributions are measured separately using bitumen droplets and clays, for example, each has its unique zeta potential distribution centered at ζ_B and ζ_C, respectively. These two distributions are overlaid schematically in Figure 4.5a as a reference. When bitumen and clays are mixed together under the same physicochemical condition, the measured zeta potential distribution of the resultant suspension varies, depending on the characteristic of the interactions between the two components. If the bitumen and clay do not coagulate with each other, a bimodal zeta potential distribution with two peaks centered at ζ_B and ζ_C as shown in Figure 4.5b is anticipated. In this case, a slight shift of ζ_B and ζ_C towards each other may be observed, due to hydrodynamic interaction of moving particles at different electrophoretic mobility. This phenomenon is known as electrokinetic retardation (reduction of ζ_B for fast moving bitumen droplets) and enhancement (increase of ζ_C for slowly moving clay particles).

In the case that the bitumen strongly coagulates with the clay particles, the measured zeta potential distribution would show only one distribution peak, with the peak position depending on the bitumen to clay ratio. For illustration purpose, the clay coating on bitumen droplets is taken as an example for the analysis. At high clay to bitumen ratio, the strong coagulation would ensure a complete coverage of bitumen droplets by clay particles, as shown by the insert in Figure 4.5c. In this case, only one distribution peak centered at ζ_C would be observed. At lower clay to bitumen ratio, bitumen would be only partially covered by the clay even though all the clay particles are depleted from the

suspension due to strong attraction from bitumen droplets, a case shown by the insert of Figure 4.5d. As a result, both distribution peaks for the original bitumen droplets and clay particles disappear, accompanied by a new peak corresponding to partially clay-covered bitumen droplets as shown in Figure 4.5d. In this case, the position of the zeta potential distribution peak depends on the coverage of bitumen droplet surface by the clay particles.

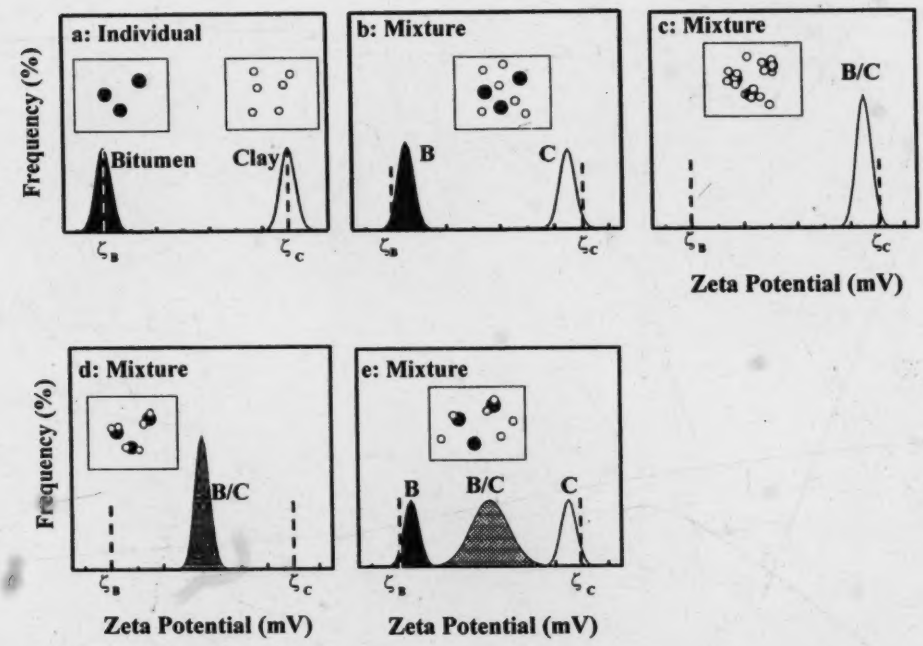

Figure 4.5 Schematic zeta potential distributions for a binary particulate component system that can be interpreted for particle interactions. In this Figure, the black and white circles represent bitumen droplets and clay particles, respectively. (a) Zeta potential distribution of the two components measured separately, but plotted together; (b) binary mixture without coagulation; (c) strong coagulation (bitumen droplets fully covered and excessive clay particles present); (d) strong coagulation (bitumen droplets partially covered with insufficient amount of clay particles); and (e) weak coagulation (some bitumen droplets partially covered with a substantial amount of individual clay particles and individual bitumen droplets). The state of particle aggregation for each case is given in the insert of corresponding cases.

For a system of weak coagulation between bitumen and clays, a zeta potential distribution featuring three peaks or a broad distribution is anticipated as shown in Figure 4.5e. In this case, a new distribution peak located between bitumen and clay peaks indicates that part of bitumen and part of clay particles are coagulated. Due to the nature of weak interactions, some of the bitumen droplets and clay particles would remain as individual particles, contributing to the presence of the remnant bitumen and clay distribution peaks in the measured overall zeta potential distribution. The state of particles in this case is illustrated in Figure 4.5e. The broadness and position of the new peak depend on both the strength of attraction between bitumen droplets and clay particles, and their ratio. At a given ratio of bitumen to clay, a stronger attraction would lead to a more significant reduction of bitumen peaks or greater shift in the peak position towards the distribution peak of clays, with a higher area ratio of the new peak to the remnant peak for clays. A similar shift is anticipated with increasing the clay to bitumen ratio. It should be noted that a similar analysis could be equally applied to the case of bitumen coating on clay surfaces.

4.4.2 Technique of zeta potential distribution measurement

Based on the above-mentioned principle, the coagulative nature for a binary colloidal system can be interpreted from the measured zeta potential distributions. In the experiment, individual component suspensions or emulsions were first used to measure the zeta potential distributions, separately. The obtained distributions were plotted together and used as a reference. The two species at a given mass ratio were then mixed and conditioned under identical conditions in an ultrasonic bath (Fisher) for about 5~15 minutes. This mixing procedure ensures particle collision with each other and provides sufficient kinetic energy to overcome the repulsive barrier between two components. The mixed suspension was used to measure the zeta potential distribution. The obtained zeta potential distribution peaks for the mixture were compared with the reference to identify the coagulative nature of the two species. To this end, it is important to note that changing the concentration of the background supporting electrolyte will compress the electrical double layer and hence cause a change in the measured zeta potential, which in turn changes their interaction force profiles and hence coagulation behaviors. The beauty of this technique is that all this can be studied collectively. The zeta potential distribution

measurement of a single component system would provide an indication of the role of the electrolyte, whether the electrical double layer compression or specific adsorption or both are involved, while the measurement with the mixture would demonstrate the degree of coagulation.

4.5 Surface force measurement (AFM technique)

A Nanoscope AFM (Digital Instrument, Santa Barbra, CA, USA) was used to measure the forces between bitumen and probe particles. The working principle and imaging techniques of AFM were described in Appendices A and B.

4.5.1 Bitumen surface preparation (spin coating technique)

Bitumen surface was prepared with a P6700 spincoater (Specialty Coating Systems Inc.). A silicon wafer was first oxidized in a well-ventilated furnace at 1100°C for 12 hours to generate a deep blue color. The oxidized wafer, referred to as silica wafer, was cut into 15x15mm square pieces. The wafer was washed with chloroform to remove adsorbed organic contaminants, rinsed with de-ionized water followed by ethanol, and finally blow-dried with ultra-pure grade nitrogen. At this stage, the contact angle of an air bubble on the wafer in deionized water was less than 10^0. Bitumen was dissolved in toluene to a concentration of 2.5 mg bitumen per ml toluene. The resultant bitumen solution was centrifuged at 15,000 g-force for 30 minutes to remove all remaining contained fine solids. About 0.1 ml of the prepared bitumen/toluene solution was dropped slowly onto the silica wafer spinning on the spincoater at 2000 rpm for 20 seconds and 5000 rpm for 1 minute. The bitumen was placed on the substrate in such a manner that the bitumen loss during the coating was minimized. The spin-coated bitumen surface was dried for about one hour in a particle-free horizontal laminar hood under ambient condition. From the volume of the bitumen used in spin coating and the werea of the wafer coated, the thickness of the bitumen layer was estimated to be ca. 100 nm. After immersing the prepared bitumen in deionized water for more than 30 minutes, an air bubble was made to contact the bitumen. After 5-minutes of contact of the air bubble with the bitumen, the static contact angle was measured using the captive bubble method. In this procedure, the measured contact angle of 70~75° can be obtained. This value was within the range of the reported contact angle values for bulk bitumen (Kasongo et al., 2000), confirming a full

coverage of the silica wafer by a bitumen film. Under optimal spin coating conditions, the bitumen-coated wafer has a black, mirror-like appearance. A typical image of spin-coated bitumen on a silica wafer was shown in Figure 4.6. On average, the roughness of the bitumen surface over a 10x10 μm werea was found to be less than 2 nm. A few protrusions up to 20 nm high were observed over the scanned werea. A similar observation was reported by Wu et al. (Wu et al., 1999a, b and 2000). It was important to note that the sparse protrusions at this scale would not affect the results of our AFM force measurement, as the contact werea of the two surfaces in our measurement was sufficiently small to minimize interference by these sparsely occuring protrusions.

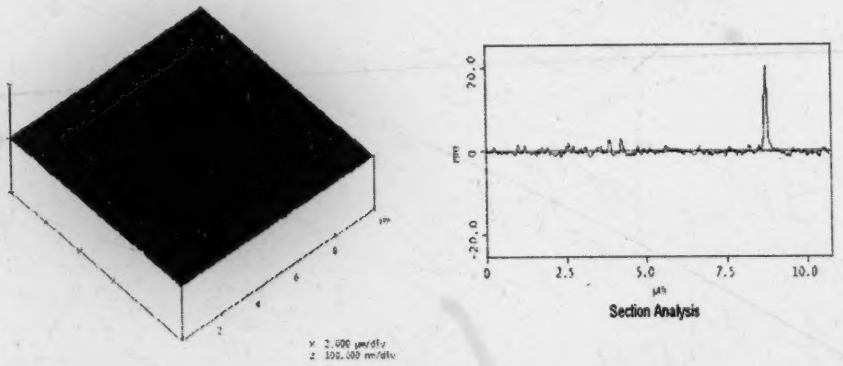

Figure 4.6 A typical AFM image of a bitumen substrate obtained with Tapping mode: three-dimensional and section analysis.

4.5.2 Probe particle preparation

The probe particles tested include single mineral particles of silica and clay, and the fines and bitumen from oil sand ores. The particles of silica, clay and fines were glued with a two-component epoxy (EP2LV, Master Bound, Hackensack, NJ, USA) onto a tip of short, wide beam AFM cantilevers. Spherical silica particles and pseudo-spherical clay particles or fines (agglomerates) of 5~10 μm size were selected under an optical microscope. The glued probe particles were allowed to dry in a vacuum desiccator for more than 24 hours. Prior to each set of experiments, the single mineral probe particles (silica and clays) were thoroughly rinsed with de-ionized water and ethanol, followed by blow-drying with ultra-pure grade nitrogen. The particles were then exposed to an ultraviolet light for more than 5 hours to remove any possible organic contaminants. The

glued fines were used directly for force measurement without further treatment. Bitumen probe surfaces were prepared by coating bitumen on a probe silica sphere using a dip-coating technique. In this case, the prepared probe silica particle was dipped into a bitumen-in-toluene solution, which was prepared in the same way as described earlier, for about 1 minute. The particle was then taken out of the solution and allowed to dry for about one hour in a particle-free horizontal laminar hood with the sphere facing up. For confirmation, the force profiles measured between dip-coated bitumen probes and silica substrates were compared with those measured between spin-coated bitumen and probe silica particles. Similar interaction force profiles obtained for the two systems can confirm successful dip-coating of bitumen on probe silica particles. Typical SEM micrographs of probe silica, bitumen-coated silica, clays and fines after the force measurement were shown in Figure 4.7.

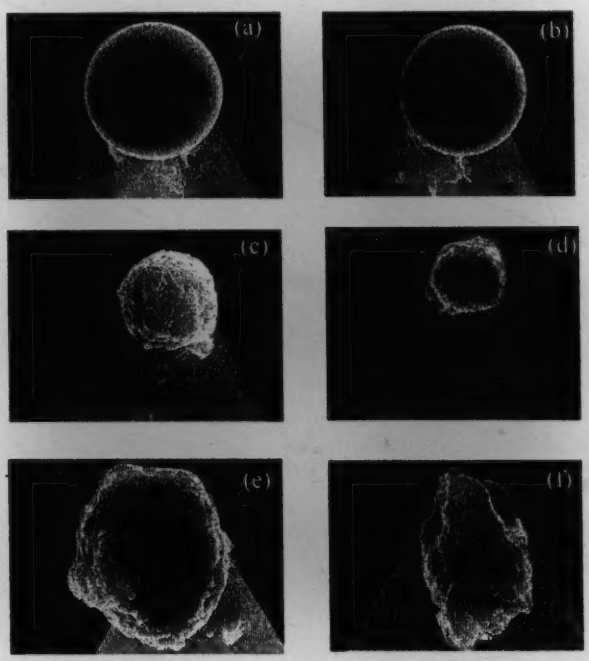

Figure 4.7 Typical SEM micrographs of probe particles on tips of AFM cantilevers. (a) Silica sphere; (b) bitumen coated silica sphere; (c) montmorillonite; (d) kaolinite; (e) fines from a poor processing ore; and (f) fines from a poor processing ore. The micrographs were obtained after the force measurements.

The exact size of the probe particles used in each set of experiments was determined from the micrographs obtained. The individual particles were characterized by x-ray microanalysis with an energy dispersive x-ray analyzer (EDX) installed on the SEM. Typical results were summarized in Table 4.3.

Table 4.3 Element wt% for probe particles with an energy dispersive x-ray analyzer (EDX) in a scanning electron microscope (SEM, K line).

Samples	O	Al	Si	K	Na	Ca	Mg	Fe	Ti
Silica	33.8	8.0	30.1	0.4	0.7	25.4	0.6	0.5	0.6
Kaolinite	51.2	18.8	28.2	-	-	0.1	0.2	0.7	0.6
Montmorillonite	46.2	11.2	23.2	0.7	1.8	4.9	6.3	4.3	0.7
Fines (good ore)	28.3	15.2	49.0	2.1	0.3	0.3	0.2	2.9	-
Fines (poor ore)	29.0	14.9	42.8	2.1	0.1	1.1	0.6	2.9	-

4.5.3 Colloidal force measurement in a fluid

Surface force measurement was conducted using a Nanoscope E AFM with a vendor-supplied fluid cell. The AFM consists of a piezoelectric translate stage, a cantilever tip, a laser beam system, a split photodiode and a fluid cell. The working principle of AFM for colloidal force measurement is illustrated in Figure 4.8. As shown in Figure 4.8A, a probe particle is glued on the AFM cantilever tip and the sample is mounted on the AFM translation stage. The particle and substrate are immersed in an aqueous solution of desired chemistry. A laser beam is focused onto the other side of the cantilever, which is coated with a thin layer of gold to increase the reflectivity of the laser light. The reflected beam is directed by a mirror to a split photodiode, which detects the deflection of the cantilever to a fraction of a nanometer resolution. When the sample on the translation stage moves towards the upper particle under the cantilever, a constant output signal is obtained initially (Figure 4.8B: a-b), indicating a zero deflection of the cantilever, i.e., zero force between the two surfaces at large separations. As the lower surface moves further towards the upper particle, either an increase or a decrease in the output signal is often seen (Figure 4.8B: b-c). An increase in the output signal indicates the cantilever being pushed away while a decrease in the output signal indicates the cantilever being

pulled towards the moving surface. The former corresponds to a repulsive force while the latter, an attractive force between the two surfaces in the liquid. Eventually, the lower surface will be brought by the translation stage into the "contact" with the upper particle. A constant compliance is then observed (Figure 4.8B: c-d), indicating that the lower solid surface is pushing the upper particle along with the cantilever upwards. From the known displacement of the piezo translation stage to which the lower surface is attached, the constant compliance allows cantilever displacement (deflection) to be calibrated in terms of output signals. The cantilever deflection can then be calculated as a function of the separation distance between the two interacting surfaces and the force calculated from the known cantilever spring constant.

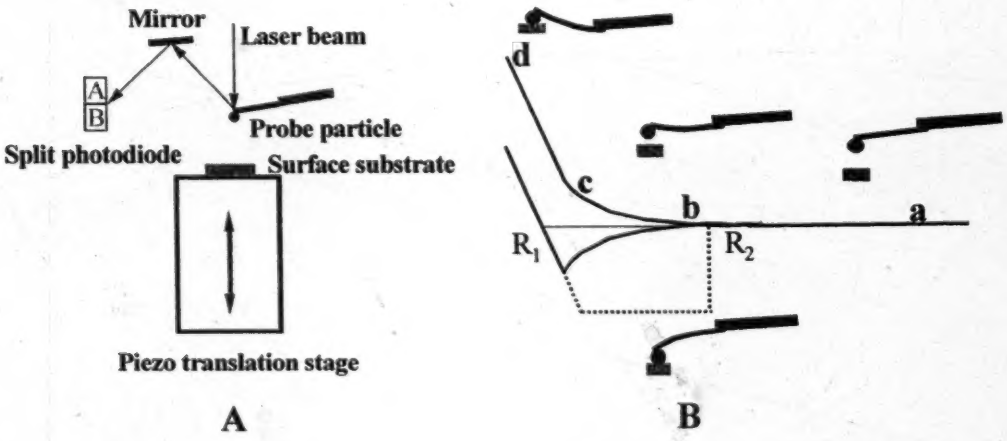

Figure 4.8 Schematics illustrating the principle of the atomic force microscope.

At the end of the extension of the piezo translation stage, the piezo starts to retract. If the colloidal force between the two surfaces is purely repulsive, an identical trace of the signal to the approaching branch is likely to be obtained. When there is an adhesion between the two surfaces, the retracting trace follows the dotted line in Figure 4.8B. In this case, the cantilever continues to follow the displacement of the piezo translation stage due to the adhesive force holding the particle on the cantilever to the surface on the translation stage. At the point where the restoring force of the cantilever exceeds the adhesive force, a sudden detachment of the particle from the substrate surface occurs, as

indicated by the signal returning to zero value. The adhesive force (pull-off force) is calculated from the displacement of the piezo between points R_1 and R_2 on retracting branch multiplied by the spring constant of the cantilever. More detailed description on the principles of the colloidal force measurement using AFM can be found in open literature (Ducker et al., 1991, 1992; Rabinovich et al., 1994; Veeramasuneni et al., 1996; Kappl and Butt, 2002).

In our experiment, the solution is injected into the fluid cell slowly with great care to avoid trapping air bubbles. Both surfaces immersed in the solution are allowed to equilibrate for 1 hour. To calculate the forces from the measured cantilever deflection, the spring constant of the AFM cantilever is determined from the measured geometry of the cantilever obtained from its scanning electron micrograph and the Young's modulus value of 1.5×10^{11} N/m^2 given in literature for the cantilever material (Sader et al., 1995; Veeramasuneni et al., 1996). The details on AFM data analysis of long-range forces are described in Appendix C. Adhesive force data are collected under loading forces of 8-10 mN/m (the loading force is defined as the maximum force in the "constant compliance region" as indicated by Figure 4.8B (d)). It is found that the adhesive force is independent of the loading force in the range examined. For quantitative comparison and theoretical analysis, both the measured interaction force and adhesive force are normalized with the mean radius R of the probe particle.

4.5.4 Reproducibility and measurement error

Our first concerns were whether the bitumen film remained stable after its contact with aqueous solution and whether the probe particles were contaminated by contacting such a sticky material as bitumen. To verify that the bitumen layer remained on the substrate during force measurements, the contact angle was measured for the same bitumen substrate after AFM force measurements. The similar contact angle values obtained before and after the AFM force measurements confirmed that the bitumen film on silica wafer remained on the substrate during force measurement. The contamination of probe particles by bitumen during repetitive contact with the bitumen was found to be negligible. This was confirmed by the reproducibility of our results obtained after solution conditions were brought back to the original after a series of measurements and

using different spheres in different sets of measurements. The reason for the minimal contamination may be attributed to the use of an ultra-thin layer of bitumen on the substrate and a short contact time (80 to 100 ms) during the AFM force measurement, although it was repetitive.

To test the reproducibility, colloidal forces were measured at different spots on the bitumen substrate for a given probe-substrate pair and measured for different probe-substrate pairs. The normalized force profiles were found to be fairly reproducible. A typical variation in magnitude of the force profiles ranges within 10~20 % for the interaction forces. For clear illustration, only a typical (most repeated) force profile was reported under a given condition for the well-defined system. For less well-defined clays and fines particles, the force measurements were repeated with at least eight bitumen-probe (clays or fines) pairs and the measured force profiles were plotted together to show a general trend. In contrast, the adhesive forces were observed to vary in a range of 20~80 %. In this case, all statistical data or an average value was reported.

4.5.5 Data fitting and nature of long-range colloidal force

To further understand the origin of the measured forces, data fitting with corresponding theories would be a good approach. The classical DLVO theory was used to describe the experimental data. From the reported Hamaker constant value of mica (10×10^{-20} J) for montmorillonite and kaolinite, 6.5×10^{-20} J for silica (Israelachvili, 1991) and 6×10^{-20} J for bitumen (Vincent, 1973), the combined Hamaker constants for bitumen/water/silica (A_{BWS}), bitumen/water/bitumen (A_{BWB}) and bitumen/water/montmorillonite or kaolinite clay (A_{BWC}) system were calculated to be 3.3×10^{-21} J, 2.8×10^{-21} J and 6.5×10^{-21} J, respectively. The values were summarized in Table 4.4. Considering the fines in oil sand ores were mainly the clays, the Hamaker constant for clays was used for the fines. The electrostatic double layer forces between two surfaces were calculated numerically by solving the non-linear Poisson-Boltzmann equation and force balance equation. A Visual basic program running on EXCEL spreadsheet was developed for a general DLVO theory of symmetrical/asymmetrical surfaces in symmetrical/asymmetrical electrolyte solutions, as shown in Appendice D and E. The program was checked with well-known systems. During the fitting exercise, Stern potentials for both surfaces as well as the decay length

(κ^{-1}) were set as adjustable parameters. The measured zeta potential values and calculated decay length were used as guides to set the initial values for Stern potentials and the decay length (κ^{-1}), respectively. It was reasonable to assume that the bitumen surface is of constant surface charge density as its surface charge mainly arises from irreversible adsorption of surfactants. Mineral (silica, clays and fines) surfaces are of constant surface potentials since its surface charge mainly arises from adsorbing ions from solution. However, the different boundary conditionds were tested for all the surfaces. A minimal discrepancy between the fitted Stern potentials and the measured zeta potentials was used to confirm the assumption of boundary conditions for the surfaces. It should be noted that the sensitivity study with the current system shows that the fitted surface potentials and decay length were not a strong function of Hamaker constant used in the calculations.

Table 4.4 Hamaker constants A (B for bitumen, C for clay, S for silica and W for water).

Material	Bitumen	Silica	Clay	Water	B-W-B	B-W-S	B-W-C
A (10^{-20} J)	6	6.5	10	3.7	2.8	3.3	6.5

When the fitting of experimental data with the classical DLVO theory was poor, the extended DLVO theory was considered by including hydrophobic force and/or steric force. Including a hydrophobic force was necessary for bitumen-bitumen systems. The hydrophobic force was calculated using equation (3-13) (Rabinovich and Yoon, 1994) by setting K as an adjustable parameter. The steric force was considered for systems involving bitumen surfaces, and evaluated using the Pincus scaling theory (equation 3-15). Since the detailed structure of macromolecules on the bitumen surface cannot be easily identified, equation (3-15) was simplified to equation (4-2) with factor f representing the characteristic of macromolecules on the bitumen surface.

$$\frac{F_s}{R} = \frac{4\pi kTN_B^2}{Cs^4}\left[\frac{1}{D} - \frac{1}{2L}\right] = f\frac{T}{C}\left[\frac{1}{D} - \frac{1}{2L}\right],\ mN \cdot m^{-1} \qquad (4\text{-}2)$$

where $f = \frac{4\pi k N_B^2}{s^4}$, $N \cdot nm \cdot K^{-1} \cdot m^{-4}$; C is molar concentration of electrolyte, $mol \cdot L^{-1}$; D is separation distance between two surfaces, nm; L is length of macromolecule tail, nm.

For a given system, the number of monomer units per chain (N_B) can be reasonably assumed to be constant. Therefore, the value of parameter f represents the density (or the average spacing s between two grafted points) of macromolecules of the asphaltene type on the bitumen surface. The bigger the f value was, the denser the macromolecule (or the smaller the s value). During the fitting exercise for the steric force at a very short range, the van der Waals forces were not considered as practiced in literature, and the density factor f and macromolecule tail length L were set as adjustable parameters.

A detailed description of data fitting procedure is given in Appendices D and E. The data fitting allows us to obtain the information on the origin of the measured forces. This helps us identify the controllable dominant colloidal forces that are adjustable by changing processing environment conditions. Normally, the controllable dominant forces are the forces other than van der Waals forces, such as the electrostatic double layer force and the hydrophobic force. The van der Waals forces are not considered as a controllable dominant force, as they vary less with changing solution conditions and relatively weaker than other forces. In our systems, the steric force is also not considered as a dominant force component since it is valid only at very short range. Through monitoring the dominant forces by adjusting the solution conditions, we can control the particle coagulation behavior. For instance, if the dominant force between bitumen and silica is the electrostatic double layer force which is related to solution pH, their coagulation behavior can be controlled by adjusting solution pH.

4.5.6 Interpretation of interaction force profiles

It is well known that the adhesive forces correspond to how strongly the two surfaces are attached, while long-range colloidal forces indicate how difficulty it is for two surfaces can approach each other.

Non-sheared colloidal system For a non-sheared colloidal system, the adhesive forces between particles are not important since the shearing force to separate particles is negligible. In this case, the classical DLVO theory is often used to predict colloidal particle interactions. It considers the van der Waals forces and electrostatic double layer force. Evaluation of the electrostatic double layer force and the van der Waals forces for various geometric configurations is well established (Israelachvili, 1991; Masliyah, 1994). To use these established theories, one would normally need to know the system parameters such as surface potentials, size and Hamaker constants of interacting colloidal particles, as well as electrolyte composition and concentration in the medium. As shown in Figure 4.9, the curve of the interaction force as a function of separation distance could be repulsive at large separation and attractive at short separation with a repulsive force barrier observed.

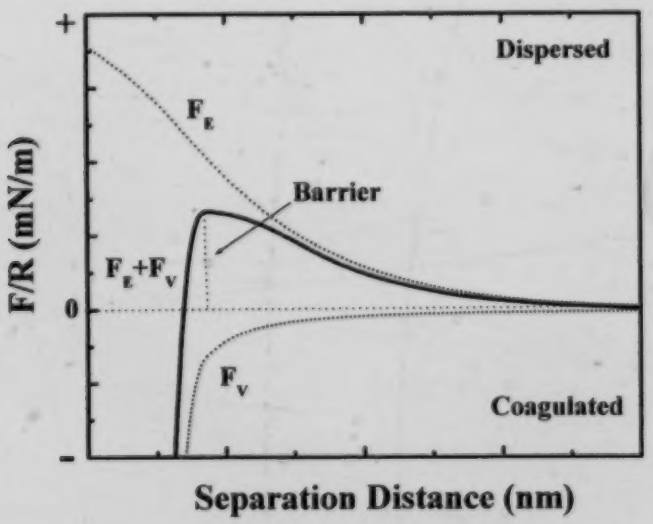

Figure 4.9 Schematics of the normalized colloidal force profile for a system with DLVO forces. F_E is the electrostatic double layer force; F_V is the van der Waals forces.

The magnitude of the repulsive barrier mainly depends on the electrostatic double layer force since the van der Waals forces are normally attractive. The coagulative nature of a colloidal system in this case is largely determined by the magnitude of the repulsive force

barrier. For instance, a colloidal system would be stable if the absolute values of the zeta potentials for colloids exceed 25 mV. At this condition, the resultant repulsive energy barrier would be greater than the kinetic energy from Brownian (thermal) motion. If the zeta potentials are less than 25 mV or two particles carry opposite charges, the system would be unstable since the repulsive barrier in this case is small or absent.

In some cases, the classical DLVO could over- or under-estimate the colloidal forces due to the existence of other forces, which are not considered in the classical DLVO theory. Under these conditions, the extended DLVO theory by including non-DLVO forces has to be used. The non-DLVO forces include repulsive hydration force for hydrophilic surfaces, attractive hydrophobic force for hydrophobic surfaces, repulsive steric force and attractive bridge force for polymer-bearing surfaces, as described in Chapter 3. In these cases, the force profiles could be more complex and diverse. As shown in Figure 4.10, the interaction force profiles may be (a) monotonically repulsive: the particles are dispersive; (b) attractive: the particles are coagulative; or (c) repulsive at larger separation and attractive at short range: the particles may be dispersive or coagulative, depending on the magnitude of the repulsive force barrier.

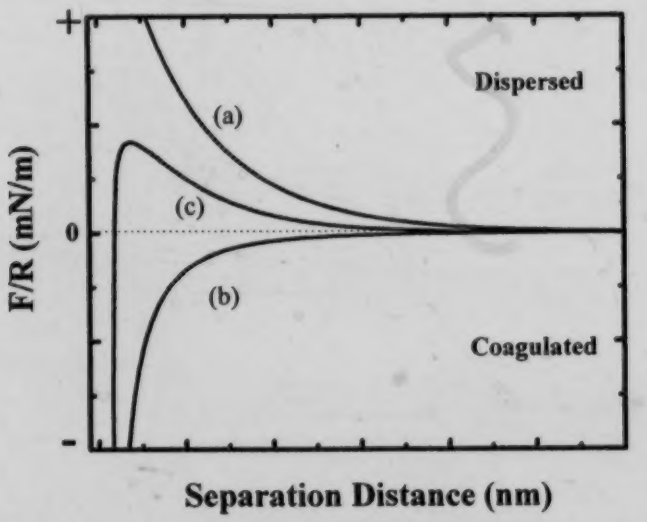

Figure 4.10 Schematics of the normalized colloidal force profile type for a system with non-DLVO forces.

Sheared colloidal system For a sheared colloidal system such as a bitumen extraction process, the DLVO or extended DLVO theory could still under- or over-estimate the coagulation behavior. In this case, both the long-range force and adhesive force have to be considered since the particles possess hydrodynamic (kinetic) energy from mechanical agitation. Comparison of long-range force barrier with adhesive forces can provide a better prediction of coagulation behavior for a dynamic colloidal system. As an example, shown in Figure 4.11 are the normalized repulsive force barrier and the contact adhesive force as a function of solution pH. This comparison provides a theoretical region or boundary between coagulation and dispersion for a given system. In general, the particles can easily coagulate in the case that the forces applied on the particles are greater than the repulsive force barriers but less than the adhesive forces (at pH<8). On the other hand, the particles would remain dispersed, should the forces applied are less than the repulsive force barriers but greater than the adhesive forces (at pH>8).

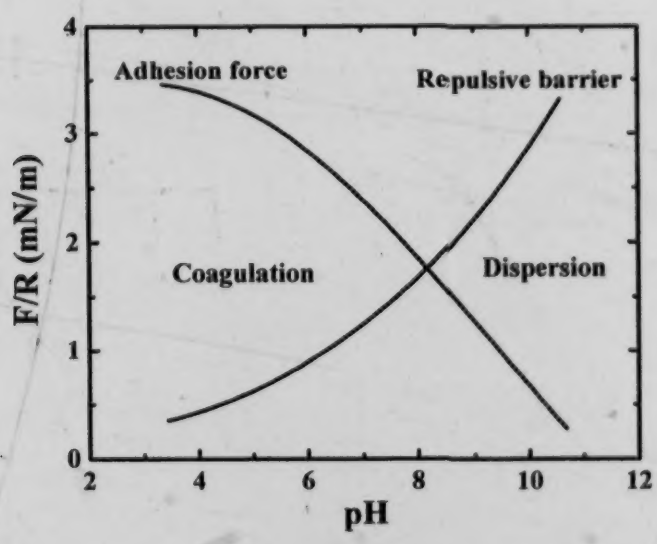

Figure 4.11 Schematics for interpreting particle coagulation behavior from the normalized repulsive force barrier and adhesive force measured with AFM.

It is conceivable that a greater difference between the repulsive barriers and adhesive forces would result in a stronger coagulation or dispersion. This provides us a clear image of the relationship between the hydrodynamic force (mechanical energy) and colloidal

force profiles. For a complex colloidal system such as an oil sands extraction system, the additional non-DLVO colloidal forces and the adhesive force cannot be simply ignored. Unfortunately, the corresponding theories describing these forces have not been well established. For this reason, one should not simply use the classical or extended DLVO theory to evaluate the coagulative state of a complex system such as bitumen extraction. Detecting these forces and predicting the coagulation behavior for the oil sands extraction system depend, to a large extent, on the experimental techniques. In this regard, the colloidal force measurement is the most direct method.

4.7 Other techniques

4.7.1 Film flotation

The surface wettability of fines was characterized using the film flotation technique, which was first adopted by Williams and Fuerstenau (1987). Methanol in water solutions of various concentrations was used as the probing solutions of various surface tensions. In each experiment, 100 ml methanol solution was placed in a plastic dish of 50 mm diameter. Precisely weighed dry fines (0.2 g) was gently sprinkled on the liquid-air interface and left for 5 minutes. Particles then sunk or remained at the interface, depending on the surface wettability of the fines. The solids sinking into solution and those remaining at the surface were collected, dried and weighed, separately. The percentage of the particles remaining at the interface was plotted as a function of the surface tension of the probe liquid. From this curve, the inflection-point was extrapolated to zero and 100 %. The corresponding surface tension values were called the "critical surface tension" of the complete wetting and non-wetting. The critical surface tension values obtained were a measure of surface hydrophobicity of particles.

4.7.2 Contact angle measurement

To evaluate the hydrophobicity of a bitumen surface, the static contact angles were measured using a captive bubble method. For the contact angle measurement of bitumen surfaces, the diluted bitumen with toluene was spin-coated on the silica wafer to represent a bitumen surface. As shown in Figure 4.12, a substrate (bitumen-coated silica wafer) was placed in an aqueous solution contained in a square glass vessel (3x3cm) with a water jacket to control temperature. A micro-syringe above the substrate was used to

generate an air bubble, which was pushed against the bitumen surface below to make contact (Figure 4.12a). The micro-syringe was then moved away from the air bubble, leaving the bubble on the bitumen surface (Figure 4.12b). The static contact angle at the three-phase contact line was allowed to equilibrate for 5min, and was measured with an optical microscope from both sides of the bubble.

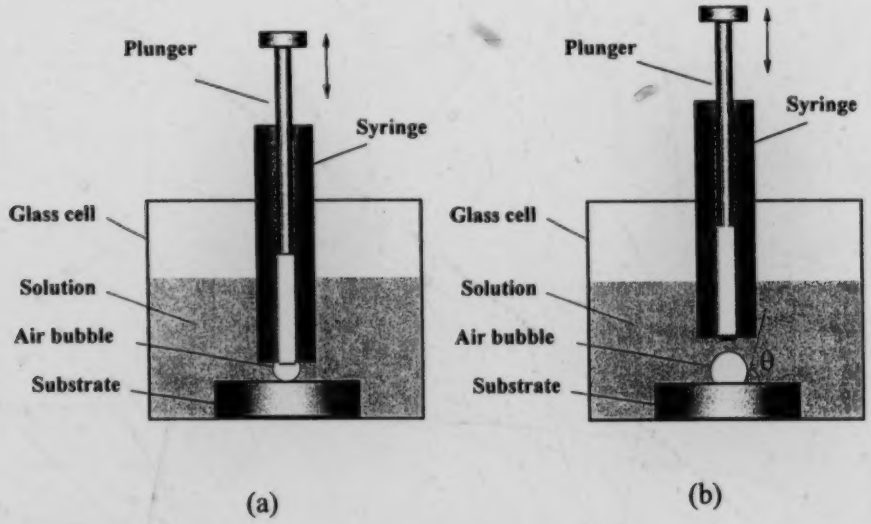

Figure 4.12 Schematics of contact angle measurement.

In the case that the contact angle is too small to make the bubble adhere to the surface, the sessile drop method is used with a Drop Shape Analysis System (DSA10, HRUSS, USA). In this case, a drop of water is placed on the bitumen surface to form a sessile drop. The drop shape is analyzed to obtain the contact angle using the built-in software. The average value of four independent measurements for both captive bubble and sessile drop methods is reported. The experimental variation is ± 5°.

4.7.3 Size distribution measurement

The size distribution of a suspension is measured with a Zetasizer (Malvern Instruments, Massachusetts, USA), In the Zetasizer, photon correlation spectroscopy measures the speed of Brownian motion of the particles in a suspension, calculates the diffusion speed

and coefficient of the particles, and then obtains the particle size through the Stokes-Einstein equation.

Chapter 5 ELECTROKINETICS OF OIL SAND COMPONENTS

The surface electric properties of oil sand components including bitumen, silica, clays and fines from real oil sand ore were presented in this chapter. The results show that solution pH, electrolyte concentration and calcium addition have a significant impact on the values of zeta potentials. The finding provides basic data for calculating electrostatic double layer forces and interpreting qualitatively colloidal interactions.

5.1 Introduction

In colloid science, many phenomena such as particle coagulation and adsorption of ionic species from solution are dependent, to a large extent, on the electrokinetics of colloids. In bitumen extraction, the coagulation behavior between oil sand components is our concern. Therefore, studying electrokinetics of oil sand components would provide an in-depth understanding of the colloidal interactions between bitumen-bitumen, bitumen-silica, bitumen-clay, and bitumen-fines.

Although there are a lot of reports regarding the zeta potentials of bitumen, zeta potentials of oil sand components including bitumen, silica, clay and fines are measured under different solution chemistry conditions to meet our special needs in this thesis. Zeta potential measurements were carried out using the procedures described in Chapter 4.

5.2 Bitumen

For a bitumen-water system, it is generally assumed that the surfactants present at the bitumen surface are responsible for the origin of surface charge. By assuming that the charge at the bitumen/water interface was derived from the ionization of carboxyl groups, Takamura and Chow (1985, 1988) applied the surface ionization model to describe the electrokinetic properties of bitumen/water interfaces. However, a discrepancy between the zeta potential values measured and derived from the model was often observed. One possible explaination is that not only carboxylate groups but also amine and sulfate groups are present at the bitumen-water interface (Liu et al., 2002).

The zeta potentials of various bitumen emulsions as a function of solution pH are shown in Figure 5.1. It is interesting to note that the coker feed bitumen, oxidized bitumen and

solvent-extracted bitumen all exhibit a similar electrokinetic response to solution pH in 1 mM potassium chloride (KCl) solutions. An iso-electric point (iep) at pH 3 is observed. Above the iep, the zeta potential becomes progressively more negative with increasing pH untill around pH7. Similar results were reported for an oil/water system in literature (Wen and Sun, 1981; Wiacek and Chibowski, 1999).

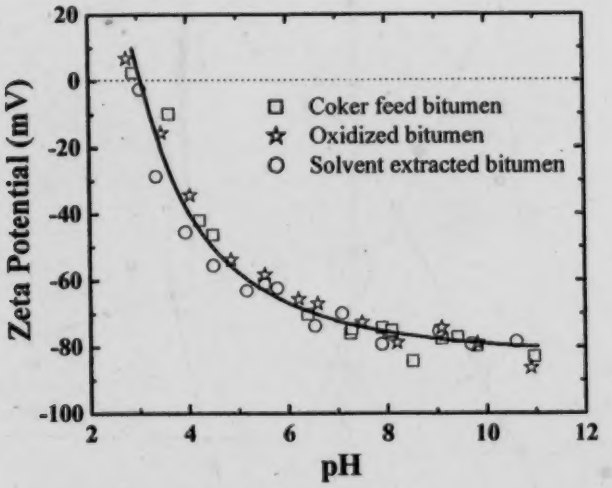

Figure 5.1 Average zeta potential of bitumen emulsion as a function of solution pH in 1 mM KCl solutions.

The effect of the supporting electrolyte (KCl) concentration on zeta potentials of bitumen emulsion is shown in Figure 5.2a. The increase of potassium chloride concentration does not alter the iep but depresses significantly the zeta potential values, indicating that potassium chloride compresses the electric double layer, as anticipated.

With the addition of calcium ions, the zeta potentials of the bitumen droplets become much less negative, as shown in Figure 5.2b. Comparision of Figure 5.2b with Figure 5.2a indicates that calcium ions even can diminish the zeta potentials more aggressively than the supporting electrolyte (KCl). Furthermore, the addition of calcium ions causes a noticeable shift in iep from pH 3.0 to pH 3.6. It is also interesting to note that the zeta potential values of bitumen emulsions with the addition of 0.1 mM calcium are only slightly different to those observed with the addition of 1 mM calcium ions. This less

sensitive response of zeta potentials to calcium concentration above 0.1 mM in bulk solution indicates that the specific adsorption of calcium ions on bitumen surface can be saturated. The observations confirm that calcium ions not only compress the electric double layer but also specifically adsorb on the bitumen surface, mainly through binding with carboxylic groups of natural surfactants contained in bitumen.

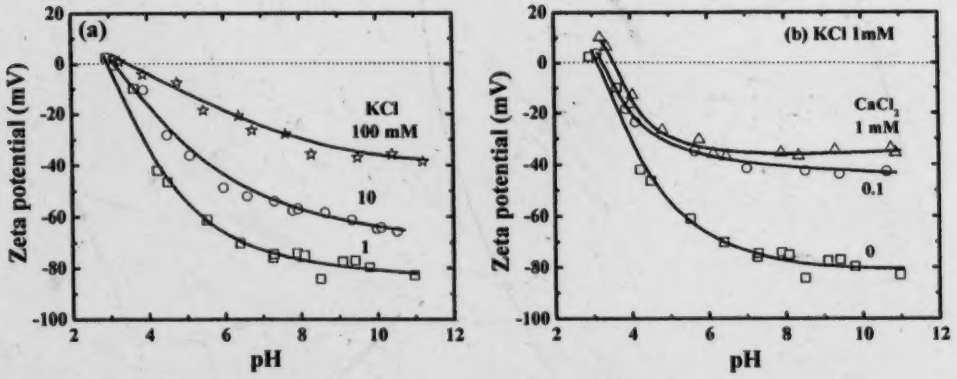

Figure 5.2 Average zeta potentials of bitumen emulsion as a function of solution pH in (a) KCl solutions; and (b) 1 mM KCl solutions containing $CaCl_2$.

5.3 Silica

The surface charge of silica originates from ionization of surface silanol groups. As a result, H^- and OH^- are the potential-determining ions. The zeta potentials of silica suspension as a function of solution pH are shown in Figure 5.3. In KCl solutions, silica particles exhibit an increasingly negative zeta potential with increasing suspension pH. The higher concentration of potassium chloride suppresses the zeta potentials substantially, as anticipated. No iep is observed over the pH range studied.

The addition of calcium ions significantly suppresses the zeta potentials of silica particles, as shown in Figure 5.3b. It is interesting to note that at a given calcium level, the zeta potentials become less negative with increasing pH greater than 7. This trend is more obvious for a higher concentration of calcium ions. For instance, the zeta potential becomes positive at pH 10.5 with the addition of 10 mM calcium ions. These results indicate a strong adsorption of calcium on the silica surface at these pH values, possibly in the form of $CaOH^+$ (King, 1982; Somasundaran and Luo, 1999).

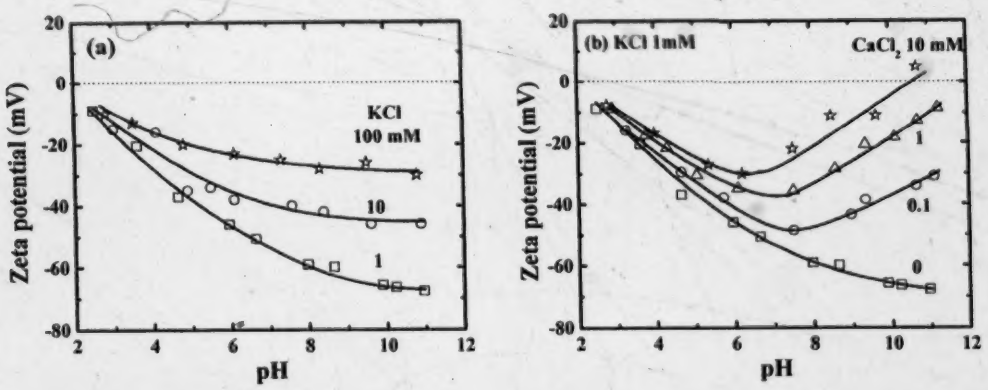

Figure 5.3 Average zeta potentials of silica suspensions as a function of solution pH in (a) KCl solutions; and (b) 1 mM KCl solutions containing $CaCl_2$.

5.4 Clays

Clay minerals are of a layer structure (Olphen, 1976). The basic building elements are two-dimensional arrays (basal planes) of silicon-oxygen tetrahedra (T) and two-dimensional arrays of aluminum- or magnesium-oxygen-hydroxyl octahedra (O). Isomorphous substitutions of Al^{3+} for Si^{4+} in the tetrahedral layer and divalent or monovalent metal ions such as Mg^{2+}, Fe^{2+}, Zn^{2+} or Li^{+} for Al^{3+} in the octahedral sheet result in an excess of negative charge on basal planes. It is evident that the surface charge of basal planes depends on the degree of isomorphous substitutions. In a real clay suspension, the plates are broken and some edges are exposed, as shown in Figure 5.4. The surface charge for the exposed edge is largely determined by solution pH with H^{+} and OH^{-} as potential-determining ions. As a result, the total surface charge for a particle is a combination of charges from both basal plane and edge. The magnitude of the net surface charge depends on the area ratio of basal plane to edge, though each may have their unique values.

Montmorillonite Montmorillonite clay is an expanding 2:1 (TOT) layer structured clay mineral (Olphen, 1976). Isomorphous substitution in the basal planes of tetrahedra and octahedra is so strong that the basal plane is considered to be of constant surface charge. This resultant excess of negative surface charge is compensated by the adsorption on the layer of cations that are too large to be accommodated in the interior of the crystal.

Therefore, the compensating cations on each side of each layer can be easily exchanged with other cations when available in solution. This unique structure results in some peculiar behaviors such as large specific surface area, great interlayer swelling and high ion exchange capacity. Since the basal plane is considered to be of constant surface charge, the surface charge for the basal plane is not sensitive to H^+ or OH^- concentration in solution. Considering that only about 1 % of the total surface area is contributed from the amphoteric edges, the pH-independent zeta potential behavior of montmorillonite clays is not unexpected (Sondi et al., 1996, 1997)

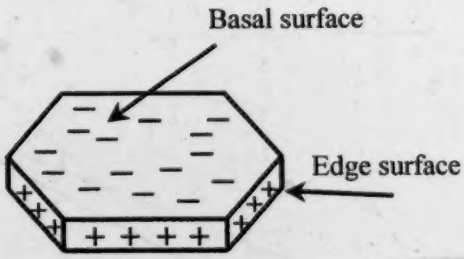

Figure 5.4 Schematic diagram of a clay plate.

The zeta potentials of montmorillonite suspension as a function of solution pH in Figure 5.5a do not show any noticeable change with pH over the pH range from 3 to 11, as expected. It is interesting to observe that changing potassium chloride concentration with the range studied has a marginal impact on the zeta potentials. This finding can be accounted for by considering ion exchange of excess K^+ with adsorbed multivalent ions. Similar results were reported by other researchers (Heath and Tadros, 1983; Sondi et al., 1996, 1997; Duran et al., 2000).

The effect of calcium addition on zeta potentials of montmorillonite clays is shown in Figure 5.5b. The montmorillonite surface remains negatively charged without iso-electric point (iep) observed. However, the magnitude becomes substantially smaller with increasing calcium ion concentration over the pH range studied, in particular at pH less than 10. The noticeable shift toward less negative zeta potentials of montmorillonite clays with calcium ion addition appears to be caused by a combination of the electric double

layer compression and specific adsorption of calcium ions. The less pronounced effect of calcium addition at pH greater than 10 is attributed to the precipitation of the added calcium ions over this pH range (King, 1982).

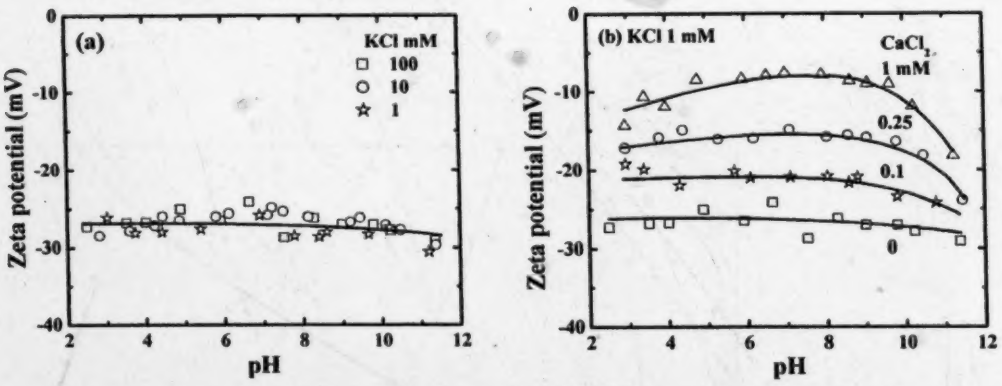

Figure 5.5 Average zeta potentials of montmorillonite suspensions as a function of solution pH in (a) KCl solutions; and (b) 1 mM KCl solutions containing CaCl2.

Kaolinite Kaolinite is a nonexpanding 1:1 (T:O) layer structured clay mineral. There is only a very small degree of isomorphous substitution and all the charge-compensating cations must adsorb on the exterior surface of the stacked layer. Therefore, surface charge for the basal plane is sensitive to H^+ or OH^- concentration in solution. Also, kaolinite does not leave any room for interlayer cations, shows a minimal swelling in water, and has a low cation exchange capacity. Since the surface charge of both the basal plane and the edge of kaolinite clay particles is sensitive to H^+ or OH^- concentration in solution, the pH dependence of its zeta potentials is therefore expected. In this case, electric double layer compression by the added electrolyte dominates the electrokinetics of the suspension.

The effect of solution pH on zeta potentials of kaolinite suspension is shown in Figure 5.6a. In contrast to the case of montmorillonite, increasing the pH of kaolinite suspensions decreases the zeta potentials steadily. High concentration of KCl depresses the zeta potential slightly, with an iep remaining unchanged at pH 3.6.

In 1 mM KCl solutions containing $CaCl_2$, the zeta potentials of kaolinite suspension becomes less negative as shown in Figure 5.6b. The diminishing of zeta potential with calcium ion addition can be partially accounted for by electric double layer compression. However, a noticeable shift in iep from pH 3.6 without calcium addition to pH 5.7 with the addition of 1 mM calcium is observed, indicating some degree of specific adsorption of calcium ions on kaolinite surface, most likely on the edges of broken clay particles.

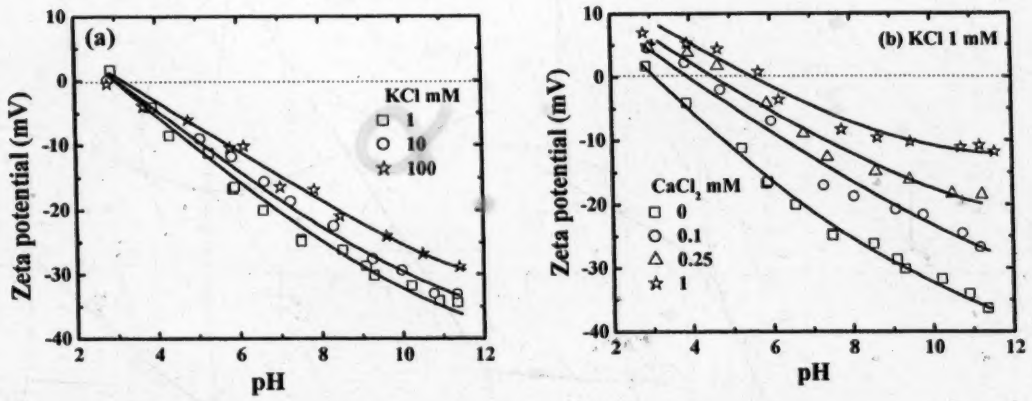

Figure 5.6 Average zeta potentials of kaolinite suspensions as a function of solution pH in (a) KCl solutions; and (b) 1 mM KCl solutions containing $CaCl_2$.

5.5 Fines from real oil sand ores

Fines extracted from real oil sand ores are mainly aluminosilicate minerals, as shown in Table 4.3. The zeta potential values of the fines as a function of solution pH are shown in Figure 5.7. It is evident that the fines from good and poor processing ores exhibit a similar electrokinetic behavior. In KCl or calcium solutions, the zeta potential of the fines become more negative with increasing solution pH and no iso-electric point (iep) is observed. With increasing supporting electrolyte (KCl) concentration, the zeta potential values of the fines became less negative, as anticipated from the electrical double layer compression (Figure 5.7a). The addition of calcium ions significantly depresses the zeta potentials of the fines as well, as a shown in Figure 5.7b. Comparison of Figure 5.7a with Figure 5.7b indicates that suppression of zeta potentials by 0.1mM and 1mM $CaCl_2$ is almost equivalent to that by 10 mM and 100mM KCl, respectively. It appears that calcium ions not only compress the electric double layer but also specifically adsorb on

the fines surface. The observed marginal difference in surface electric properties of the fines collected from good and poor processing ores would suggest a negligible difference in the electrostatic double layer interactions between bitumen and fines from the good from poor processing.

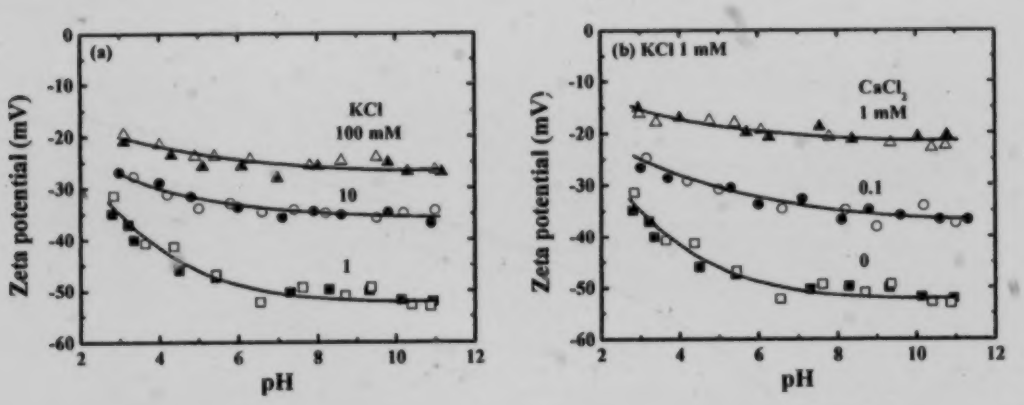

Figure 5.7 Average zeta potentials of fines suspensions as a function of solution pH in (a) KCl solutions; and (b) 1 mM KCl solutions containing $CaCl_2$. Filled symbols: fines from a good processing ore; open symbols: fines from a poor processing ore.

5.6 Implications

The obtained results can provide the data essential for calculating electrostatic double layer forces and qualitatively interpreting colloidal interactions. Qualitatively, for example, one would expect stronger repulsive electrostatic double layer forces between bitumen and sands/clays/fines with increasing solution pH, due to a substantially increased surface charge on bitumen, silica, kaolinite and fines. Therefore, a higher pH environment would be favorable for bitumen liberation from silica, kaolinite and fines. However, increasing pH is unfavorable for bitumen-bitumen coagulation and hence bitumen aeration. Therefore, a comprise needs to be made to optimize bitumen extraction. Since high concentration of electrolyte, in particular divalent electrolyte, depresses profoundly the zeta potentials of bitumen, silica, clays and fines, the resultant weaker repulsive electrostatic double layer forces are unfavorable for bitumen liberation, but are desirable for bitumen-bitumen coagulation and bitumen aeration. These

hypothetical implications from the zeta potential measurements will be further tested later in the thesis.

5.7 Summary of chapter

- The zeta potentials of bitumen, silica, kaolinite and fines show a pH-dependence, and their values become more negative with increasing solution pH. However, the zeta potentials of montmorillonite suspension exhibit pH-independent characteristics.
- High concentration KCl suppresses the zeta potentials of bitumen, silica and fines, but only slightly affect the zeta potentials of kaolinite and montmorillonite clays.
- Calcium ion addition significantly depresses the zeta potentials of bitumen, silica, kaolinite, montmorillonite, and fines.

CHAPTER 6 INTERACTIONS BETWEEN BITUMEN AND SILICA*

The surface forces between bitumen (spin-coated on silica wafer) and silica particles in aqueous solutions measured with an atomic force microscope are reported in this chapter. The effect of solution pH, salinity, divalent ion addition, and temperature on the interaction/adhesive forces was studied. The results show that higher solution pH and temperature, and lower salinity and calcium concentration result in a system with a stronger repulsive force and a weaker adhesive force, which is favorable for bitumen detachment from silica surface and the subsequent stabilization. At separation distance of greater than 2~4 nm, the long-range interaction force profiles between bitumen and silica can be well described with the classical DLVO theory, suggesting that the electrostatic forces play a dominant role in a bitumen-silica colloidal system. An additional repulsive force is observed at a relatively short separation, which is attributed to a polymer-like steric force. The implication of the measured interaction forces by AFM is confirmed by the zeta potential distribution measurements. The quantitative description of the interactions between bitumen and silica provides fundamental insights into bitumen "liberation/separation" mechanism in Water-Based Extraction systems and justifies the industrial use of caustics.

6.1 Introduction

In the Water-Based Extraction process of bitumen from oil sands, "liberation" of bitumen from sands and the subsequent stabilization against heterocoagulation of the liberated bitumen with sand grains, as shown in Figure 2.2a, are the prerequisites for bitumen extraction. Since silica sands constitute the main minerals in an oil sand ore, successful separation of bitumen from silica would greatly enhance the bitumen recovery and lead to a high quality froth. It is evident that bitumen liberation is largely determined by adhesion strength of bitumen with sand grains while the heterocoagulation is controlled by both long-range forces and adhesive forces between the two components. As a result, controlling the colloidal interactions between bitumen and sands is of great importance to bitumen extraction process and vast interest to researchers. Although the early studies

* A revised version of this chapter, co-authored by J. Liu, Z. Xu and J. Masliyah, has been published in *Langmuir*, Vol. 19(9), 3911-3920.

based on visualization and model calculation have advanced our knowledge on bitumen-sand interactions, they are mostly indirect and/or qualitative in nature.

To have a better understanding of bitumen "liberation" in the WBE process, quantitative studies of bitumen/sand interactions are highly relevant and beneficial. To our knowledge, there has not been any research work reported in open literature on quantifying bitumen/silica interactions relevant to bitumen extraction systems. This chapter focuses on the measurement of long-range and adhesive forces between bitumen and silica in aqueous solutions using an atomic force microscope. The practical implication from these colloidal force measurements are supported by the results from zeta potential distribution measurements. The normalized force profiles are fitted with the extended DLVO theory by including a steric force at very short range. The measured repulsive force barrier coupled with the adhesive force is used to predict the colloidal coagulation behavior between bitumen and silica.

6.2 Colloidal force measurement

6.2.1 System characteristics

It is known that bitumen is a deformable, extremely viscous honey-like material. To avoid complication of data analysis incurred by bitumen deformation, using a thin layer of bitumen on a smooth, hard substrate is desirable. For this reason, a molecularly smooth silica wafer was used as the substrate for supporting bitumen film. To avoid forming a thick layer of bitumen, it was necessary to fine-tune spin-coating operating parameters by adjusting the toluene to bitumen ratio and spin speed. The prepared bitumen surface was found to be acceptably smooth for colloidal force measurement, as shown in Figure 4.6. During the initial force measurement, it was observed that about half an hour was required for the measured force profile to be reproducible. This time-dependent behavior is attributed to the reorganization of the surface active molecules at bitumen/water interface. It is conceivable that the surfactant molecules in extremely viscous bitumen take time to migrate to the interface and to be dissociated or dissolved into the aqueous phase when the bitumen is contacted with aqueous solution. To ensure reaching the equilibrium, the system is allowed to incubate at each condition for at least one hour before collecting force profile data.

6.2.2 Deformation of bitumen surface

When dealing with soft, deformable surfaces such as oil droplets (Yoon et al., 1995, Basu and Sharma, 1996; Mulvaney et al., 1996; Synder et al., 1997; Aston and Berg, 1998; Hartley et al., 1999; Rabinovich et al., 2002) or air bubbles (Ducker et al., 1994) in a colloidal force measurement, the surface deformation is always a concern. The degree of surface deformation depends to a large extent on the geometry and the elasticity of the deformable solid or fluid interface. For a given system, a higher loading force would also cause a greater degree of deformation. Although a number of approaches including elastic model (Ducker et al., 1994; Fielden et al., 1996; Preuss and Butt, 1998; Hartley et al., 1999), contact mechanics theory (Johnson et al., 1971; Derjaguin et al., 1975; Meyer et al., 1998; Vakarelski, 2003) and augmented Young-Laplace equation (Miklavic et al., 1995; Bachmann and Miklavic, 1996; Miklavic, 1996; Horn et al., 1996; Aston and Berg, 2001; Bhatt et al., 2001; Chan et al., 2001; Attard, 2001) have been proposed to deal with the deformation of a deformable surface, the application of these approaches remains rather limited to a few special cases. To ensure that the deformation does not contribute to errors in the force analysis, the bitumen film in this study is prepared to be sufficiently thin so that the deformation under the applied force could be considered negligible.

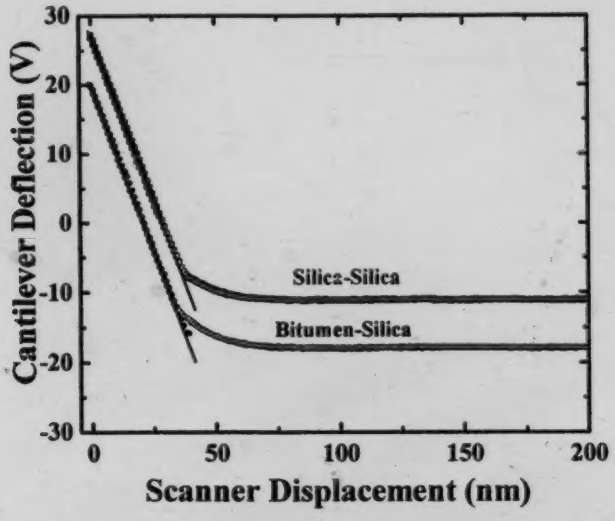

Figure 6.1 Raw data from typical surface force measurements between the silica-silica wafer and silica-bitumen (coated on silica wafer) in 1 mM KCl solutions at pH 8.2.

Shown in Figure 6.1 are the raw force profiles obtained using a probe silica particle against both silica and bitumen-coated silica surfaces in an aqueous KCl solution at pH 8.2. The open symbols represent the approaching branch while the solid symbols, the retracting branch. Even though a small adhesive force is observed between bitumen and silica in contrast to between a silica-silica pair, the constant compliance region for the two pairs of surfaces show the same slope (solid lines). This observation confirms the absence of any noticeable deformation of bitumen film under the applied force from the silica sphere.

6.2.3 Effect of pH

The solution pH is a critical operating parameter in bitumen recovery, and in most cases, the controlling parameter for surface charge. In a 1mM KCl solution, the effect of pH on the interaction forces between the bitumen and silica particle is shown in Figure 6.2. Over the pH range tested, the measured force profiles are monotonically repulsive. The repulsion increases with increasing pH. Even at pH 3.5, a weak repulsive force is observed.

The adhesive (pull-off) forces between bitumen and silica measured by the retracting branch of AFM force profiles are shown in the insert of Figure 6.2. A strong adhesion of 8 mN/m is measured at pH 3.5. A drastic decrease of adhesive force occurs from pH 5.7 to 8.2, and the adhesion disappears eventually at pH 10.5. Since the interfacial chemistry plays an important role in controlling colloidal interactions, the pH-dependent dissociation of cationic/anionic surfactants at the bitumen/water interface (King, 1992, Liu et al., 2002) could be a reason for the observed variations of adhesive forces with pH.

Comparison of the repulsive force barrier and the adhesive force is shown in the insert of Figure 6.2. The results in this Figure suggest that bitumen can be easily liberated from silica sand at a pH greater than 7~8. This finding is consistent with other observations (Dai and Chung, 1995, 1996; Zhou et al., 1999).

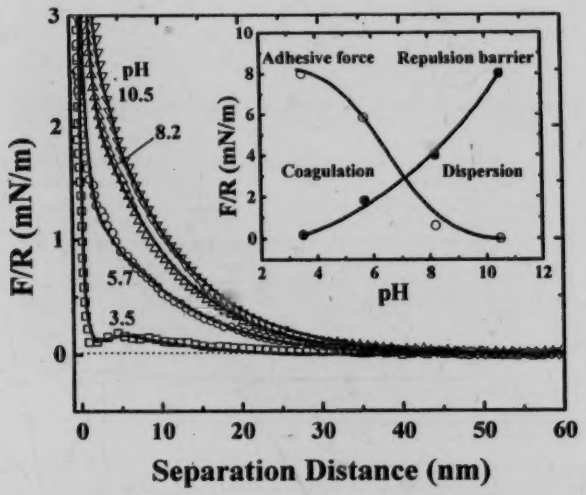

Figure 6.2 Normalized interaction forces (F/R) between bitumen and silica as a function of separation distance in 1 mM KCl solutions at different solution pH. Solid lines represent the fitting of the extended DLVO theory using A_{132}=3.3X10^{-21} J with the best-fitted decay length, Stern potential, macromolecule density factor f and tail length L being: pH 3.5 (down triangle) - $\kappa^{-1} = 9.6\,nm$, ψ_B=-15 mV, ψ_S=-20 mV, f=2.5x10^{-6} $N \cdot nm \cdot K^{-1} \cdot m^{-4}$, L=2 nm; pH 5.7 (circle)-$\kappa^{-1} = 9.1\,nm$, ψ_B=-51 mV, ψ_S=-41 mV, f=5x10^{-6} $N \cdot nm \cdot K^{-1} \cdot m^{-4}$, L=3 nm; pH 8.2 (up triangle) - $\kappa^{-1} = 8.9\,nm$, ψ_B=-72 mV, ψ_S=-56 mV, f=8x10^{-6} $N \cdot nm \cdot K^{-1} \cdot m^{-4}$, L=4 nm; and pH 10.5 (square) - $\kappa^{-1} = 9.2\,nm$, ψ_B=-75 mV, ψ_S=-62 mV, f=10x10^{-6} $N \cdot nm \cdot K^{-1} \cdot m^{-4}$, L=4 nm. Insert: interaction force barriers and adhesive forces measured at loading forces of 8~10 mN/m as a function of solution pH.

6.2.4 Effect of electrolyte (KCl) concentration

The concentration of an electrolyte is also an important factor to consider in a surface force analysis and is a process variable for a bitumen extraction system. The effect of electrolyte (KCl) concentration on the interaction forces between bitumen and silica at pH 8.2 is shown in Figure 6.3. All the force profiles are repulsive but the range of the repulsive forces decreases with increasing electrolyte concentration, as anticipated.

Although the long-range repulsive forces are suppressed by increasing electrolyte concentration, the adhesive forces between bitumen and silica are affected only marginally, as shown in the insert of Figure 6.3. This observation is anticipated as the electrolyte added should have only a minimal effect on surface ionization/dissociation and hence cause little change in interfacial chemistry. Since salinity has only a marginal impact on the repulsive force barrier and adhesion as shown in the insert of Figure 6.3, electrolyte addition could not greatly influence the coagulation behavior of bitumen with silica sand grains.

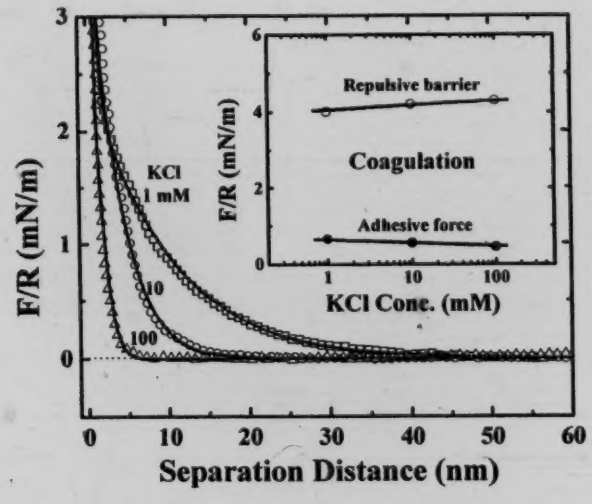

Figure 6.3 Normalized interaction forces (F/R) between bitumen and silica as a function of separation distance in KCl solutions at pH 8.2. Solid lines represent the fitting of the extended DLVO theory using A_{132}=3.3X10^{-21} J with the best-fitted decay length, Stern potential, macromolecule density factor f and tail length L being: 1 mM KCl (square) - $\kappa^{-1} = 8.9\,nm$, ψ_B=-72 mV, ψ_S=-56 mV, f =8x10^{-6} $N \cdot nm \cdot K^{-1} \cdot m^{-4}$, L=4 nm; 10 mM KCl (circle) - $\kappa^{-1} = 3.1\,nm$, ψ_B=-56 mV, ψ_S=-44 mV, f =60x10^{-6} $N \cdot nm \cdot K^{-1} \cdot m^{-4}$, L=2.5 nm; and 100 mM KCl (up triangle) - $\kappa^{-1} = 1\,nm$, ψ_B=-35 mV, ψ_S=-30 mV, f =100x10^{-6} $N \cdot nm \cdot K^{-1} \cdot m^{-4}$, L=2 nm. Insert: interaction force barriers and adhesive forces measured at loading forces of 8~10 mN/m as a function of KCl concentration.

6.2.5 Effect of calcium ions

Calcium is one of the divalent ions normally present in a bitumen extraction system. A substantial amount of calcium ions are introduced into bitumen extraction systems through recycling of process water from tailings treatment in which gypsum is added as a process aid to form consolidated tailings (Sheeran, 1995). A significant impact of calcium ions on the colloidal and adhesive forces between the bitumen and silica is expected, as calcium could compress the electric double layer and specifically adsorb on the bitumen and silica surfaces. the effect of calcium ion addition on the long-range and adhesive forces between bitumen and silica is studiesd by measuring these forces as a function of solution pH.

At pH 8.2, for example, calcium ion addition depresses the repulsive forces substantially, as shown in Figure 6.4. Meanwhile, the adhesive force between bitumen and silica increases from 0.2 mN/m without the addition of calcium ions to 5 mN/m with the addition of 1 mM calcium. Comparison of the repulsive force barrier and the adhesive force shown in the insert of Figure 6.4 clearly shows that the bitumen can easily coagulate with silica sands at calcium ion concentration greater than 0.1 mM at a solution pH 8.2. Using the DLVO theory, Takamura and Chow (1983) arrived at a similar conclusion.

A much more dramatic effect of calcium addition on both the long-range colloidal force and the contact adhesive force is observed at pH of 10.5, as shown in Figure 6.5. The colloidal forces change progressively from repulsive to attractive with increasing calcium ion addition to 1 mM, while the adhesive forces increase from zero to 8 mN/m. The change of interaction force profiles can be attributed to the diminished electrostatic double layer forces and the specific adsorption of calcium ions. To account for an attractive force profile with 1 mM calcium addition, the charge on the silica and bitumen surfaces at the Stern plane must have been drastically suppressed and is significantly different, which will be further confirmed by the zeta potential measurements of corresponding colloidal suspensions. Comparison of the repulsive force barrier and adhesive force shown in the insert of Figure 6.5 clearly shows that the bitumen can easily coagulate with silica sands at calcium ion concentration greater than 0.03 mM at a

solution pH of 10.5. The implication from these results is that excess caustic addition to increase pulp pH may not be always beneficial for bitumen digestion when calcium ions are present in the system. This fundamental finding provides an important justification as to why industrial scale bitumen extraction operates at a pulp pH around 8.5 as a compromise.

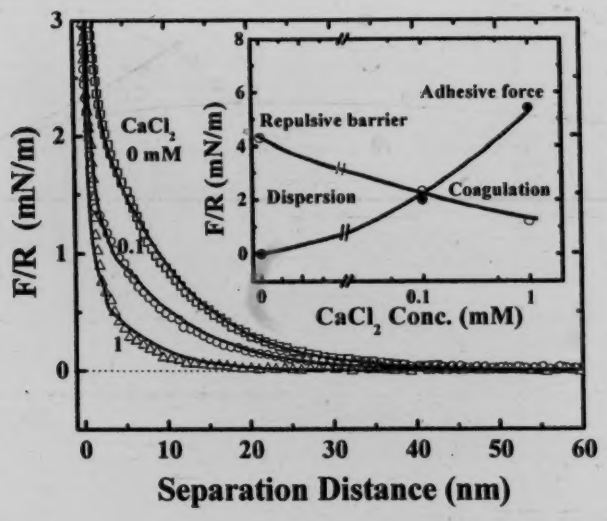

Figure 6.4 Normalized interaction forces (F/R) between bitumen and silica as a function of separation distance in 1 mM KCl solutions containing $CaCl_2$ at pH 8.2. Solid lines represent the fitting of the extended DLVO theory using A_{132}=3.3X10^{-21} J with the best-fitted decay length, Stern potential, macromolecule density factor f and tail length L being: 0 mM $CaCl_2$ (square) - $\kappa^{-1} = 8.9\,nm$, ψ_B=-72 mV, ψ_S=-56 mV, f=8x10^{-6} $N \cdot nm \cdot K^{-1} \cdot m^{-4}$, L=4 nm; 0.1 mM $CaCl_2$ (circle) - $\kappa^{-1} = 8.5\,nm$, ψ_B=-45 mV, ψ_S=-48 mV, f=5x10^{-6} $N \cdot nm \cdot K^{-1} \cdot m^{-4}$, L=3 nm; and 1 mM $CaCl_2$ (up triangle) - $\kappa^{-1} = 4.6\,nm$, ψ_B=-35 mV, ψ_S=-25 mV, f=3x10^{-6} $N \cdot nm \cdot K^{-1} \cdot m^{-4}$, L=2.5 nm. Insert: interaction force barriers and adhesive forces measured at loading forces of 8~10 mN/m as a function of calcium ion concentration.

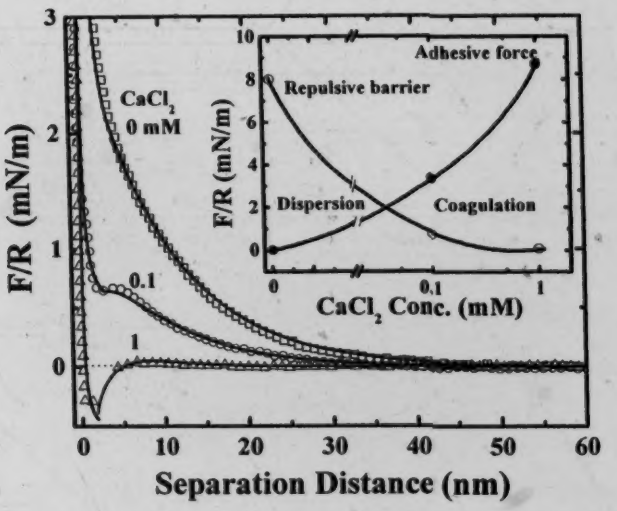

Figure 6.5 Normalized interaction forces (F/R) between bitumen and silica as a function of separation distance in 1 mM KCl solutions containing $CaCl_2$ at pH 10.5. Solid lines represent the fitting of the extended DLVO theory using A_{132}=3.3X10^{-21} J with the best-fitted decay length, Stern potential, macromolecule density factor f and tail length L being: 0 mM $CaCl_2$ (square) - $\kappa^{-1} = 9.2\,nm$, ψ_B=-75 mV, ψ_S=-62 mV, f=10x10^{-6} $N \cdot nm \cdot K^{-1} \cdot m^{-4}$, L=4 nm; 0.1 mM $CaCl_2$ (circle) - $\kappa^{-1} = 7.9\,nm$, ψ_B=-45 mV, ψ_S=-35 mV, f=4x10^{-6} $N \cdot nm \cdot K^{-1} \cdot m^{-4}$, L=3 nm; and 1 mM $CaCl_2$ (up triangle) - $\kappa^{-1} = 4.8\,nm$, ψ_B=-35 mV, ψ_S=-8 mV, f=2x10^{-6} $N \cdot nm \cdot K^{-1} \cdot m^{-4}$, L=2 nm. Insert: interaction force barriers and adhesive forces measured at loading forces of 8~10 mN/m as a function of calcium ion concentration.

6.2.6 Effect of temperature

Temperature is another critical operating parameter in bitumen extraction by hot water process. Elevated temperature is usually considered to reduce the viscosity of bitumen, which in turn facilitate bitumen-air bubble attachment and engulfment (Drelich and Miller, 1994; Drelich et al., 1994; Dai and Chung, 1995, 1996). To appreciate the role of increased temperature in bitumen digestion/liberation, the colloidal forces are measured at different temperatures in a solution of pH 8.2. As shown in Figure 6.6, increasing the

temperature makes the long-range forces between bitumen and silica slightly more repulsive. The increased repulsion can be accounted for by considering an increase in surface charge density at the bitumen/water interface. The adhesive forces, on the other hand, disappear at a solution temperature higher than 35°C, as shown in the insert of Figure 6.6. Comparison of the repulsive force barrier and the adhesive force shown in the insert of Figure 6.6 clearly shows that increasing process temperature facilitates bitumen liberation from silica sands.

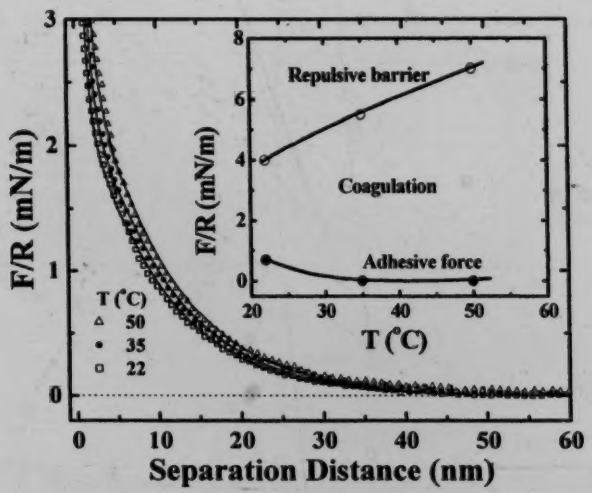

Figure 6.6 Normalized interaction forces (F/R) between bitumen and silica as a function of separation distance in 1 mM KCl solutions at pH 8.2 and different temperatures. Solid lines represent the fitting of the extended DLVO theory using A_{132}=3.3X10^{-21} J with the best-fitted decay length, Stern potential, macromolecule density factor f and tail length L being: 22°C (square) - $\kappa^{-1} = 9.2\,nm$, ψ_B=-72 mV, ψ_S=-56 mV, f=8x10^{-6} $N \cdot nm \cdot K^{-1} \cdot m^{-4}$, L=4 nm; 35°C (circle) - $\kappa^{-1} = 8.6\,nm$, ψ_B=-77 mV, ψ_S=-59 mV, f=10x10^{-6} $N \cdot nm \cdot K^{-1} \cdot m^{-4}$, L=5 nm; and 50°C (up triangle) - $\kappa^{-1} = 8.8\,nm$, ψ_B=-79 mV, ψ_S=-63 mV, f=12x10^{-6} $N \cdot nm \cdot K^{-1} \cdot m^{-4}$, L=5.5 nm. Insert: interaction force barriers and adhesive forces measured at loading forces of 8~10 mN/m as a function of temperature.

6.2.7 Data fitting and nature of colloidal force

To further understand the nature of the colloidal forces measured in the various systems mentioned earlier, the measured force profiles are fitted with the extended DLVO theory by considering a steric force for an asymmetric system. The boundary conditions of constant surface charge density and constant Stern potential are set to bitumen and silica surfaces, respectively, as discussed in Chapter 4. A typical surface force profile measured at pH 8.2 in 1mM KCl solution is shown in Figure 6.7. The measured force profiles at separation distance of greater than 4 nm can be satisfactorily described by the classical DLVO theory, as shown by the dash line in Figure 6.7. It is important to note that similar fittings with boundary conditions of constant surface charge density for both surfaces or constant surface potential for both surfaces would result in a bigger discrepancy between the fitted Stern potentials and the measured zeta potentials. At a very short separation (less than 4 nm), however, the observed repulsive force deviates from the predicted force profiles by the DLVO theory, suggesting the presence of an additional repulsive force. Considering various macromolecules of the asphaltene type present at the bitumen/water interface (Boukir et al., 2001; Zhang et al., 2003a, b), this additional repulsive force can be attributed to a steric force originated from the macromolecule brushes. The good description of the additional repulsive forces by the Pincus scaling theory (equation 4-2) confirms its steric nature, as shown by dotted line in Figure 6.7. The excellent fit of the force profiles with the extended DLVO theory suggests that the long-range forces do arise from the electrostatic double layer force, the van der Waals forces and the steric force. The electrostatic double layer force is the dominant force that controls the interactions between bitumen and silica.

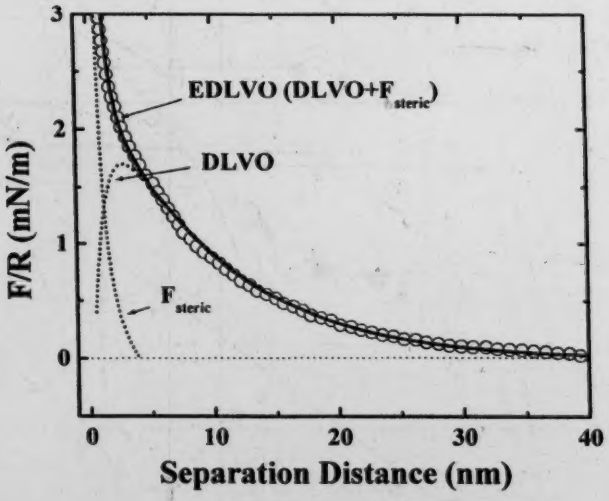

Figure 6.7 Normalized interaction forces (F/R) between bitumen and silica as a function of separation distance in a 1 mM KCl solution at pH 8.2. Solid line represents the fitting of the extended DLVO theory using A_{132}=3.3X10^{-21} J with the best-fitted decay length, Stern potential, macromolecule density factor f and tail length L being: $\kappa^{-1} = 8.9\ nm$, ψ_B=-72 mV, ψ_S=-56 mV, f =8x10^{-6} $N \cdot nm \cdot K^{-1} \cdot m^{-4}$, L=4 nm.

The same procedure is applied to all the force profiles measured between bitumen and silica. As shown by the solid lines of Figures 6.2~6, the measured force profiles between bitumen and silica can be described with the extended DLVO theory by considering a steric force. To further confirm the electrostatic nature of the relatively longer range (greater than 4 nm) repulsive forces, the fitted decay length from the measured force profiles is compared with those calculated using the well known Debye-Huckel approximation formula (Israelachvili, 1991) and the actual electrolyte concentration used in the force measurement. As shown in Figure 6.8, an excellent agreement between the two sets for all the force profiles presented confirms our interpretation of the electrostatic nature of the long-range repulsion.

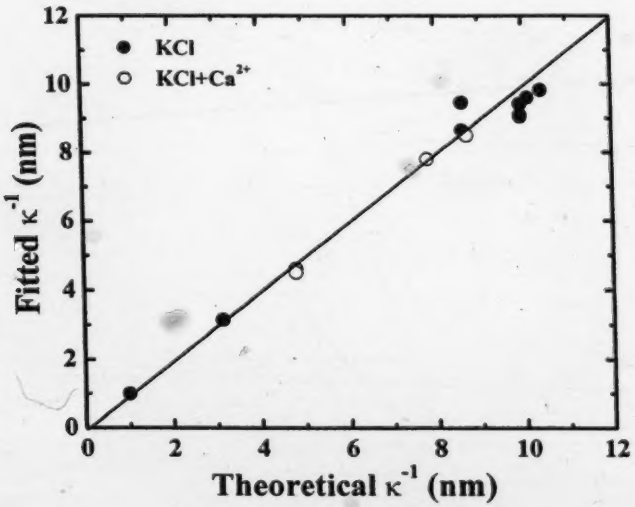

Figure 6.8 Comparison of best-fitted decay length from the measured force profiles with calculated decay length using Debye-Huckel theory from the actual electrolyte concentration used in the corresponding force measurement.

Further tests are performed to compare the fitted Stern potentials with the measured zeta potentials of bitumen droplets and silica particles. The zeta potentials of bitumen droplets and silica particle are shown in Figure 5.2 and 5.3, respectively. The zeta potential results are fairly informative to interpret the measured force profiles. Without calcium addition, repulsive force profiles are anticipated between negatively charged bitumen and silica as shown in Figure 6.2. With the addition of 1 mM calcium ions, on the other hand, the less negatively charged silica and more negatively charged bitumen at pH 10.5 would result in an attractive force profile, which is indeed measured as shown in Figure 6.5 (Triangles). Quantitatively, the plot of the measured zeta potentials against the corresponding fitted Stern potentials of the measured force profiles with the DLVO theory exhibits an excellent agreement as shown in Figure 6.9. The close match between the measured zeta potential and the fitted Stern potential confirms that the measured repulsive forces indeed originate from electrostatic double layer interactions.

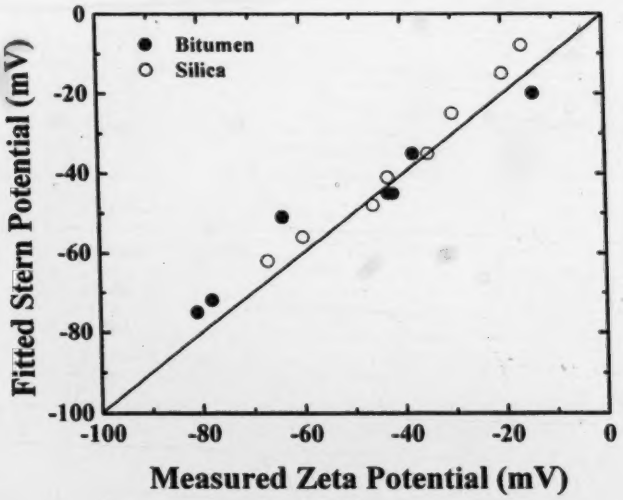

Figure 6.9 Comparison of the best-fitted Stern potential from the measured force profiles with the classical DLVO theory and the measured corresponding zeta potentials of silica (open symbols) and bitumen droplets (filled symbols).

The deviations of measured forces from the classical DLVO theory at separations less than 2~4 nm are attributed to the presence of steric forces. It is also known that when bitumen is brought into contact with an aqueous phase, the bitumen surface would become relaxed or reorganized such that the polar molecules are concentrated at the bitumen/water interface or even migrate into the aqueous phase, depending on the polarity of their head groups and the length of carbon chain in molecules. In this manner, the presence of surface-active macromolecules at the bitumen/water interface results in a brush-like surface configuration as observed in polymer systems, and thereby induces a brush-type of repulsive force. The observed strong repulsive force at short range can be well described with the Pincus scaling theory. The fitted tail length L and structure factor f are dependent on solution pH, salinity, calcium addition and temperature. Higher pH, higher temperature and lower salinity can reduce the viscosity of bitumen and hence facilitates the dissociation, release, and stretching of the macromolecules at the bitumen/water interface, and thereby corresponds to a longer tail (L) and a denser polymer (bigger f), i.e. a strong repulsive force. For example, the fitted tail length L increases with increasing solution pH, as shown in Figure 6.10. As electrolyte

concentration increases, the fitted scaling parameters L decreases while density factor f increases. Although the exact reason is not clear, one can image that electrolyte at higher concentration can compress the electric double layer and thereby decrease the distance between the charged groups. However, divalent calcium ion addition decreases fitted scaling parameters L and f. This is expected since calcium ions make the macromolecule tails more condensed by charge neutralization or calcium bridge.

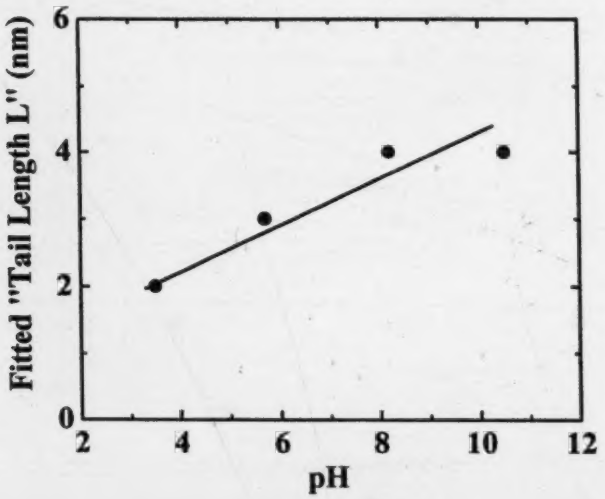

Figure 6.10 The best-fitted macromolecule "Tail Length L" of steric forces with the extended DLVO theory of the measured force profiles as a function of solution pH.

The above results and analysis of colloidal forces clearly show that the colloidal interactions between bitumen and silica sand grains are largely controlled by the electrostatic double layer forces. Although the short-range steric repulsive force is determined to be significant, it does not contribute to the coagulative nature due to the attraction (jump-in) beyond this range. However, the existence of short-range steric repulsion will determine the structure of aggregates as in the case that particles are coagulated at an attractive well. This general finding suggests that to avoid detrimental hetero-coagulation of bitumen with silica sand grains in a water-based bitumen recovery process, creating a suitable surface charge condition by controlling the slurry pulp chemistry is necessary.

6.2.8 Nature of adhesive force

The adhesive force (pull-off force) is found to be highly dependent on solution pH and calcium addition. The adhesive force between two particles generally originates from the molecular/atomic interactions in the contact area, such as electrostatic interaction, chemical bond, and hydrogen bonding. These contact forces are highly sensitive to surface composition. In the present system, silica surfaces are dominated by OH^- group and can specifically adsorb calcium ions at higher pH, while bitumen surface bears various types of natural surfactants (Liu et al., 2002), which could become protonated or dissociated, depending on solution pH (King, 1982; Laskowski, 1999). At low pH, the cationic surfactants on bitumen surface are protonated to generate cationic sites (RNH_3^+), which can interact with OH^- group on the silica surface to induce a strong adhesive force. At high pH, the dissociated anionic surfactants ($RCOO^-$ and $ROSO_3^-$) dominate bitumen surface. These anionic surface groups have little affinity to the OH^- groups on the silica surface, making the system non-adhesive. These interpretations are consistent with our experimental observations shown in the insert of Figure 6.2. With the addition of calcium ions, the specific adsorption of calcium ions on the silica surface in the form of $CaOH^+$ at high pH (Figure 5.3) is responsible for the observed strong adhesion (at pH 10.5 in the insert of Figure 6.5) between bitumen and silica through chemical binding of carboxylate on the bitumen surface with calcium ion on the silica surface.

6.3 Zeta potential distribution measurement

The current study clearly shows that the tuning of colloidal forces by changing solution pH, salt concentration, divalent cation addition, and system temperature can be confidently attributed to their ability to alter the electrostatic double layer forces and the adhesive forces. Since the measurements with AFM are performed using single particles, even though a number of particles are used in the measurements, its generalization to a system of colloidal interactions between bitumen and silica remains a concern.

To further confirm the conclusions derived from the force profiles and adhesion forces measured with AFM, the zeta potential distributions of bitumen emulsion and silica suspension, individually and in a mixture, are measured and the results are interpreted in terms of colloidal interactions. For illustrative and confirmative purposes, only the results

with and without calcium addition at a solution pH of 10.5 are presented here. The zeta potential distributions measured with bitumen droplets or silica particles alone in a 1mM KCl solution without calcium addition are centered at -82 and -67 mV, respectively, as shown in the overlaid histogram of Figure 6.11a. A similar zeta potential distribution histogram is obtained for the mixture of the two species as shown in Figure 6.11b. The presence of two distinct distribution peaks at -82 and -69 mV indicates that bitumen droplets and silica particles in the mixture are non-coagulative, i.e. they are present separately as individual particles. This observation agrees with the presence of a strong repulsive force between the two components as shown in the AFM force measurement (Figure 6.2).

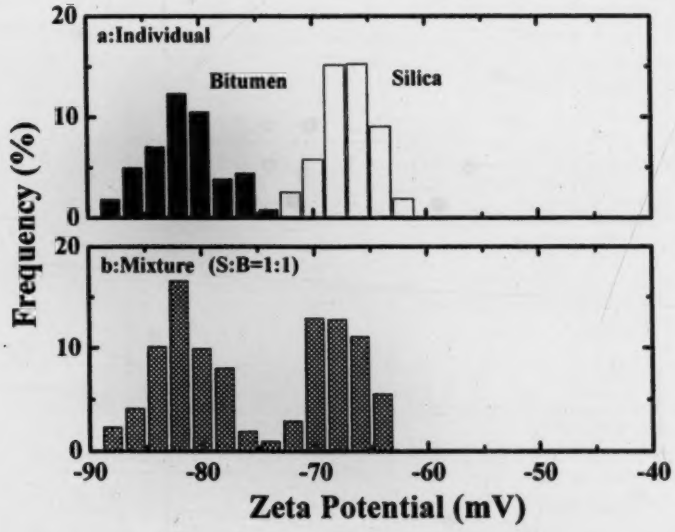

Figure 6.11 Zeta potential distributions in 1 mM KCl solutions at pH 10.5 without calcium ion addition. (a) Individual bitumen emulsion and silica suspension; and (b) their mixture at a mass ratio of 1:1.

When 1 mM calcium ions are added, the zeta potential distribution histograms for bitumen droplets and silica particles measured separately are found to be much less negative, as shown in Figure 6.12a. When zeta potential distribution is measured with the mixture of the two species, only a single broad distribution peak located in between the two original peaks is observed, as shown in Figure 6.12b. The disappearance of the

original distribution peaks of silica and bitumen and the appearance of a new broad distribution peak in between suggest that the silica particles and bitumen droplets are hetero-coagulated to form composite aggregates. This behavior indicates a strong attraction between the two components, as anticipated for a system of an attractive long-range force profile with a finite adhesion measured with the AFM (see Figure 6.5).

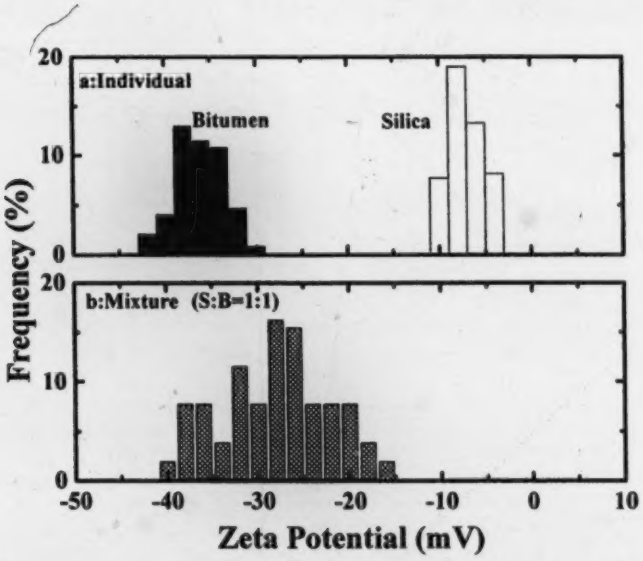

Figure 6.12 Zeta potential distributions in 1 mM KCl solutions containing 1 mM $CaCl_2$ at pH 10.5. (a) Individual bitumen emulsion and silica suspension; and (b) their mixture at a mass ratio of 1:1.

6.4 Relevance to the oil sands industry

It is well known that the adhesive force determines bitumen attachment onto silica surfaces, while long-range forces are the key for dispersion or coagulation of silica-bitumen colloidal systems. In general, long-range forces described by the DLVO theory or extended DLVO theory can be used satisfactorily to interpret the stability of colloidal systems. However, for a dynamic colloidal system such as a bitumen extraction process, both the long-range forces and adhesive forces have to be considered. For instance, the interaction forces between bitumen and silica are repulsive in simple electrolyte solution at pH less than 8 (Figure 6.2), where no coagulation between them is anticipated. This anticipation is in contrast to the visual observations of poor bitumen detachment from a

sand grain in neutral pH aqueous medium made by other researchers (Dai and Chung, 1995; Zhou et al., 1999). To reconcile the observed discrepancy and to further understand bitumen digestion from silica sand grains, the adhesive forces between bitumen and silica have to be considered. As shown in the insert of Figure 6.2, at a pH below 7, strong adhesion compounded with a weak long-range repulsive force barrier between bitumen and silica is responsible for the observed poor bitumen digestion or coagulation of bitumen with silica. This is consistent with the results from coagulation tests (Dai and Chung, 1995; Zhou et al., 1999). The finding suggests that bitumen is unlikely to be liberated from sand grains at solution pH below 7. At pH greater than 7 the adhesive forces become extremely weak and approach zero, with a strong repulsive force profile observed. Such a system facilitates bitumen liberation from sand grains and is consistent with the required caustic addition to adjust pulp pH above 8 in industrial bitumen extraction processes.

However, excessive caustic addition to increase pulp pH may not be always beneficial for bitumen digestion when calcium ions are present in the system. The stronger adhesion and long-range attraction induced by calcium addition at pH 10.5 as shown in Figure 6.5 will not facilitate bitumen liberation from sand grains. Clearly the presence of calcium ions in bitumen extraction process is detrimental to bitumen separation, as it would hinder the detachment of bitumen from sand grains due to increased adhesive forces between the two components. This study provides a legitimate justification as to why the industrial bitumen extraction system operates at pulp pH around 8.5 as a compromise. It is also evident from the direct force measurement that increasing the electrolyte concentration only marginally impacts the interaction between bitumen droplet and silica particle as the repulsive barriers and adhesive forces are not greatly influenced although the ranges of long-range repulsive forces are reduced, as shown in Figure 6.3. The elevated temperature could increase the repulsive interaction force and decrease the adhesive force as shown in Figure 6.6. The results suggest that in addition to the commonly accepted role of high temperature in reducing bitumen viscosity, the elevated temperature can, to some extent, facilitate bitumen liberation by controlling long-range and adhesive forces.

It is evident that for a bitumen extraction system, a repulsive colloidal force profile and zero adhesive force represent a "stable" colloidal state, resulting in easy liberation and absence of coagulation between bitumen and silica sand. From the direct force measurement, this condition can be realized by operating the process at high temperature and/or high pH without calcium addition. This favorable condition for bitumen extraction is practiced in some commercial bitumen extraction operations (Hepler and Hsi, 1989; Hepler and Smith, 1994). For a system of repulsive colloidal force with a finite adhesive force, a careful balance between hydrodynamic forces and colloidal forces is required to create a favorable condition for bitumen separation. This would be a difficult situation to create for a dynamic system if the energy barrier is smaller than the adhesive force, should it exist. The particles can usually obtain kinetic energy enough to overcome the repulsive force barrier and become coagulated with each other, but not enough to overcome the adhesive force and detach from each other. This case is seen for low solution pH in the insert of Figure 6.2. For a system with an attractive interaction force and a finite adhesive force as in case of 1mM calcium ion addition and at pH 10.5 (Figure 6.5), it is extremely difficult if not impossible to separate the bitumen from the sand grains.

6.5 Summary of chapter

The results presented here demonstrated that AFM force measurement in conjunction with the spin-coating technique is a powerful tool to quantitatively investigate the bitumen/silica interactions. This provides further insight into the bitumen liberation mechanism in the HWE process. The following are general conclusions derived from the results in this chapter.

- Solution pH is a critical factor that controls the bitumen-silica interactions. With increasing solution pH, the long-range repulsive force increases and the adhesive force decreases.

- With the addition of calcium ions, the repulsive force between bitumen and silica becomes smaller and even reversed from repulsive to attractive, depending on the pH

and calcium ion concentration. The adhesive force increases profoundly with calcium ion addition.

- At temperatures higher than room temperature, increasing the temperature leads to a slight increase in repulsive interaction force and a decrease in the adhesive force.

- Increasing the salinity depresses the repulsive forces between bitumen and silica significantly but only has a marginal effect on the adhesive forces.

- The surface force measurement identifies the conditions of hetero-coagulation between bitumen and silica above pH 10 with 1 mM calcium ion addition, which is substantiated by the zeta potential distribution measurement. The results justify the industrial operation at slurry pH around 8.5 as a compromise.

- At separation of greater than 2~4 nm, the measured long-range colloidal forces can be well fitted with the classical DLVO theory, with the fitted Debye lengths and Stern potentials being in an excellent agreement with those calculated and measured, respectively. Deviation from the classical DLVO theory is observed at separation less than 2~4 nm, which is attributed to a short-range steric repulsion.

- The results show that the electrostatic double layer forces play a dominant role in the interactions between bitumen and silica.

CHAPTER 7 INTERACTIONS BETWEEN BITUMEN AND BITUMEN*

The surface colloidal forces between bitumen surfaces in aqueous solution were measured with an Atomic Force Microscope (AFM). The results show that the solution pH, salinity, calcium and montmorillonite clay addition have a significant impact on both the long-range and adhesive forces. The measured long-range forces were compared with the adhesive forces to predict the coagulative nature of bitumen droplets. Weaker repulsive forces were observed under conditions of lower solution pH, higher salinity and higher calcium concentration. Stronger adhesive forces occurred at lower solution pH, lower salinity and lower calcium concentration. The addition of montmorillonite clays increased the repulsive forces and decreased the adhesive forces, particularly co-added with calcium ions. The measured force profiles were fitted with the extended DLVO theory. The results show that the electrostatic double layer force and hydrophobic force dominate the interactions between bitumen and bitumen. At very short range (less than 4~6 nm), strong repulsive forces were observed, which is of steric origin. These results provide a fundamental understanding of bitumen emulsion stability and the mechanism of bitumen "aeration" in bitumen extraction systems.

7.1 Introduction

Fine particle processing is one of the large challenges in mineral processing. One of the reasons is the low attachment efficiency between particle and air bubble due to low inertia of fine particle (Ralston, et al., 1984; Kent and Ralston, 1985). In bitumen extraction from oil sands, the "aeration" of bitumen with air bubbles is affected by the size of bitumen droplets in the context of collision efficiency. It has been recognized that the bitumen droplet size has a very good correlation to bitumen recovery in bitumen flotation systems (Dai and Chung, 1996). For good processing ores, for example, one can easily obtain over 93 % bitumen recovery with a generated bitumen droplet size of up to several hundred microns, while for poor processing ores bitumen recovery can be as low as 30 % with a generated bitumen droplet size of less than 100 microns. The size of

* A revised version of this chapter, co-authored by J. Liu, Z. Xu and J. Masliyah, has been published in *Langmuir*, Vol. 19(9), 3911-3920, 2003.

bitumen droplets is highly dependent on the coagulation and coalescence behavior between bitumen droplets, as shown in Figure 2.2b(I). The coagulation behavior is controlled by interaction forces between bitumen droplets. Therefore the direct surface force measurement between bitumen surfaces would provide us some fundamental knowledge on bitumen "aeration". The earlier work by Yoon et al. (1995, 1999) and Wu et al. (2000) on quantifying the interactions between bitumen droplets laid foundations for our further study. In this chapter, surface forces between bitumen coated on silica spheres and bitumen coated on silica wafers are measured to further investigate the effects of various factors such as solution pH, salinity, calcium and fine clay addition on the their interactions. The normalized force profiles are fitted with the extended DLVO theory by including a hydrophobic force and a steric force at very short separation range.

7.2 Interactions in the absence of fines

7.2.1 General observation

In surface force measurements, it has been a challenge for people how to choose a proper set-up for a fluid surface. Directly generating a fluid droplet is a simple choice. Techniques like dip-coating, Langmuir-Bologgett (L-B) deposition and spin coating are the options to prepare a smooth fluid material-like surface. However, the deformation of the prepared fluid surface would complicate the treatment and interpretation of the experimental data. Although some methods of coping with the deformation of fluid surfaces have been developed recently (see Chapters 4 and 6), the best way is to make the deformation of fluid interfaces negligible under the premise of keeping surface properties of the coated film the same as that of bulk fluid. For a bitumen system, unlike pure oil, methods used to prepare bitumen surfaces may greatly impact the bitumen/water interfacial properties. For instance, the L-B deposition technique would result in a bitumen monolayer of selective species of whole bitumen with a mutation surface that is different from that of whole bitumen. In L-B deposition, preferential orientation of deposited molecules is also a concern. Therefore, the method of preparing bitumen surfaces should be delicately considered because of the complexity of bitumen composition. Dipping a substrate or a particle into the bitumen, spin-coating bitumen or just generating a bitumen droplet can produce a bitumen film that possesses the same surface properties as whole bitumen. However, this kind of bitumen film would be so

thick that a noticeable deformation of the bitumen surface becomes inevitable. In the worst cases, two surfaces may stick together to impede the probing process, in particular when strong attractive forces exist. To obtain a representative bitumen film, diluting bitumen with toluene is a good approach. In this study, spin-coating was found suitable for bitumen to be coated on silica wafers, while the bitumen coating on silica spheres by dip-coating was deemed satisfactory. Contact angle measurements indicated that the surface properties of bitumen-coated silica wafers were similar to those of whole bitumen. The smoothness of the coated film wais found to be acceptable from AFM imaging (see Figure 4.6). The negligible deformation of the coated bitumen film in colloidal force measurement was confirmed, as described in Chapter 6. To confirm the satisfactory nature of the bitumen film coated on the silica sphere, the measured force profile of a bitumen-coated substrate interacting with a silica probe sphere is compared with the force profile obtained for a silica substrate interacting with a bitumen-coated probe, as shown in Figure 7.1. The two force profiles are almost identical, confirming that the bitumen film spin-coated on a silica wafer and bitumen film dip-coated on a silica probe possess the same surface features.

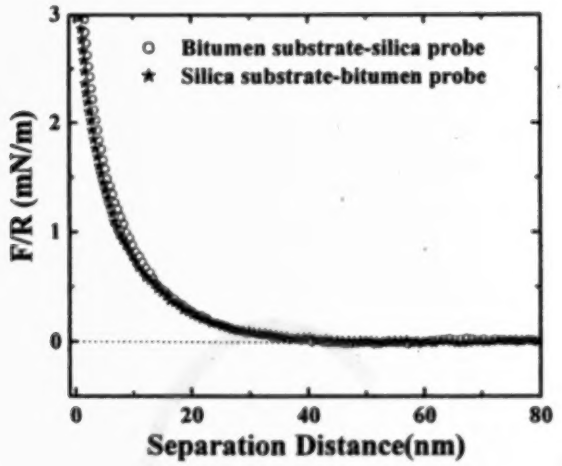

Figure 7.1 Normalized interaction forces (F/R) between bitumen and silica as a function of separation distance in 1 mM KCl solutions at pH 8.2. (a) Open circle: pair of bitumen coated on silica wafer - silica sphere; and (b) filled star: pair of silica wafer - bitumen coated on the silica sphere surface.

As in the bitumen-silica system discussed in Chapter 6, the measured force profiles between bitumen surfaces are also time-dependent. As shown in Figure 7.2, the repulsive interaction forces between bitumen surfaces increased with increasing incubation time. About 30 min is required to obtain the repeatable force profiles. This kind of time-dependant behavior can be attributed to the presence of polar molecules in the bitumen and honey-like flexibility of bitumen as described in Chapter 6. To ensure that the surface is fully equilibrated prior to collecting force data, 1 hr of incubation time was used for the following experiments.

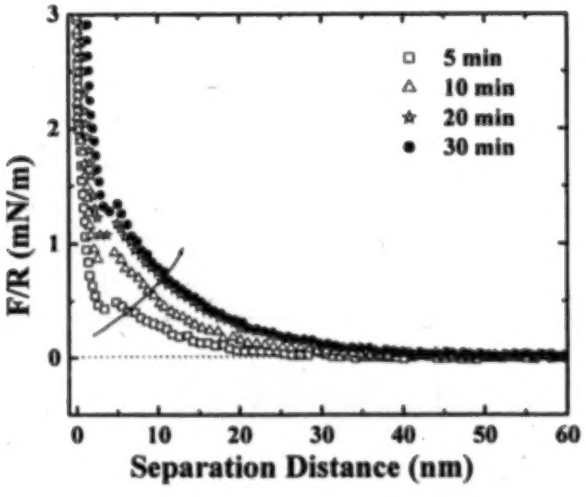

Figure 7.2 Normalized interaction force (F/R) profiles as a function of incubation time in a 1 mM KCl solution at pH 5.7.

7.2.2 Effect of solution pH

The solution pH is recognized as an important operating parameter in bitumen recovery. The effect of solution pH on the interaction force between the bitumen surfaces is shown in Figure 7.3. In a 1 mM KCl solution, the solution pH has a significant impact on both the colloidal force and adhesive force. The long-range interaction force profile changes from attractive at pH 3.5 to repulsive as the solution pH increased from 5.7 to 10.5. At a separation of ca. 5~8 nm, the force profiles exhibit a noticeable jump-in motion in solutions of pH 3.5~8.2, but no such jump-in is observed in the solution at pH 10.5. Immediately after jump-in, a stronger repulsive force at separation of less than 4~5 nm is

encountered. This type of force profile indicates the complex nature of the bitumen surface and force origin. With an increase in solution pH, the normalized adhesive force decreases significantly from 12 mN/m at pH 3.5 to nearly 0 mN/m at pH 10.5. The insert of Figure 7.3 clearly shows that at a solution pH less than 9, a weaker repulsive force and a stronger adhesive force between bitumen droplets are highly desirable for bitumen coagulation.

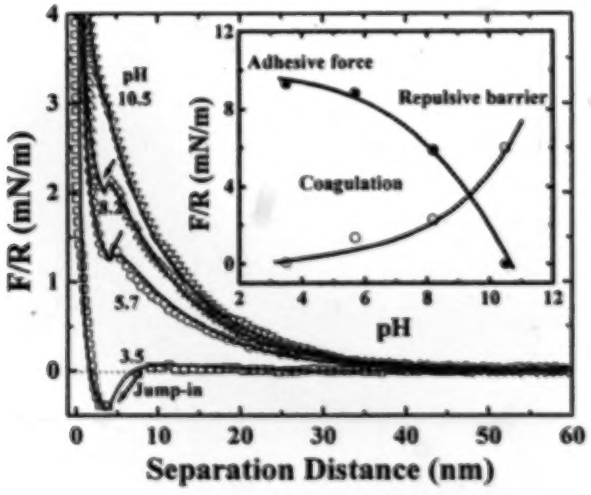

Figure 7.3 Normalized interaction forces (F/R) between bitumen surfaces as a function of separation distance in 1 mM KCl solutions at different solution pH. Solid lines represent the fitting of the extended DLVO theory using A_{131}=2.8x10^{-21} J with the best-fitted decay length, Stern potential, hydrophobic force constant K, macromolecule density factor f and tail length L being: pH 3.5 (square) - $\kappa^{-1} = 9.4\ nm$, ψ_B=-22 mV, K =10x10^{-20} J, f =3x10^{-6} $N \cdot nm \cdot K^{-1} \cdot m^{-4}$, L=2 nm; pH 5.7 (circle) - $\kappa^{-1} = 9.4\ nm$, ψ_B=-60 mV, K =10x10^{-20} J, f =6x10^{-6} $N \cdot nm \cdot K^{-1} \cdot m^{-4}$, L=3 nm; pH 8.2 (up triangle) - $\kappa^{-1} = 9.4\ nm$, ψ_B=-74 mV, K =10x10^{-20} J, f =8x10^{-6} $N \cdot nm \cdot K^{-1} \cdot m^{-4}$, L=3 nm; and pH 10.5 (down triangle) - $\kappa^{-1} = 9.4\ nm$, ψ_B=-80 mV, K =5x10^{-20} J, f =10x10^{-6} $N \cdot nm \cdot K^{-1} \cdot m^{-4}$, L=3.5 nm. Insert: interaction force barriers and adhesive forces measured at loading forces of 8~10 mN/m as a function of solution pH.

7.2.3 Effect of electrolyte concentration

At solution pH 8.2, the colloidal force between bitumen-bitumen surfaces was measured as a function of KCl concentration. As shown in Figure 7.4, increasing potassium chloride (KCl) concentration depresses repulsive long-range forces and adhesive forces significantly.

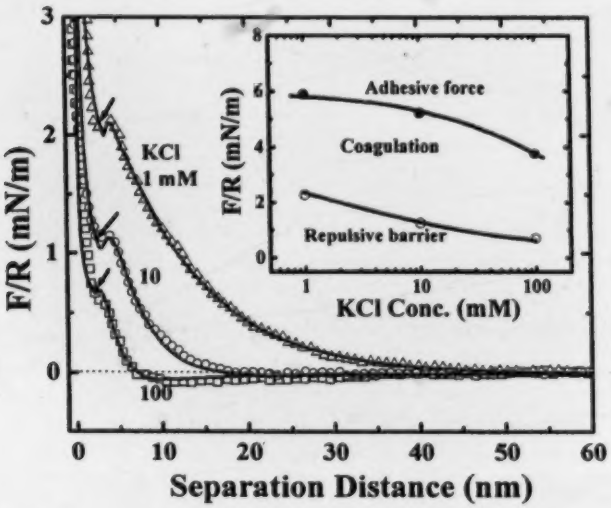

Figure 7.4 Normalized interaction forces (F/R) between bitumen surfaces as a function of separation distance in KCl solutions at pH 8.2. Solid lines represent the fitting of the extended DLVO theory using A_{131}=2.8x10^{-21} J with the best-fitted decay length, Stern potential, hydrophobic force constant K, macromolecule density factor f and tail length L being: 1 mM KCl (up triangle) - $\kappa^{-1} = 9.4\ nm$, ψ_B=-74 mV, K =10x10^{-20} J, f =8x10^{-6} $N \cdot nm \cdot K^{-1} \cdot m^{-4}$, L=3 nm; 10 mM KCl (circle) - $\kappa^{-1} = 3.4\ nm$, ψ_B=-58 mV, K =10x10^{-20} J, f =50x10^{-6} $N \cdot nm \cdot K^{-1} \cdot m^{-4}$, L=2.5 nm; 100 mM KCl (square) - $\kappa^{-1} = 1.2\ nm$, ψ_B=-45 mV, K =7x10^{-20} J, f =120x10^{-6} $N \cdot nm \cdot K^{-1} \cdot m^{-4}$, L=2 nm. Insert: interaction force barriers and adhesive forces measured at loading forces of 8~10 mN/m as a function of KCl concentration.

In a solution containing 1 or 10 mM KCl, the long-range force shows a monotonic repulsion at a separation distance of greater than 5 nm and a jump-in at a separation

distance of 5 nm, with a strong repulsion at a separation distance of less than 4 nm. However, in the solution containing 100 mM KCl, a weakly attractive force at a separation distance of 8~20 nm, a repulsive force at a separation distance of less than 8 nm, a jump-in at separation of 4 nm, and another strong repulsion at separation distance of less than 3 nm are observed. The magnitude and range of interaction forces decrease with increasing salt concentration, demonstrating the compression of the electric double layer by salt addition. As shown by the insert of Figure 7.4, the adhesive force also decreases from 5.8 mN/m in a 1 mM KCl solution to 3.5 mN/m in a 100 mM KCl solution. These results suggest that although bitumen droplets in higher salinity environment easily coagulate to each other, the aggregates are readily broken down due to the low adhesive forces.

7.2.4 Effect of calcium addition

Calcium ions can not only compress the electric double layer, but also specifically adsorb on the bitumen surface to change bitumen surface properties. Therefore, a significant impact of calcium addition on the surface forces is expected. At pH 8.2, for example, the addition of calcium ions alters both the interaction force and adhesive force between bitumen surfaces in a 1 mM KCl solution, as shown in Figure 7.5. The repulsive force is reduced with increasing calcium ion addition while jump-ins at a separation of ca. 5nm remained. The adhesive force between the bitumen surfaces also decreases from 5.8 mN/m to 2 mN/m upon the addition of 1 mM calcium. The reduced adhesion is attributed to the saturated adsorption of calcium ions on the bitumen surface, as discussed in Chapter 5.

The reduction in the repulsive force barriers and the adhesive forces in the presence of calcium ions suggests that calcium addition would facilitate bitumen droplet coagulation, but cause aggregates to be readily broken down at same time.

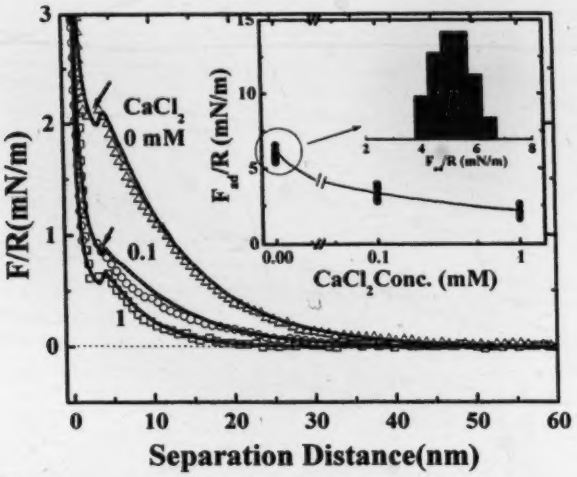

Figure 7.5 Normalized interaction forces (F/R) between bitumen surfaces as a function of separation distance in 1 mM KCl solutions containing $CaCl_2$ at pH 8.2. Solid lines represent the fitting of the extended DLVO theory using A_{131}=2.8x10^{-21} J with a best-fitted decay length, Stern potential, hydrophobic force constant K, macromolecule density factor f and tail length L being: 0 mM $CaCl_2$ (up triangles) - $\kappa^{-1} = 9.4\,nm$, ψ_B=-74 mV, K =10x10^{-20} J, f =8x10^{-6} $N \cdot nm \cdot K^{-1} \cdot m^{-4}$, L=3 nm; 0.1 mM $CaCl_2$ (circles) - $\kappa^{-1} = 8.3\,nm$, ψ_B=-41 mV, K =6x10^{-20} J, f =6x10^{-6} $N \cdot nm \cdot K^{-1} \cdot m^{-4}$, L=2.5 nm; 1 mM $CaCl_2$ (squares) - $\kappa^{-1} = 4.8\,nm$, ψ_B=-31 mV, K =3.5x10^{-20} J, f =3x10^{-6} $N \cdot nm \cdot K^{-1} \cdot m^{-4}$, L=2 nm. Insert: normalized adhesive forces (F_{ad}/R) measured at loading forces of 8~10 mN/m as a function of calcium ion concentration. Inner insert: distribution of normalized adhesive forces (F_{ad}/R) in a 1 mM KCl solution.

7.3 Interactions in the presence of montmorillonite clay

Since fine clay particles are always present in bitumen extraction systems, it is desirable to study interactions between bitumen surfaces in the presence of fines. For this reason, the forces between bitumen surfaces conditioned with montmorillonite clay suspensions were measured. Montmorillonite clay suspension was prepared by dispersing ground montmorillonite clays in water at a concentration of 0.1 wt% under ultrasonication for 10 minutes, followed by settling for 6 hours to remove any coarse particles. The supernatant

was used to condition bitumen surfaces. During force measurement, the supernatant was first injected into the fluid cell in AFM to contact the bitumen surfaces for about half an hour, and was then replaced with a clear electrolyte solution to minimize the disturbance from suspended solids in the medium. With this procedure, the measured force profiles reflect the interactions of bitumen surfaces after contacting montmorillonite suspensions. The measurements for a given bitumen-bitumen pair were repeated with different spots on the substrate, and the most repeatable one was chosen to represent the force profile for this bitumen-bitumen pair. For each given condition, at least eight force profiles from at least eight bitumen-bitumen pairs were reported.

7.3.1 In the absence of calcium ions

The bitumen surface was conditioned with a 0.1 % fine montmorillonite clay suspension containing 1 mM KCl in the absence of calcium ions. The measured colloidal surface forces are shown in Figure 7.6.

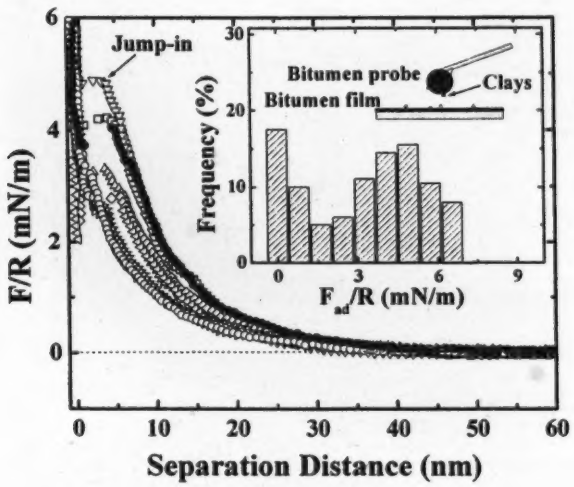

Figure 7.6 Normalized interaction forces (F/R) between bitumen surfaces as a function of separation distance in 1 mM KCl solutions at pH 8.2. The surfaces are conditioned before AFM force measurement with a 0.1 % montmorillonite suspension containing 1 mM KCl. Insert: distribution of normalized adhesive forces (F_{ad}/R) measured at loading forces of 8~10 mN/m.

It is evident that the force profiles from different pairs are highly variable; indicating a statistical nature of contact positions resulting from the presence of deposited clay particles, as shown from the inner insert of Figure 7.6. Nevertheless, it is evident that the repulsive forces between bitumen-bitumen surfaces conditioned by montmorillonite suspensions are substantially increased. To account for the very strong repulsive forces, one needs to assume some coverage of fine montmorillonite clay particles on the bitumen surface. It is interesting to note that in some cases, a noticeable "jump-in" is observed after encountering a strong repulsive force barrier at a separation distance of 5~8 nm, shown by the arrows in Figure 7.6. The observed sudden "jump-in" after encountering a strong repulsive force barrier cannot be explained by either van der Waals or hydrophobic forces. A possible explanation is that the montmorillonite clay particles deposit weakly and sparsely on the bitumen surface. This is plausible since only the amphoteric edge of layer-structured clay particles is amenable for deposition on the negatively charged bitumen surface and the edge accounts for only 1 % of the total surface area of particles (Sondi et al., 1996, 1997). As schematically illustrated in Figure 7.6, the weakly and sparsely bound clay particles on bitumen surfaces are pushed laterally under a threshold force applied by the AFM cantilever when the two surfaces are brought close to each other. A similar observation was reported when forces are measured between an AFM tip and a mica surface bearing adsorbed aggregates of DTAB (Ducker and Wanless, 1996). The observed "jump-in" after encountering a strong repulsive force was attributed to the "squeezing out" of the surfactant aggregates. The presence of montmorillonite clay particles on the bitumen surface can be further inferred from the distribution nature of the measured adhesive force. Compared with the adhesive force distribution measured between bitumen surfaces without conditioned by clay suspensions as shown in the inner inset of Figure 7.5, the adhesive forces between bitumen surfaces conditioned by montmorillonite clay suspensions are much more widely distributed as shown in the insert of Figure 7.7. The adhesive forces between bitumen surfaces conditioned with the clay suspensions are mostly distributed in the range of 4~7 mN/m, a range very similar to the case observed in the absence of fines. However, in a number of cases, the measured adhesive forces decrease all the way to zero, which can be attributed to the deposition of some clays on the bitumen surfaces. The observed wide

variation of adhesive forces further confirms the weakness and sparseness of montmorillonite particle deposition on the bitumen surface. The results of force profiles clearly indicate that conditioning bitumen surfaces with 0.1 % montmorillonite clay suspension can, to a small extent, increase the repulsive force barriers and diminish the adhesive forces between bitumen surfaces. This implies that the presence of montmorillonite particles in the suspension without the addition of calcium ions has only a weak impact on the bitumen-bitumen interactions.

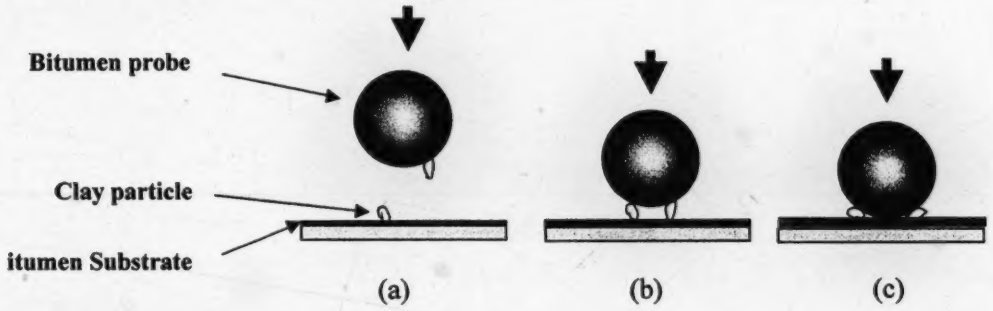

Figure 7.7 Schematics of possible interactions between bitumen surfaces after conditioning with 0.1 % montmorillonite suspension containing 1 mM KCl at pH 8.2 in AFM. (a) Approaching with sparse montmorillonite particles attached weakly on the bitumen surface; (b) initial contact; and (c) "jump-in" when "squeezing-out" of montmorillonite particle under threshold forces.

7.3.2 In the presence of calcium ions

When bitumen surfaces are conditioned with 0.1 % montmorillonite clay suspensions containing 1 mM calcium ions, the force profiles between the bitumen surfaces become monotonically repulsive without "jump-in", as shown in Figure 7.8. With calcium ion addition, the range of the repulsion is reduced substantially. The force profiles cannot be fitted with the classical or extended DLVO theory. The adhesive forces, on the other hand, are reduced significantly, in most cases to zero, as shown in the insert of Figure 7.8. Compared with Figures 7.5 and 7.6, the absence of "jump-in" in the force profiles of Figure 7.8 and reduction in the adhesive force imply a strong and dense deposition of montmorillonite clay particles on bitumen surface in the presence of 1mM calcium ions,

as depicted in the insert of Figure 7.8. Since both the edge and basal plane of montmorillonite particles can attach to the bitumen surface with calcium ions as a bridge, the strongly coated clay particles cannot be squeezed out under the limited force provided by the AFM cantilever anymore. As a result, the bitumen surface bearing densely coated montmorillonite particles becomes clay-like. The finding indicates that the montmorillonite fines in the presence of calcium would greatly hinder the coagulation of bitumen droplets and air-bitumen attachment. The strong attachment of montmorillonite to bitumen in the presence of calcium ions will be further illustrated in Chapter 8.

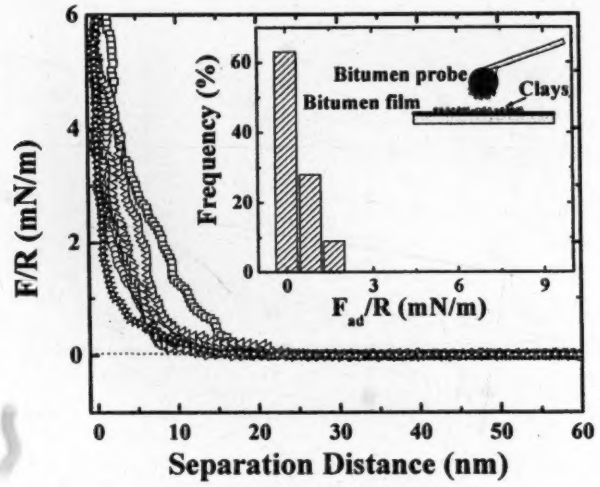

Figure 7.8 Normalized interaction forces (F/R) between bitumen surfaces as a function of separation distance in 1 mM KCl solution containing 1 mM $CaCl_2$ at pH 8.2. The surfaces are conditioned before AFM force measurement with a 0.1 % montmorillonite suspension containing 1 mM KCl and 1 mM $CaCl_2$. Insert: distribution of normalized adhesive forces (F_{ad} / R) measured at loading forces of 8~10 mN/m.

7.4 Data fitting and nature of colloidal force

To better control the forces, it is beneficial to understand the nature of the forces operating in a given system. For this purpose, data fitting of the measured force profiles with DLVO and extended DLVO theory, by considering a hydrophobic force and a steric force, were carried out. Constant surface charge density was set as the boundary

condition for bitumen surfaces in solving non-linear Poisson-Boltzmann equation. The general fitting procedure is described in Chapter 4 and Appendices D and E. Figure 7.9 is an example for fitting a typical measured force profile between bitumen surfaces in a 1mM KCl solution at pH 5.7. As shown by one of the dotted line in Figure 7.9, the force profile at separation distance of greater than ca.18 nm can be described well with the classical DLVO theory. At separation distance of less than 18 nm, however, a noticeable deviation of force profile from the classical DLVO theory is observed. To best fit the data, as shown by the solid line in Figure 7.6, an extra attractive force has to be involved. To account for this additional attractive force, the contact angle of an air bubble on a bitumen surface in water is measured to be about 70^0. With such a contact angle value, the bitumen surfaces can be considered sufficiently hydrophobic to induce a hydrophobic force.

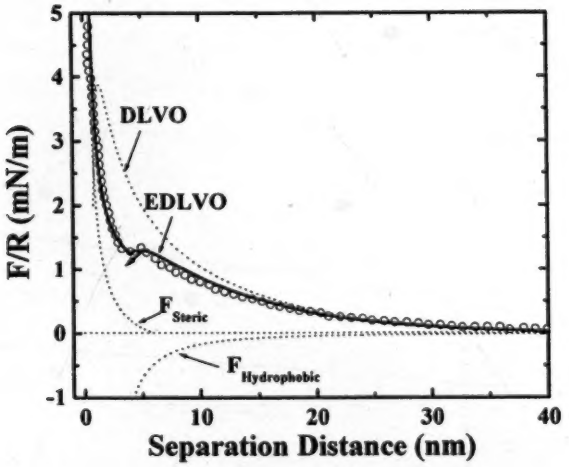

Figure 7.9 Normalized interaction forces (F/R) between bitumen surfaces as a function of separation distance in a 1 mM KCl solution at pH 5.7. Solid line represents the fitting of the extended DLVO theory using A_{131}=2.8x10^{-21} J with the best-fitted decay length, Stern potential, hydrophobic force constant K, macromolecule density factor f and tail length L being: κ^{-1} = 9.6 nm, ψ_B=-63 mV, K =10 x10^{-20} J, f =6x10^{-6} $N \cdot nm \cdot K^{-1} \cdot m^{-4}$, L=3 nm.

At very short separation range (less than 4~6 nm), a strong repulsive force is encountered after jump-in. The strong repulsion is contradictory to the attractive regime resulting from

the van der Waals forces and the hydrophobic force between bitumen surfaces. To account for this strong repulsion, the steric force originating from the macromolecules on the bitumen surface (Boukir et al., 2001; Zhang et al., 2003) need to be considered. The force profiles over this short separation range can be well described with Pincus scaling theory (equation 4-2). By including a hydrophobic attraction and a steric repulsion, the extended DLVO theory shown by solid line in Figure 7.9 describes the measured force profile exceptionally well.

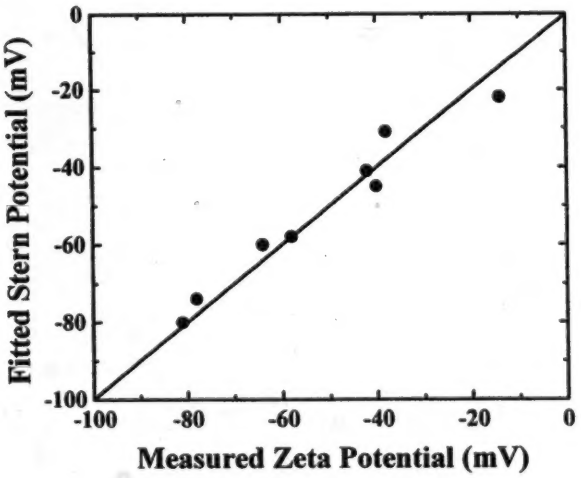

Figure 7.10 Comparison of the best-fitted Stern potentials from the measured force profiles with the extended DLVO theory and the measured corresponding zeta potentials of bitumen droplets.

Similar fitting procedures are applied to all the measured force profiles. As shown by the solid lines in Figures 7.3~5, the colloidal force profiles between bitumen surfaces in the *absence* of the fines can be reasonably described with the extended DLVO theory. The fitted Debye decay lengths (κ^{-1}) agree well with those calculated using the Debye-Huckel theory for the electrolyte concentrations as used in the experiments. Furthermore, the measured zeta potentials of bitumen (Figure 5.2) are in good agreement with the fitted Stern potentials as shown in Figure 7.10. This implies that the repulsion component in the long-range forces at separation distance of greater than 4~6 nm arise from the electrostatic double layer force. The best-fitted hydrophobic force constant (K) values

exhibit a good correlation to the measured contact angles, as shown in Figure 7.11. For example, a bitumen surface with a contact angle of 65~75^0 corresponds to a hydrophobic force constant K of 10x10^{-20} J. This constant value is much greater than Hamaker constant A_{131} (0.28x10^{-20} J), implying that the hydrophobic force is much greater than the van der Waals forces in this case. Yoon et al. (1997) obtained a similar value (7~20x10^{-20}J) for a pair of silanated silica surfaces with a contact angle of 81^0. The agreement between the K values obtained from two completely different systems indirectly confirms that the detected attractive component in the long-range forces do arise from the hydrophobicity of the bitumen surfaces. Reflected by the reduced K values, the hydrophobic forces are found to decrease with increasing solution pH and divalent electrolyte concentration. These variations can be anticipated. For example, increasing solution pH would ionize more organic acid groups, which in turn reduces the surface hydrophobicity. With the addition of calcium, the bitumen surface can adsorb calcium ions through reacting with carboxylate groups on the bitumen surface. In this case, the adsorbed cations are of hydrophilicity, which in turn reduce the hydrophobicity of the bitumen surface.

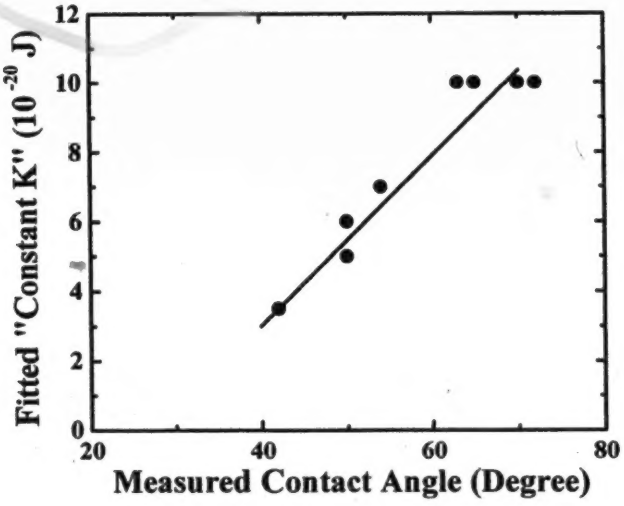

Figure 7.11 Comparison of the values of best-fitted hydrophobic force constant K from the measured force profiles with the extended DLVO theory and the measured contact angle values of air bubbles on the bitumen surface in aqueous solution.

The fitted macromolecule tail length L and density factor *f* for steric forces are found to vary with solution pH, salinity and calcium addition. For example, the fitted tail length L increases as increasing solution pH, as shown in Figure 7.12. The fitted tail length L in the current system is about 2~4 nm. These values are the same as those obtained from the system of bitumen and silica (Figure 6.10 in Chapter 6). This finding further confirms that the strong repulsion at short range is of steric force originating from the brush-like bitumen surface. However, these repulsions occur over a much shorter separation range than those reported by Yoon et al. (1995, 1999). The difference can be attributed to the different methods used in preparing bitumen surfaces. In Yoon's work, bitumen surfaces were prepared by an L-B deposition method, in contrast to our dip-coating and spin-coating methods. It is likely that asphaltene aggregates dominate the prepared bitumen monolayer in Yoon's work. For the bitumen film prepared by the dip-coating or spin-coating method, asphaltene aggregates are embedded in maltene component and therefore less or small protrusions are present. As a result, the steric force arising from protrusions of asphaltene aggregates would be of shorter range between bitumen surfaces prepared with spin-coating or spin-coating than between bitumen surfaces with L-B depositing.

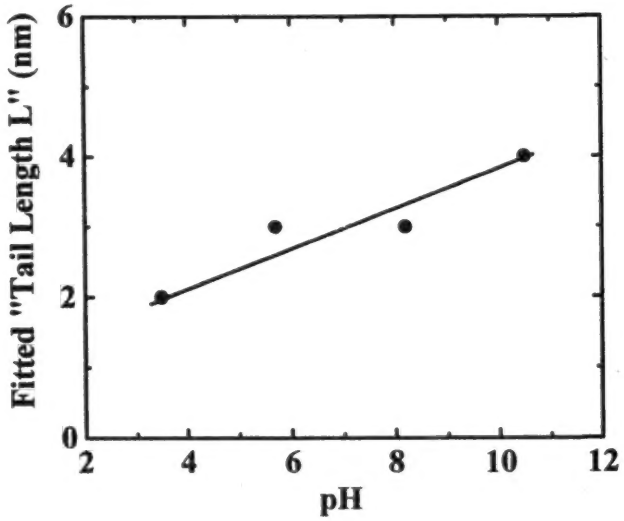

Figure 7.12 The best-fitted macromolecule "Tail Length L" for steric force from the measured force profiles with the extended DLVO theory as a function of solution pH.

The good fit of the measured force profiles with the extended DLVO theory confirms that both electrostatic double layer forces and hydrophobic forces play a dominant role in controlling the interactions between bitumen surfaces. The implication here is that we can control the bitumen coagulation behavior through monitoring the electrostatic double layer force and hydrophobic force. Since the electrostatic double layer force in terms of zeta potential and the hydrophobic force in terms of contact angle are greatly affected by solution pH and calcium addition, we can control the bitumen coagulation behavior by adjusting solution pH and calcium ion concentration.

Attempts are also made to fit the measured force profiles between bitumen surfaces conditioned by montmorillonite suspensions. Unfortunately, no satisfactory fitting could be obtained with either the classical DLVO theory or the extended DLVO theory. The lack of fitting is attributed to the deposition of clay particles on bitumen surfaces, which will be further studied in Chapter 8.

7.5 Nature of adhesive force

Adhesive force results from the molecular or atomic interaction between two surfaces in contact. To quantitatively describe the adhesive forces, a few contact mechanic theories (Johnson et al., 1971; Derjaguin et al., 1975; Meyer et al., 1998; Burnham and Kulik, 1999) were developed. According to these theories, the adhesive force equation (4-2) can be simplified as a function of the bitumen/water interfacial tension, γ_{BW}.

$$\frac{F_{ad}}{R} = 2m\gamma_{BW} \tag{7-1}$$

where m is the coefficient ranged from $\pi \sim 2\pi$. In AFM measurement, however, the contact time (typically 0.1s) is too short for the contact system to reach equilibrium, therefore a much lower coefficient m is expected. This equation can qualitatively explain the measured adhesive forces. The normalized adhesive force has a linear relation to the interfacial tension at bitumen/water. According to Moran et al.'s report (2000), the interfacial tension γ_{BW} at the bitumen/water interface is strongly pH-dependent. Values reported were with 23 mN/m at pH 3.5 diminishing to 1 mN/m at pH 10.5. These two sets of data do have a good linear relationship, with coefficient m being 0.25.

7.6 Relevance to the oil sands industry

The surface force measurements show that the coagulation of bitumen droplets is impacted by the solution pH, salinity, divalent calcium addition and the presence of fine clays. For example, a lower pH corresponds to a weaker repulsion and stronger adhesive force between bitumen droplets, which is favorable for bitumen coagulation. However, higher pH is needed for oil sands digestion as well as mitigation of slime coating (hetero-coagulation between bitumen and fines) (Hepler and Hsi, 1989; Hepler and Smith, 1994; Chapter 6, 8, 9). The results justify a need for choosing an optimal solution pH for bitumen extraction in commercial operations. These findings are consistent with the other reports (Sanford, 1983; Dai and Chung, 1996) stating that a critical NaOH amount was needed to achieve optimal effect. Over-dose of NaOH would cause bitumen to emulsify and result in small size bitumen droplets, which are unfavorable for bitumen aeration.

The reduction in the repulsive force barrier in the presence of calcium leads us to conclude that in the absence of fines the presence of calcium ions would be favorable for bitumen droplet coagulation. However, in a commercial system, the fines are always present. In the presence of fines, calcium can cause clay fines to strongly attach to the bitumen surface and this hinders the coagulation between bitumen droplets. From the bitumen extraction perspective, the presence of montmorillonite clays on bitumen in the presence of 1 mM calcium would set up an obstacle for bitumen droplet coagulation and attachment to air bubbles. These effects lead to a poor "aeration" during bitumen extraction.

7.7 Summary of chapter

- AFM can be used to investigate the colloidal interactions between bitumen surfaces. The results clearly show that the solution pH, salinity, calcium and montmorillonite clay addition have a significant impact on both the long-range forces and adhesive forces.

- The lower solution pH corresponds to a weaker repulsive force and a stronger adhesive force, which is favorable for bitumen droplet coagulation. Higher concentration of monovalent (KCl) and divalent cation (Ca^{2+}) can substantially

reduce both the repulsive and the adhesive forces. The presence of montmorillonite clays causes a strong repulsive force and a weaker adhesive force between bitumen surfaces, particularly in the presence of 1 mM calcium, which is unfavorable for bitumen droplet coagulation.

- In the absence of clay fines, the measured force profiles at separation of greater than 4~6 nm can be well described with the extended DLVO theory by considering a hydrophobic force. The fitted Debye lengths and Stern potentials are in an excellent agreement with those calculated and measured, respectively. The fitted hydrophobic force constant K values correlate well with the values of contact angle measured. Deviation from the classical DLVO theory is observed at separations less than 4~6 nm, which is attributed to a short-range steric repulsion.

- The results show that the electrostatic double layer force, hydrophobic force and the presence of clay fines play dominant roles in the interactions between bitumen surfaces.

CHAPTER 8 INTERACTIONS BETWEEN BITUMEN AND CLAYS*

The colloidal interactions between bitumen and clays in aqueous solutions were studied with zeta potential distribution measurement and colloidal force measurement. The hetero-coagulation behaviors between bitumen-kaolinite and bitumen-montmorillonite with and without calcium addition were investigated. The zeta potential distribution peaks of the individual components (emulsified bitumen droplets or clay suspension) were compared with those of bitumen/clays mixture to identify the coagulative nature of clays with bitumen. The results show a stronger deposition of montmorillonite clays on the bitumen surface in the presence of 1 mM calcium. Such a deposition was *not* observed between bitumen and montmorillonite or kaolinite in the absence of calcium, or between bitumen and kaolinite in the presence of 1 mM calcium. Colloidal force measurements show that stronger adhesive forces exist between bitumen and montmorillonite than between bitumen and kaolinite, in particular when calcium ions are present, although long-range repulsive forces between bitumen-kaolinite and bitumen-montmorillonite are similar. The stronger adhesive forces are responsible for the stronger coagulation of bitumen with montmorillonite clay than with kaolinite clay when calcium ions are present. The results provide a fundamental understanding of slime coating in bitumen "aeration" and also demonstrate that zeta potential distribution measurement could be a powerful tool to study hetero-coagulation phenomena for complex colloidal systems.

8.1 Introduction

Fines are one of the important components in oil sand ores, especially in poor processing ores. Most of the fines in oil sand ores are clay minerals with kaolinite clays being the most representative. Although montmorillonite clays are present as a minor component, the behavior of montmorillonite clays with their unique surface properties cannot be overlooked. The significant impact of fine clays present in the slurry and water chemistry on oil sand ore processibility has been recognized both in industrial operations and in laboratory tests (Sanford et al., 1979, 1983; Takamura and Wallace, 1988; Hepler and

* A revised version of this chapter, co-authored by J. Liu, Z. Zhou, Z. Xu and J. Masliyah, has been published in *J Colloid Interface Sci*, Vol.252, 409-418, 2002.

Hsi, 1989; Smith and Schramm, 1992; Hepler and Smith, 1994; Zhou et al., 1998, 1999; Kasongo et al., 2000; Yang et al., 2000a, b; Gu et al., 2003; Masliyah et al., 2003). The coating of fine mineral solids on bitumen surfaces would lead to a decrease in hydrophobicity of bitumen surface, resulting in small sized bitumen droplets and a low bitumen "aeration" efficiency as shown in Figure 2.2b Due to the complex nature of oil sand ores, no conclusive guidelines are currently available as to whether it is the individual variables alone or in combination with others that play a dominant role in depressing bitumen recovery. To discern the role of ore characteristics and water chemistry in bitumen flotation, it is necessary to use an ideal and well-controlled experimental system. In such a system, the effect of each known variable, individually or in combination, on bitumen recovery can be isolated and their critical levels can be identified.

The early studies suggested that the depressed bitumen recovery by the addition of 1 mM calcium and 1 wt% montmorillonite clays is due to the hetero-coagulation of montmorillonite clays on bitumen surfaces (Kasongo et al., 2000; Yang et al., 2000a, b; Gu et al., 2003, Masliyah et al., 2003). To experimentally confirm this hypothetical depression mechanism, it would be instructive to examine *directly the interactions between bitumen and clays*. Although extensive research efforts have been devoted to visual observation of clay coatings on bitumen, little progress has been made due to experimental challenges. In this chapter, the novel method of zeta potential distribution measurement is used to investigate the fine clay coating on bitumen in aqueous solutions. Surface forces between bitumen and montmorillonite or kaolinite clays are also measured with an atomic force microscope to disclose the essence of the slime coating phenomenon. For the less well-defined clay particles (Figure 4.7), the surface force measurements were repeated with at least 8 bitumen-clay pairs and plotted together to show a general trend. The normalized force profiles are fitted with the classical DLVO theory using the combined Hamaker constant of 6.5×10^{-21} J (as described in Chapter 4).

8.2 Surface properties of clay mineral

As discussed in Chapter 5, montmorillonite and kaolinite clays have different structures and possess different surface properties. As shown in Figure 8.1, montmorillonite clays

exhibit a large capacity for cation adsorption from a solution than kaolinite. Adsorption tests were conducted by conditioning montmorillonite or kaolinite clays in a 1 mM calcium solution at 1 g/L (clay/solution). After conditioning for a given time, the suspension was filtered to remove the solids. The supernatant was then analyzed with the A.A. (Atomic Absorption) technique. The results show that one gram of montmorillonite clay can adsorb up to 10.5 mg calcium in 5 minutes from a 1 mM calcium solution, while one gram of kaolinite clay with a similar average particle size as montmorillonite clay can only adsorb 1.6 mg calcium in 500 minutes.

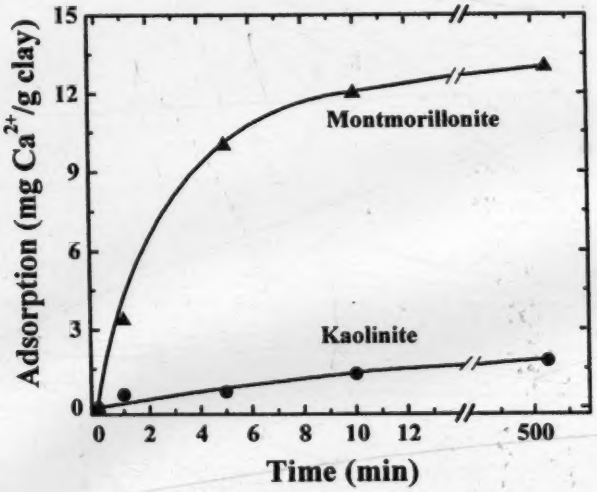

Figure 8.1 Calcium adsorption on clay minerals as a function of time in solutions containing initially 1 mM $CaCl_2$ at a solid to liquid ratio of 1g/L.

Similarly, there are great differences in zeta potentials of kaolinite and montmorillonite clays, as presented in Chapter 5. These differences in surface properties lead to the different coagulative behaviors between bitumen and montmorillonite or kaolinite clays.

8.3 Zeta potential distribution measurement

From zeta potential distribution measurement using single component emulsions or suspensions (see Chapter 5), it is evident that bitumen emulsions feature their own electrokinetics, which are significantly different from those for kaolinite and

montmorillonite clay suspensions. Therefore, tracking the electrokinetic distributions of individual sample and the mixture of bitumen emulsion and clay suspension could be a convenient, yet powerful means to investigate their interactions. Since industrial bitumen extraction is performed in a pulp of pH around 8.2, this pH was chosen for the investigation of bitumen-clay interactions using zeta potential distribution measurement.

8.3.1 Bitumen-montmorillonite clay

Zeta potential distributions of bitumen emulsions and montmorillonite clays measured separately in 1 mM KCl solution at pH 8.2 are overlaid in Figure 8.2a. Both bitumen droplets and montmorillonite clay particles exhibits a net negative zeta potential with the distribution peaks centered at -73 and -23 mV, respectively. The zeta potential distribution measured with a mixture of bitumen emulsion and montmorillonite clay suspension at a clay to bitumen mass ratio of 1:1 exhibits two distinct distribution peaks centered at -59 and -24 mV as shown in Figure 8.2b. The distribution peak at -24 mV is almost identical to the value measured with montmorillonite clay suspension alone. However, the peak at -73 mV measured for bitumen emulsion alone shifts significantly to -59 mV, in the direction towards the distribution peak of montmorillonite clay particles. The distribution peak of -59 mV is much broader, indicating a more heterogeneous nature of the clay-coated bitumen droplets. The observed peak shift and broadening appear to suggest a partial coating of montmorillonite clay particles on bitumen droplets. The results obtained here suggest a weak coagulation between bitumen droplets and montmorillonite clay particles at a mass ratio of 1:1 in a 1 mM KCl solution at pH 8.2, as schematically shown in the insert of Figure 4.5e.

Since calcium ions are often present in oil sand industrial extraction system, it is interesting to examine the effect of calcium addition on the interactions between bitumen droplets and montmorillonite clay particles. The zeta potential distributions measured with a bitumen emulsion and a montmorillonite clay suspension in a 1 mM KCl solution containing 1 mM calcium ions at pH 8.2 are overlaid in Figure 8.3a. Both bitumen droplets and montmorillonite clay particles exhibit new zeta potential distribution peaks centered at -38 and -9 mV, respectively, due to the double layer suppression and specific adsorption of calcium ions. Such a reduction in the magnitude of zeta potentials is

anticipated to diminish the repulsive energy barrier to facilitate both homo- and hetero-coagulation. Furthermore, the adsorption of calcium ions on both bitumen and montmorillonite surface could trigger a strong coagulation between them with calcium ions acting as a bridge. To confirm this hypothesis, the zeta potential distribution of a bitumen emulsion and a montmorillonite clay suspension binary mixture at a 1:1 mass ratio was measured under similar conditions. As shown in Figure 8.3b, a single distribution peak centered at -13 mV is observed for the mixture. This peak position is close to the value for montmorillonite clay suspension measured alone under the same condition. It is evident that under this condition, a sufficient number of montmorillonite clay particles are strongly deposited on the bitumen surface to cause a full surface coverage. This is equivalent to the case shown in Figure 4.5c. By comparing Figures 8.2 with 8.3, it is not difficult to conclude that zeta potential distribution measurement is a powerful tool for studying colloidal particle interactions. The conclusion derived from this measurement is that calcium ions activate slime coating of fine montmorillonite clay particles on the surface of bitumen droplets.

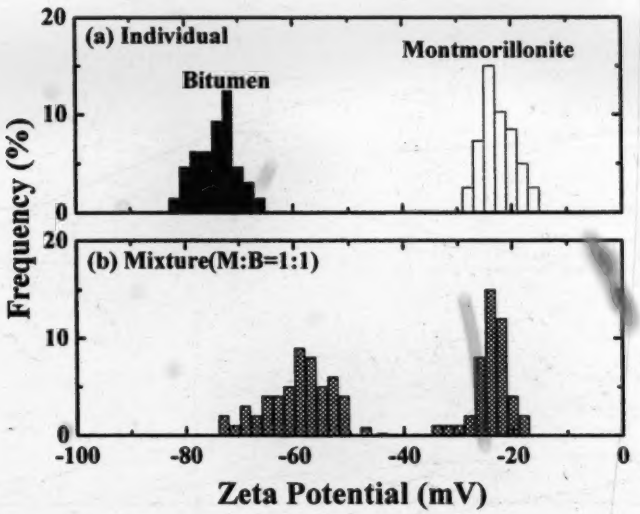

Figure 8.2 Zeta potential distributions in 1 mM KCl solutions at pH 8.2. (a) Individual bitumen emulsion and montmorillonite clay suspension; and (b) their mixture at a mass ratio of 1:1.

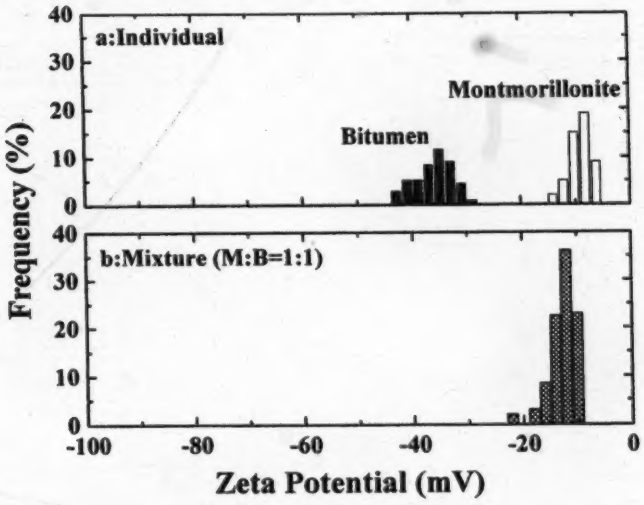

Figure 8.3 Zeta potential distributions in 1 mM KCl solutions containing 1 mM $CaCl_2$ at pH 8.2. (a) Individual bitumen emulsion and montmorillonite clay suspension; and (b) their mixture at a mass ratio of 1:1.

To further explore the capabilities of the technique, the zeta potential distributions of the binary mixture at various mass ratios of bitumen to montmorillonite clay are measured in 1 mM KCl solutions containing 1 mM calcium at solution pH 8.2. The results in Figure 8.4a show that even at a ratio as low as 0.05:1, a single modal zeta potential distribution is observed, although a much broader distribution peak exists at around -28 mV. This is an equivalent case to that shown in Figure 4.5d, confirming a strong attraction between bitumen and montmorillonite clay particles and suggesting an insufficient amount of montmorillonite clay particles in the suspension to fully cover the bitumen droplets. Under this condition, the bitumen droplets are only partially covered by montmorillonite clay particles as illustrated in the insert of Figure 4.5d. An increase in montmorillonite clay to bitumen mass ratio to 0.5:1 forms a single zeta potential distribution peak centered at -15 mV as seen in Figure 8.4c. This value is much closer to the value obtained with single montmorillonite clay suspension as shown in Figure 8.4a. It is evident that under this condition, bitumen droplets are close to being fully covered by montmorillonite clay particles. By further increasing in the mass ratio of montmorillonite

clay to bitumen to 1:1, only a marginal change in the position of the single zeta potential distribution peak occurs, which is centered at the same zeta potential value of -13 mV as measured with montmorillonite clay suspension alone. It is interesting to note that at this ratio, the measured distribution is almost identical to that obtained with montmorillonite suspension alone, in terms of not only peak position but also range of distribution, suggesting an excess of montmorillonite particles. The current finding corresponds well with the bitumen floatation results obtained by adding 1 wt% of montmorillonite and 40 ppm calcium ions (Kasongo et al., 2000). Both the depressed bitumen flotation and the observed single zeta potential distribution peak at the location for the montmorillonite suspension under the same conditions suggest that bitumen droplets in the flotation process are covered by montmorillonite clays to such an extent that the bitumen surface becomes montmorillonite-like to air bubbles, thereby bitumen is unable to be aerated and floated.

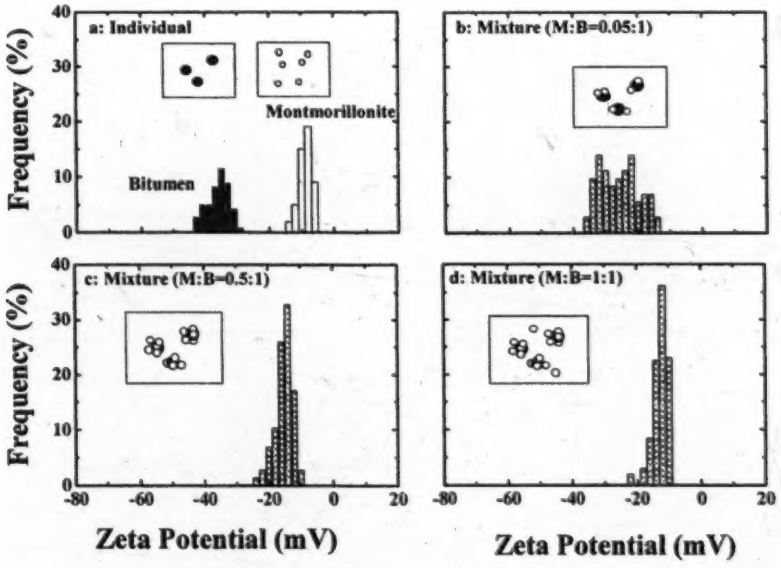

Figure 8.4 Effect of the mass ratio of montmorillonite clays to bitumen on zeta potential distributions measured in 1 mM KCl solutions containing 1 mM $CaCl_2$ at pH 8.2.

The peak position of the measured single modal zeta potential distribution in Figure 8.4 can be summarized in Figure 8.5 as a function of montmorillonite clays to bitumen ratio. From this figure, it is clear that the measured distribution peak position of the mixture decreases from the original value for bitumen alone towards the value corresponding to montmorillonite clay suspension alone. The required montmorillonite clay to bitumen ratio for near complete surface coverage of montmorillonite clay particles on bitumen can be readily determined as 1:1.

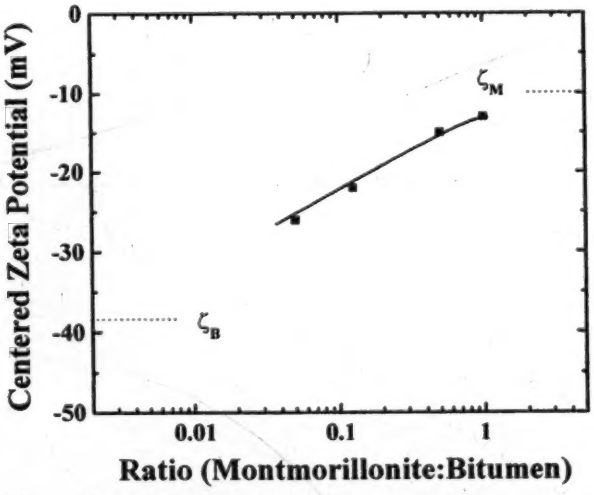

Figure 8.5 Peak position of single modal zeta potential distribution measured with a mixture of montmorillonite clay suspension and bitumen emulsion at different mass ratios. The measurement is conducted in 1 mM KCl solutions containing 1 mM $CaCl_2$ at pH 8.2.

8.3.2 Bitumen-kaolinite clay

The zeta potential distribution of kaolinite clay suspension alone measured in a 1 mM KCl solution at pH 8.2 is superimposed on the zeta potential distribution histogram of bitumen emulsion in Figure 8.6a. The zeta potential distribution of the kaolinite clay suspension is centered at -28 mV. When the zeta potential distribution is measured with a binary mixture at a kaolinite clay to bitumen mass ratio of 1:1, two distinct distribution peaks are obtained as shown in Figure 8.6b. The shape of the distribution peaks remains

invariant from those measured with the bitumen emulsion and kaolinite suspension separately, but the peak positions moves towards each other in the case of the mixture. Considering the similar distribution peaks in the two cases, the observed shift in distribution peak position can be well accounted for by the hydrodynamic retardation and enhancement as explained in Figure 4.5b. As in the case of the mixture of bitumen emulsion and montmorillonite clay suspension without calcium addition, the measured zeta potential distributions clearly indicate a marginal, if there is any, hetero-coagulation between bitumen droplets and kaolinite clay particles.

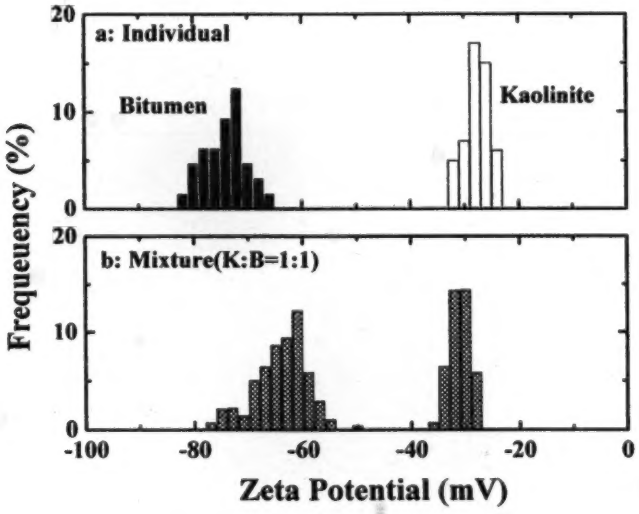

Figure 8.6 Zeta potential distributions in 1 mM KCl solutions at pH 8.2. (a) Individual bitumen emulsion and kaolinite clay suspension; and (b) their mixture at a mass ratio of 1:1.

With the addition of 1 mM calcium ions, the zeta potential distribution peak position of kaolinite clay suspension shifted from -28 mV to -15 mV as shown in Figure 8.7a. This shift is similar to that observed in the case of montmorillonite clay suspensions as shown in Figure 8.3a and one would expect a heterocoagulation between bitumen and kaolinite with calcium as a bridge as in the case of montmorillonite. When the bitumen emulsion and kaolinite suspension are mixed at a mass ratio 1:1 of clay to bitumen, two distinct zeta potential distribution peaks are observed as shown in Figure 8.7b. This is in distinct

contrast to the observations made with the mixture of bitumen emulsion and montmorillonite clay suspension (see Figure 8.3). Careful examination of the distribution in Figure 8.7b reveals that the peak corresponding to the original bitumen emulsion shifted substantially to -29 mV, indicating a partial coverage. This distribution feature suggests a system of weak coagulation between the two dispersed components, which is the case illustrated in Figure 4.5e. Considering that the binding strength of calcium ions with kaolinite is much weaker than with montmorillonite, a much weaker coagulation between bitumen and kaolinite is expected.

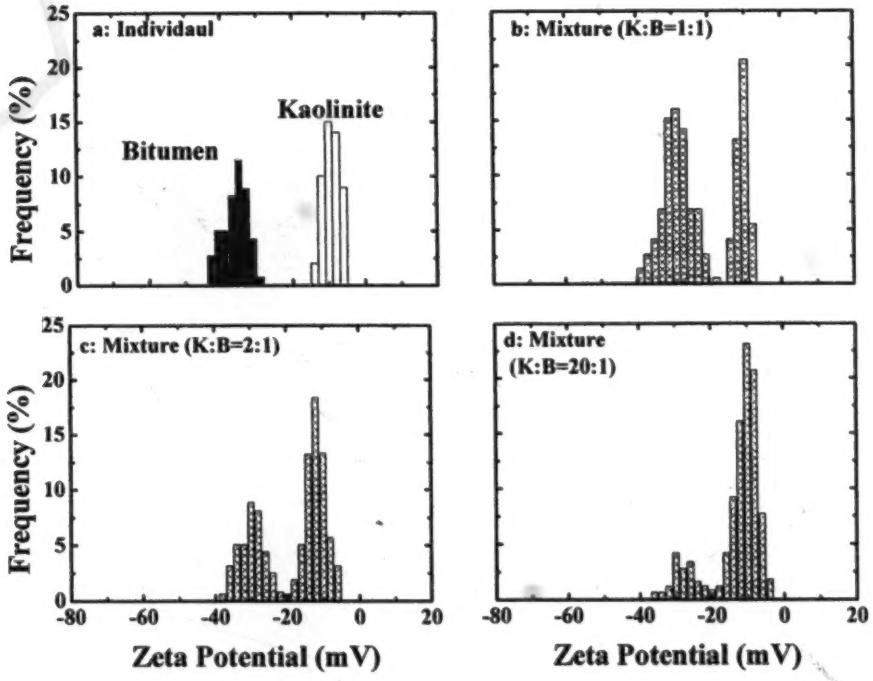

Figure 8.7 Effect of kaolinite clays to bitumen mass ratio on zeta potential distributions measured in 1 mM KCl solutions containing 1 mM $CaCl_2$ at pH 8.2.

To further confirm a weak interaction of bitumen with kaolinite, the zeta potential distribution measurements are performed at increased kaolinite clay to bitumen mass ratios. The results are shown in Figure 8.7c and 8.7d for a mass ratio of 2:1 and 20:1, respectively. For all the cases examined, a bimodal zeta potential distribution is obtained

although the distribution peak position corresponding to the original bitumen emulsion further shifted towards the value for the kaolinite clay suspension with increasing kaolinite to bitumen mass ratio. As anticipated, this finding indicates an increased slime coating of kaolinite clay particles on bitumen with increasing kaolinite clay to bitumen ratio.

8.3.3 Practical implication

The zeta potential distribution measurements presented above clearly demonstrate a more severe slime coating of bitumen by montmorillonite than by kaolinite clay particles, particularly when 1 mM calcium is added, suggesting a much stronger coagulation of bitumen with montmorillonite than with kaolinite. This finding bears a significant practical implication. In bitumen extraction (Kasongo et al., 2000), for example, it has been shown that doping a good oil sand ore with kaolinite clay, montmorillonite clay or calcium alone showed a marginal depression in bitumen recovery. This finding indicates that these components alone have little impact on bitumen flotation. Co-addition of kaolinite clay and calcium at pH 8 also did not show any substantial impact on bitumen recovery. In contrast, the combination of calcium > 30 ppm with montmorillonite clay at a much reduced montmorillonite clay to bitumen ratio suppressed bitumen recovery significantly, causing a reduction of bitumen recovery from above 90 % to below 70 %. This observation can be now confidently explained with the results of our zeta potential distribution measurements. In the case of kaolinite clay with or without calcium addition, the measured bimodal zeta potential distribution indicates at most a weak coagulation between the bitumen and kaolinite clay particles. In this case, the attached fraction of kaolinite clay particles partially covering the bitumen surface can be removed under the hydrodynamic conditions encountered in the bitumen flotation. As a result, the contact of air bubbles with solids-free regions on the bitumen surface leads to an effective air-bitumen attachment and hence flotation. In the case of montmorillonite clays, on the other hand, the addition of calcium initiates a strong coagulation between the bitumen and montmorillonite clay particles as confirmed by a single modal zeta potential distribution. The hydrophilic montmorillonite clay particles coated on bitumen surface prevent intimate contact of air bubbles with bitumen in a flotation system, resulting in low attachment efficiency and hence low bitumen flotation recovery. In this case, the

divalent cations are considered as a bridge or binder. Therefore a "bitumen-calcium-clay fines" model can be proposed, as shown in Figure 8.8

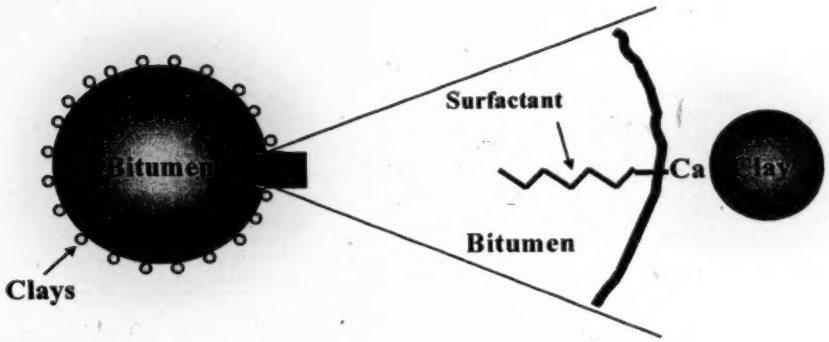

Figure 8.8 Schematics of calcium as a binder for the interaction between bitumen and clay fines.

8.4 Colloidal force measurement

Zeta potential distribution measurements can qualitatively describe the interaction between bitumen and clays. To further confirm the interaction mechanism, the surface force between bitumen and clay particles is directly measured using AFM.

8.4.1 Bitumen-montmorillonite clay

The measured force profiles for a number of bitumen-montmorillonite clay pairs are shown in Figure 8.9. In 1 mM KCl solutions at pH 8.2 without calcium addition (Figure 8.9a), the interaction forces are highly repulsive, setting up a barrier for montmorillonite clays to approach the bitumen surface. The presented force profiles are obtained with a number of different clay particles. As would be anticipated, the data are highly scattered. This is due to the variation of surface roughness of the clay particles, as shown in Figure 4.7c. From the larger number of measurements, the trend is clear and the general conclusion derived from the data is valid, as would be further illustrated with the measurements under different conditions. In 1 mM KCl solutions containing 1 mM calcium ions at pH 8.2 (Figure 8.9b), the long-range repulsive forces are depressed significantly. The substantially decreased force barrier suggests that a montmorillonite clay particle can easily approach a bitumen surface.

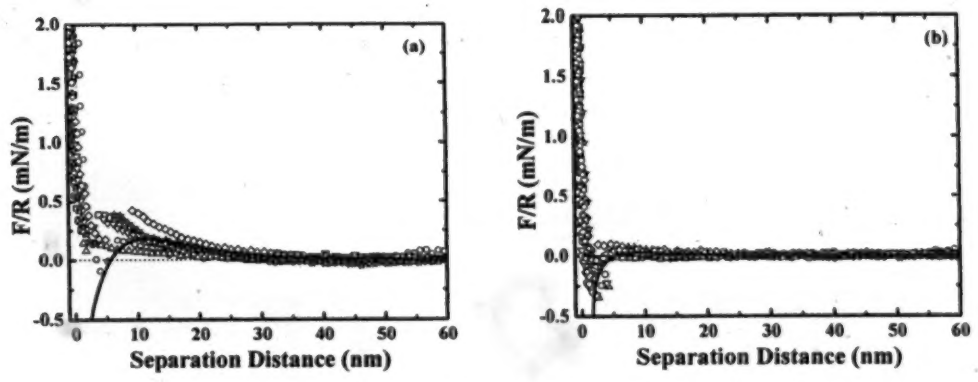

Figure 8.9 Normalized interaction forces (F/R) between bitumen and montmorillonite as a function of separation distance at pH 8.2. Solid lines represent the fitting of the classical DLVO theory using $A_{132}=6.5\times10^{-21}$ J with the best-fitted decay length and Stern potential being: (a) in 1 mM KCl solutions, $\kappa^{-1}=9.4\ nm$, ψ_B=-70 mV, ψ_M=-18 mV; and (b) in 1 mM KCl solutions containing 1 mM $CaCl_2$, $\kappa^{-1}=4.8\ nm$, ψ_B=-30 mV, ψ_M=-6 mV.

The normalized adhesive force distribution for a number of bitumen-montmorillonite clay pairs is shown in Figure 8.10. In 1 mM KCl solutions without calcium addition at pH 8.2 (Figure 8.10a), the adhesive force is centered at around 4 mN/m. Adding 1 mM calcium ions (Figure 8.10b) cause a significant increase in the adhesive force up to about 9 mN/m. The observed increase can be attributed to the fact that calcium ions strongly adsorb on both the montmorillonite clays (Figure 8.1) and bitumen surfaces as discussed in Chapter 5. These dual adsorption characteristics lead to bridging between bitumen and montmorillonite clay particles. The results clearly indicate that calcium addition can depress the repulsive force barrier and enhance the adhesive force between bitumen and montmorillonite clay particles, thereby facilitating slime coating of montmorillonite clay particles on the bitumen surface. This conclusion is consistent with observation from the zeta potential distribution measurement (Figure 8.4). The strong attachment of montmorillonite clays on the bitumen surface is also inferred from the measured force profiles between bitumen surfaces in the presence of montmorillonite clays, as discussed in Chapter 7.

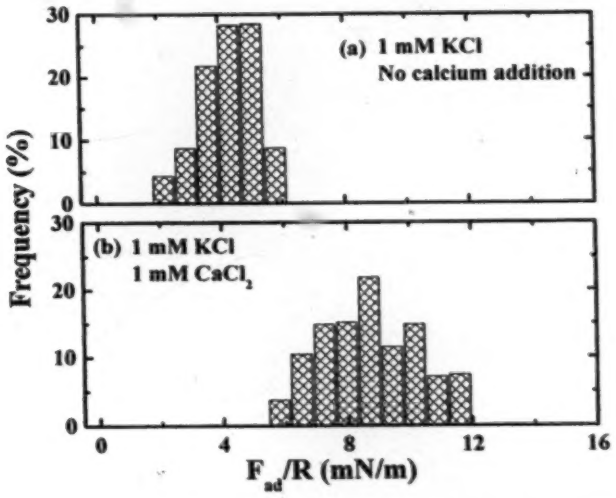

Figure 8.10 Distribution of normalized adhesive forces (F_{ad} / R) between bitumen and montmorillonite measured at loading forces of 8~10 mN/m. (a) In 1 mM KCl solutions; and (b) in 1 mM KCl solutions containing 1 mM $CaCl_2$.

8.4.2 Bitumen-Kaolinite clay

Between bitumen and kaolinite clays, strong repulsive forces are also observed in a 1mM KCl solution at pH 8.2 as shown in Figure 8.11a. By adding 1 mM calcium ions, the repulsive force is depressed to zero as shown in Figure 8.11b. From the consideration of long-range colloidal forces, one would expect kaolinite clay particles to coat the bitumen surface in the presence of calcium as is in the case of montmorillonite clays. However, zeta potential distribution measurements showed that, compared with montmorillonite clays, only a marginal slime coating of kaolinite on the bitumen surface is observed (Figures 8.6, 8.7; Kasongo et al., 2000; Yang et al., 2000a, b; Gu et al., 2003; Masliyah et al., 2003). To reconcile this apparent conflict, the adhesive forces have to be considered. As shown in Figure 8.12, the adhesive forces between bitumen and kaolinite clay particle range from 0 to 4mN/m, which is lower than that between the bitumen and montmorillonite clay particles. More importantly, calcium addition did not enhance the adhesive forces between the bitumen and kaolinite clay particles. This is probably due to the weaker adsorption of calcium on the kaolinite clay surface, compared with the case of montmorillonite. The present results indicate that kaolinite clay can only weakly attach to the bitumen surface even with calcium ion addition.

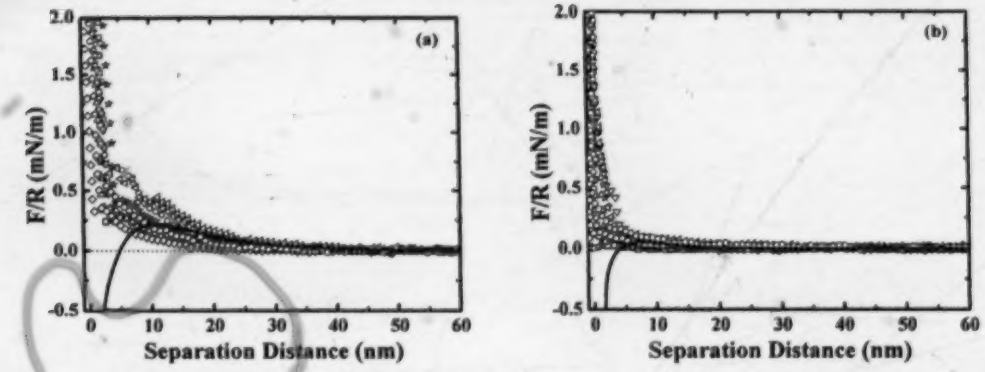

Figure 8.11 Normalized interaction forces (F/R) between bitumen and kaolinite as a function of separation distance at pH 8.2. Solid lines represent the fitting of the classical DLVO theory using A_{132}=6.5x10^{-21} J with the best-fitted decay length and Stern potential being: (a) in 1 mM KCl solutions, $\kappa^{-1} = 9.4\ nm$, ψ_B=-71 mV, ψ_K=-20 mV; and (b) in 1 mM KCl solutions containing 1 mM $CaCl_2$, $\kappa^{-1} = 4.8\ nm$, ψ_B=-32 mV, ψ_K=-8 mV.

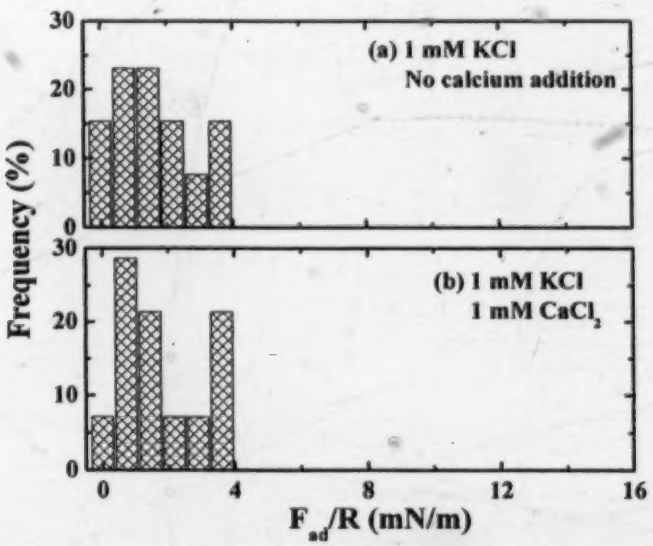

Figure 8.12 Distribution of normalized adhesive forces (F_{ad} / R) between bitumen and kaolinite measured at loading forces of 8~10 mN/m. (a) In 1 mM KCl solutions; and (b) in 1 mM KCl solutions containing 1mM $CaCl_2$.

8.4.3 Data fitting and implication

Although the force-distance profiles obtained from the surface force measurements show a large degree of scatter, the trends are clear and they shed a light on a complex industrial system. The measured force profiles were fitted by the classical DLVO theory with constant surface charge density for bitumen and constant surface potential for clays as boundary conditions. The force profiles at a separation of greater than 6~8 nm for a large number of bitumen-clay pairs can be predicted with the classical DLVO theory within the scatter range, as shown by solid lines running through the middle of scattered force profiles in Figure 8.9 and 8.11. The observed strong repulsion at a separation of less than 6~8 nm could be of steric origin as described in Chapters 6 and 7. The fitted Debye decay lengths (κ^{-1}) agree well with those calculated for the electrolyte concentrations used in the experiments. Furthermore, the fitted Stern potentials (see figure captions) are slightly smaller than the measured zeta potentials (see Chapter 5), as shown in Figure 8.13.

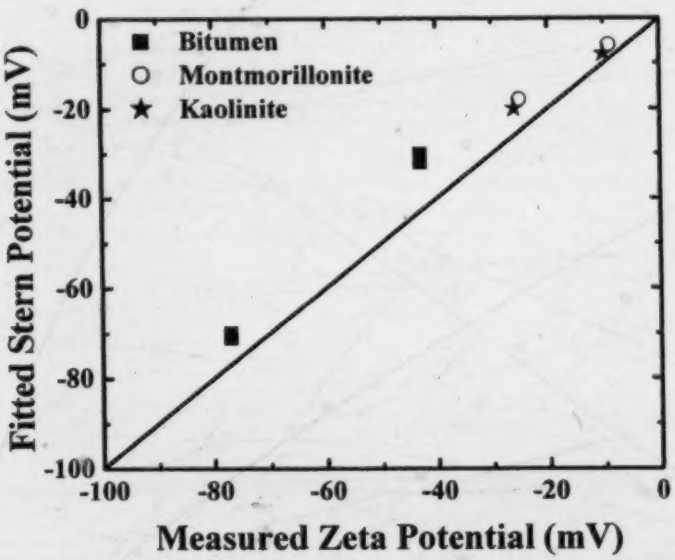

Figure 8.13 Comparison of the best-fitted Stern potentials of the measured force profiles with the classical theory and the measured corresponding zeta potentials of bitumen droplets (square symbols), montmorillonite (circle symbols) and kaolinite (star symbols).

Considering the roughness of the clays used in the force measurement, this level of discrepancy is expected. It is important to note that similar fittings with a boundary condition of constant surface charge density for both surfaces result in the fitted Stern potentials much smaller than the measured zeta potentials. The reasonable agreement implies that the electrostatic double layer force dominates the interactions between bitumen and clays. Strong slime coating of montmorillonite clays on the bitumen surface in the presence of 1 mM calcium is a good candidate as being the main cause for depressed bitumen recovery of poor processing ores containing high content of fines and divalent cations. It is anticipated that any changes that cause an increase in the electrostatic repulsion and reduction in adhesive forces between bitumen and clays by dispersant addition, such as sodium silicates or phosphates, would mitigate the depression of bitumen recovery by flotation.

8.5 Summary of chapter

The results in this chapter provide insights into the mechanism of slime coating and bitumen aeration in a model system. It is also demonstrated that the novel method based on the zeta potential distribution measurements developed in this thesis to study the interactions between bitumen and clays in aqueous solutions is simple, yet informative.

- Montmorillonite clay possesses some unique surface properties. It exhibits a large capacity for calcium ion adsorption, and a pH-independent zeta potential. Kaolinite, on the other hand, behaves as a typical mineral.

- Montmorillonite clays can weakly attach to a bitumen surface in the absence of calcium. With the addition of 1 mM calcium, montmorillonite clays attach strongly to the bitumen surface. The depressed electrostatic double layer forces and increased adhesion between the bitumen and montmorillonite clays in the presence of 1 mM calcium are responsible for the observed strong attachment, thereby presenting a barrier for bitumen droplets to coagulate with each other and to attach to air bubbles, leading to poor bitumen recovery.

- Kaolinite clays can only weakly attach to the bitumen surface in the absence or presence of calcium ions. Although the electrostatic double layer forces are

suppressed with the addition of 1 mM calcium, the weak adhesion between the two surfaces is responsible for weak attachment of kaolinite to bitumen.

- At a separation greater than 5~6 nm, the measured force profiles between bitumen and clays can be reasonably described with the classical DLVO theory. The electrostatic double layer force is the dominant force to control the interactions between bitumen and clays.

- The results interpreted from zeta potential distribution measurements are in excellent agreement with the predications from surface force measurement using AFM.

- The conclusions obtained further justify our mechanistic hypothesis for the observed depression of bitumen flotation by montmorillonite but not by kaolinite clay addition when calcium ions are added. This behavior accounts for the observed detrimental synergetic effect of montmorillonite clays and calcium ions on bitumen recovery by flotation.

CHAPTER 9 INTERACTIONS BETWEEN BITUMEN AND FINES*

The colloidal interactions between bitumen and fines, extracted directly from oil sand ores, were investigated with zeta potential distribution measurement and surface force measurement using an atomic force microscope (AFM). A solution containing 1 mM calcium was used as the probing medium to investigate the effect of calcium ions, while process water from a bitumen flotation system was used to represent real flotation medium. The zeta potential distribution peaks of the individual component (emulsified bitumen droplets or fines suspension) were compared with those of bitumen/fines mixtures and emulsified flotation froth to identify coagulative nature of the fines with bitumen. The results show that the fines from a poor processing ore attach to bitumen surface more strongly than fines from a good processing ore. The presence of calcium ions enhances the attachment of fines from the poor processing ore to bitumen. A similar enhancement was observed when the corresponding process water was used. The surface force measurements show that there is an attractive hydrophobic force between bitumen and fines collected from the poor processing ore, while such an attractive force between bitumen and the fines from the good processing ore is not identified. The higher content of divalent ions in the process water of the poor processing ore coupled with moderate surface hydrophobicity of the fines results in attractive long-range forces and strong adhesion between bitumen and the fines in a real flotation system. The strong attachment of the fines in the poor processing ore onto bitumen surface (slime coating) is responsible for the low bitumen flotation recovery of poor processing ores. Potential approaches to mitigate the slime coating are proposed.

9.1 Introduction

Bitumen extraction from a good processing ore with the HWE process is successful in a number of commercial operations and a total bitumen recovery above 93 % is not uncommon. However, there are many technical challenges in bitumen extraction from poor processing ores. For example, low bitumen recovery or/and poor froth quality is/are

* A revised version of this chapter, co-authored by J. Liu, Z. Xu and J. Masliyah, has been sumitted to *Can J Chem Eng*, Aug. 2003.

often experienced when processing poor processing ores. Normally, the fines content and divalent ion concentration in poor processing ores are much higher than these in good processing ores. The difference in the processibility between good and poor processing ores has been recognized both in industrial operations and in laboratory tests (Sanford and Seyer, 1979; Sanford, 1983; Takamura and Wallace, 1988; Smith and Scharmm, 1992). Understanding the difference would help find avenues for improving the processibility of poor processing ores.

In earlier studies, model systems were often used to investigate the role of mineral fines and water chemistry in bitumen flotation systems (Kasongo et al., 2000; Yang et al., 2000; Masliyah et al., 2003). In such systems, single mineral clays such as montmorillonite, kaolinite and illite were used as a model sample to represent fines so that the effect of individual operating parameters on oil sand ore processibility and bitumen-bubble interaction could be studied. The observed bitumen flotation recovery (Kasongo et al., 2000), consistent with bitumen-bubble attachment using impinging jet technique (Yang et al., 2000, Masliyah et al., 2003) and induction time (Gu et al., 2003) suggested that the depressed bitumen recovery by the addition of 1 mM calcium and 1 wt% montmorillonite clay is due to the hetero-coagulation of montmorillonite clays on bitumen surfaces. As presented in Chapter 8, zeta potential distribution measurement and surface force measurement have confirmed this hypothesis.

Although the earlier studies identified the role of model fine clays in bitumen extraction, the question remains whether these clays are representative of the fines in oil sand ores. Since the real mineral fines in oil sand ores are much more complex than single mineral clays, the role of real fines in oil sands processing needs to be validated. Therefore, it becomes necessary to study the colloidal interactions between bitumen and the fines directly extracted from real oil sand ores. In this chapter, the colloidal interactions between bitumen and fines are investigated using the methodology based on zeta potential distribution and surface force measurement. To investigate the effect of water chemistry on their interactions, three types of probing solutions were used. They were de-ionized water with 1 mM KCl, de-ionized water with 1 mM KCl and 1 mM calcium, and the process water from batch bitumen extraction tests. For the less well-defined fines

particles (Figure 4.7), the surface force measurements are repeated with at least 8 bitumen-fines pairs and plotted together to show a general trend. The normalized force profiles are fitted with the classical DLVO theory or extended DLVO theory with the combined Hamaker constant of 6.5×10^{-21} J (as described in Chapter 4).

9.2 Sample characterization

9.2.1 Justification of samples

To study the colloidal interactions between bitumen and fines in the context of bitumen extraction, it is better to directly use the fines from the flotation froth. However, obtaining fines from the froth with a solvent extraction method would alter the surface properties of the original fines. Our first concern was whether the fines extracted from the tailings in our bitumen extraction experiments could represent the fines present in the froth. In our test, the fines from tailings and from froth were first characterized by x-ray microanalysis and particle size distribution measurement. As shown in Figure 4.2, the fines from the tailings and the froth show a bimodal particle size distribution with the major and minor distribution peaks centered at around 10 and 0.6 μm, respectively, for both the good and poor processing ores. This result indicates that the obtained fines from the tailings using our procedure (see Chapter 4) were suitable for the purpose of our study. In the subsequent tests, the fines obtained from tailings were used, unless otherwise specified. X-ray microanalysis (Table 4.3) and XRD pattern as shown in Figure 9.1 indicate that the fines extracted form the good processing ore and the poor processing ore are basically similar in composition and structure, possibly aluminosilicate minerals or a mixture of silica and clays.

It should be noted that the solvent-extracted bitumen from "good processing ores" and "poor processing ores" shows indistinguishable surface properties in terms of zeta potential, induction time for air bubble-bitumen attachment, and colloidal force between bitumen-silica sand grains.

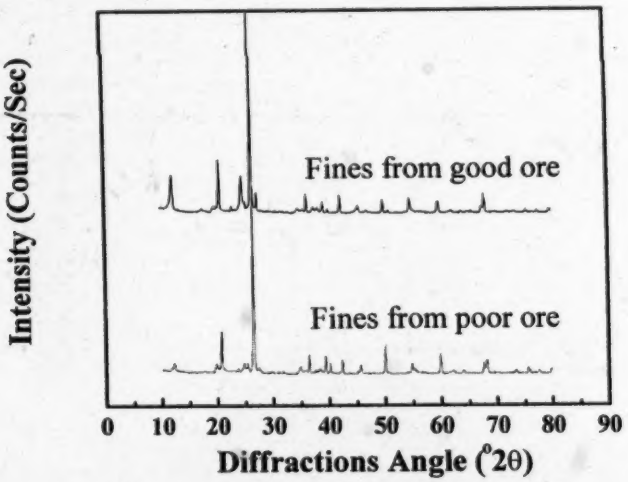

Figure 9.1 X-ray diffraction patterns of fines from oil sand ores. CuKα radiation (with graphite monochrometer), scanned at 0.05 °2θ step and 4 s per step.

9.2.2 Surface properties of fines

The surface electric properties reveal a marginal difference for the fines collected from good and poor processing ores, as shown in Figure 5.7. The zeta potentials of the fines become more negative with increasing solution pH, without an iso-electric point (iep) observed. For solvent-extracted bitumen (Figure 5.2), however, an iep at about pH 3 is observed. Compared with the zeta potentials of the fines, a more pronounced decrease in zeta potentials with increasing solution pH is observed for bitumen than for the fines. This finding indicates that the obtained fine solids feature their unique surface electric properties and are not covered with bitumen. The difference in zeta potentials between bitumen and fines also allows us to study the bitumen/fine interactions with zeta potential distribution measurements.

However, the fines from the good processing ore exhibit a distinct difference in surface hydrophobicity from the fines from the poor processing ore. As shown in Figure 9.2, the "critical surface tension" of the fines from poor processing ore is 30~45 mN/m, while the fines from good processing ore could be wetted even by water with a surface tension 72 mN/m. The results indicate that the fines from the poor processing ore are much more hydrophobic than the fines from the good processing ore. Although the origin of the

hydrophobicity for the fines from the poor processing ore is not clear, it can be certain that the hydrophobicity is not merely from the coating of bitumen since the fines from the poor processing ore exhibited the same zeta potential values over a wide solution pH range as the fines from the good processing ore, as shown in Figure 5.7. More importantly, the fines from the poor processing ore are still hydrophobic with a "critical surface tension" of 43~52 mN/m, even after washing with toluene. A possible reason for the hydrophobicity of the fines from the poor processing ore is the strong adsorption of surfactants on the fines from the poor processing ore that contains high multivalent metal ions, such as calcium and magnesium ions as shown in Table 4.3. The difference in the particle hydrophobicity could result in a significant difference in interaction behaviors between the bitumen and the fines.

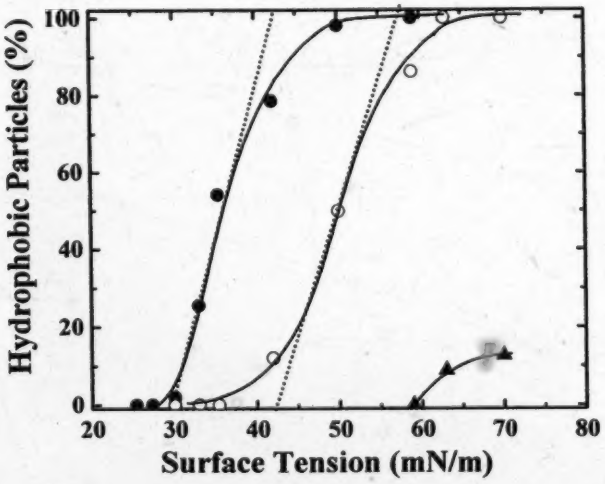

Figure 9.2 Partition of the fines at air-aqueous methanol solution interface. Filled circles: fines from a poor processing ore; open circles: fines from a poor processing ore washed with toluene; and filled triangles: fines from a good processing ore.

9.3 Zeta potential distribution measurement

9.3.1 Fines from good processing ore

In 1mM KCl solutions At pH 8, zeta potential distributions of the emulsified solvent-extracted bitumen and fines suspension measured separately are shown in Figure 9.3a.

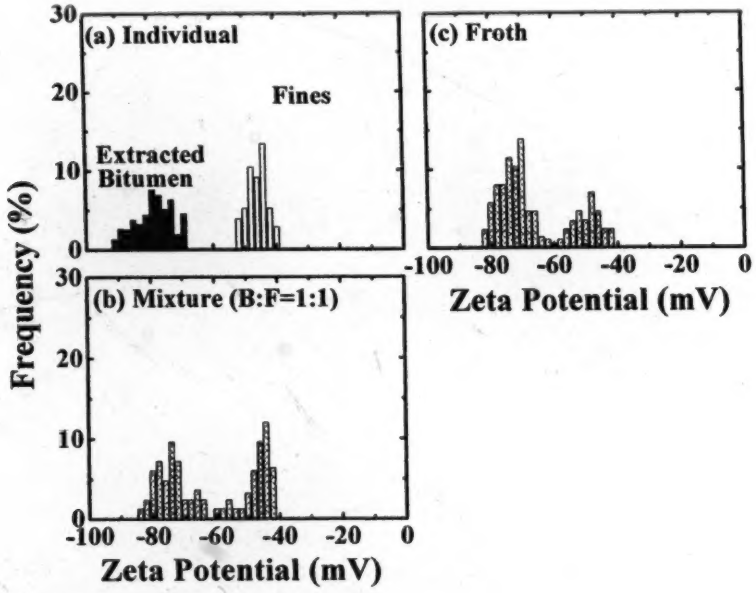

Figure 9.3 Zeta potential distributions in 1 mM KCl solutions at pH 8. (a) Emulsified bitumen and fines suspension measured separately; (b) their mixture at a mass ratio of 1:1; and (c) emulsified froth from a good processing ore.

The distribution peaks are centered at -78 and -45 mV for bitumen and fines, respectively. The broader distribution peak of the bitumen is attributed to its complex chemical composition, while a narrower distribution peak for the fines indicates that the obtained fines are more homogeneous. The zeta potential distribution for the mixed suspension of solvent-extracted bitumen and fines is shown in Figure 9.3b. Two distinct peaks are observed, centered at -74 and -46 mV, representing bitumen and fines, respectively. This observation suggests a negligible coagulation between bitumen droplets and fines particles in the 1 mM KCl solution. For the emulsified froth from the extraction test of the good processing ore, Figure 9.3c also shows two distinct zeta potential distribution peaks centered at -72 and -48 mV. These peak values are almost identical to those for the bitumen and fines, respectively. The results confirm that for the good processing ore, there is minimal attachment between the bitumen droplets and fines. The appearance of the peak for the fines from the emulsified froth suggests that the

bitumen froth from the good processing ore carries some fine solids. These fines are likely to report to the froth by mechanical entrainment/entrapment.

In 1 mM $CaCl_2$ solutions To study the effect of calcium ions, the zeta potential distributions of the individual components in the presence of 1 mM calcium ions were measured.

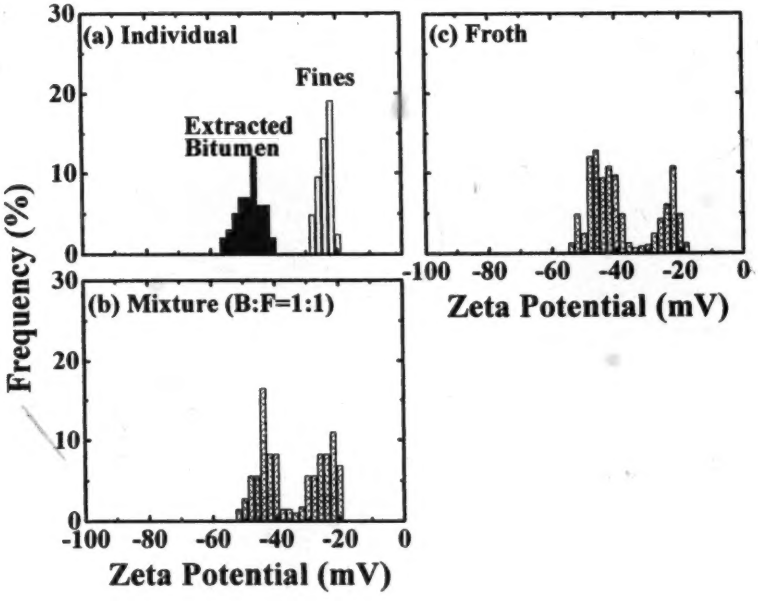

Figure 9.4 Zeta potential distributions in 1 mM KCl solutions containing 1 mM $CaCl_2$ at pH 8. (a) Emulsified bitumen and fines suspension measured separately; (b) their mixture at a mass ratio of 1:1; and (c) emulsified froth from a good processing ore.

As shown in Figure 9.4a, the zeta potentials of the emulsified solvent-extracted bitumen and fines suspension are suppressed, and the distribution peak is centered at -48 and -24 mV, respectively. The electric double layer compression and specific adsorption of calcium ions contributes to the suppression of zeta potentials. For the zeta potentials of the mixed suspension of the bitumen and fines, two distinct distribution peaks centered at -44 and -25 mV, respectively, are again observed, as shown in Figure 9.4b. This finding confirms a negligible attachment of the fines to the bitumen even with the addition of 1

mM calcium ions. The emulsified froth also shows a bi-modal zeta potential distribution, as shown in Figure 9.4c. One zeta potential distribution peak corresponds to the bitumen and the other to the fines, illustrating a negligible coagulation between the two components. Compared with the results shown in Figure 9.3, one can conclude that calcium ion addition does not enhance attachment of fines from the good processing ore to the bitumen droplets.

In processing water The zeta potential distributions of fines and bitumen were also measured using the corresponding process water derived from the extraction experiment of a good processing ore.

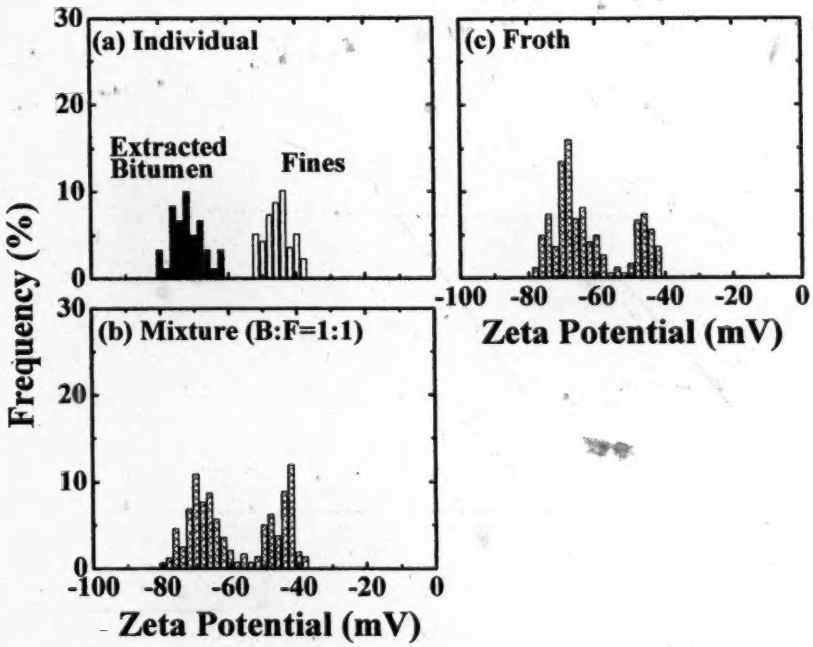

Figure 9.5 Zeta potential distributions in its corresponding process water. (a) Emulsified bitumen and fines suspension measured separately; (b) their mixture at a mass ratio of 1:1; and (c) emulsified corresponding froth from a good processing ore.

In this case, zeta potential distributions of bitumen and fines are centered at -71 and -45 mV, respectively, as shown in Figure 9.5a. These distribution peak values are similar to

those measured in 1 mM KCl solutions, suggesting the presence of a negligible amount of divalent ions, such as calcium in the process water. For the mixture of bitumen and fines, two distinct distribution peaks in Figure 9.5b are observed, as anticipated. The zeta potential values correspond to those for bitumen and fines, respectively, illustrating a negligible coagulation between the two components in a real flotation system. Measurement with the emulsified froth shows two distinct distribution peaks in Figure 9.5c, also corresponding to those for the bitumen and fines, respectively. The results confirm that there is a negligible coagulation between the bitumen and fines. The weak coagulation between the bitumen and fines translates to less slime coating of the bitumen by the fines in a commercial flotation environment. Therefore, a high bitumen flotation rate from good processing ores is anticipated as often being the case in practice.

9.3.2 Fines from poor processing ore

In 1 mM KCl solutions Zeta potential distributions of emulsified solvent-extracted bitumen and fines suspension measured separately are shown in Figure 9.6a. Two distinct distribution peaks at -78 and -46 mV are observed. These peak values are not substantially different from those observed for the good processing ore. However, the zeta potential distribution for the mixed suspension of the solvent-extracted bitumen and fines is quite different. Figure 9.6b shows a major distribution peak at a zeta potential value corresponding to that of the fines, with a continuous spread towards the distribution peak for the bitumen alone. The results suggest that bitumen droplets are partially covered by the fine solids. This observation indicates a weak coagulation between the two components. The result of the emulsified froth in a 1 mM KCl solution is shown in Figure 9.6c. Only one broad distribution peak located at the zeta potential value close to that for the fines is observed. This observation illustrates that most of the bitumen droplets are fully covered with fines. It should be noted that the fines content in the froth is much higher than that in the mixture of bitumen and fines at 1:1 mass ratio. Compared with the case of the good processing ore, the attachment of the fines to bitumen droplets in the poor processing ore is much more noticeable. It can be concluded that the fines in the froth from the poor processing ore is carried over mostly by slime coating.

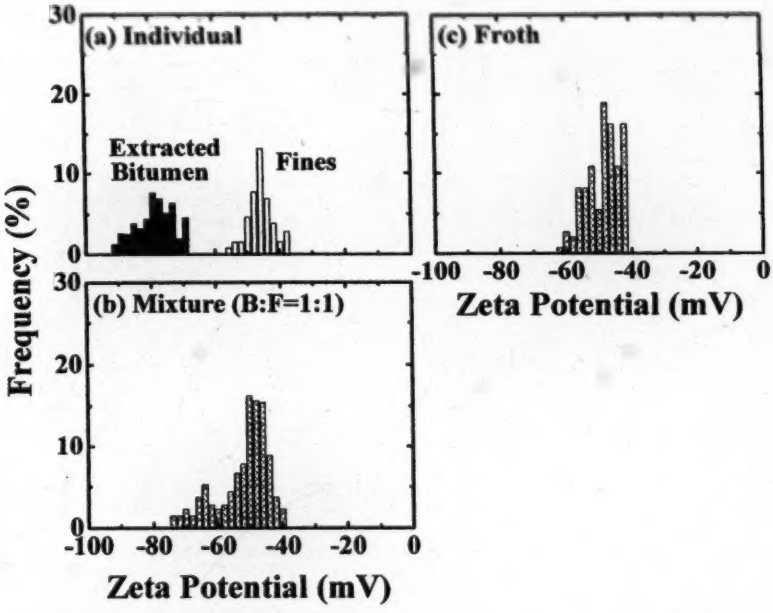

Figure 9.6 Zeta potential distributions in 1 mM KCl solutions at pH 8. (a) Emulsified bitumen and fines suspension measured separately; (b) their mixture at a mass ratio of 1:1; and (c) emulsified froth from a poor processing ore.

In 1 mM $CaCl_2$ solutions With the addition of 1 mM calcium ions, the zeta potential distributions of the bitumen and fines in a single component system are shown in Figure 9.7a. Compared to the case where calcium is absent, shown in Figure 9.6a, the peak positions for bitumen and fines are shifted substantially to less negative values of -48 and -24 mV respectively, suggesting a strong calcium adsorption on both bitumen and fines. For the mixture of the solvent-extracted bitumen and fines, one continuous distribution as shown in Figure 9.7b is observed. This zeta potential distribution features with a major peak corresponding to the peak of fines and a tail spreading towards bitumen direction. Compared with the case without calcium addition, a larger surface coverage of the fines on the bitumen surface is evident. This observation suggests a stronger attraction between the two components in the presence of calcium ions. For the emulsified froth, only one narrow zeta potential distribution is observed in Figure 9.7c. This distribution peak is located at -25 mV, which corresponds to the peak position of the fines. The absence of a

bitumen peak from the froth suggests that all the bitumen droplets are fully covered with the fines, due to a stronger attraction between the bitumen and fines and the presence of a larger amount of fines in the froth. Compared with Figure 9.6, these results suggest that calcium ion addition enhances the attraction between the bitumen droplets and fine solids from the poor processing ore.

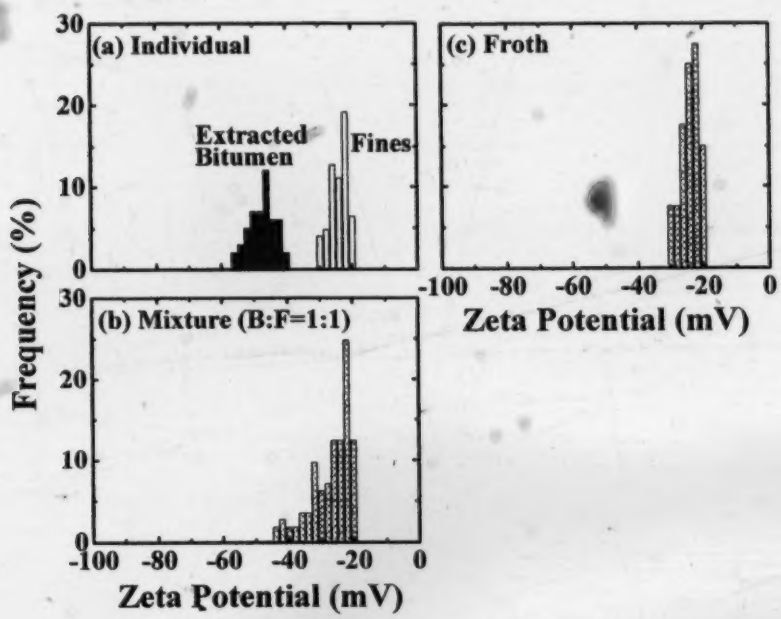

Figure 9.7 Zeta potential distributions in 1 mM KCl solutions containing 1 mM $CaCl_2$ at pH 8. (a) Emulsified bitumen and fines suspension measured separately; (b) their mixture at a mass ratio of 1:1; and (c) emulsified froth from a poor processing ore.

In process water The zeta potential distributions in the corresponding process water for each component are shown in Figure 9.8a. The distribution for the emulsified bitumen and fines suspension peaks at -50 and -28 mV, which is similar to the case with 1 mM calcium ion addition in 1 mM KCl solution. This observation suggests the presence of calcium and/or magnesium ions in the process water of the poor processing ore (Table 4.3). With the mixture of bitumen and fines, a major distribution peak at the zeta potential value corresponding to that for the fines is observed in Figure 9.8b, with a small tail towards the distribution peak of the bitumen. Again, this result suggests a stronger

attachment between the bitumen and fines in the process water than in the case of adding 1 mM calcium ions. The results of Figure 9.8c for the emulsified froth show only one very narrow distribution peak at the same zeta potential value as that for the fines, indicating a strong attachment of fines on bitumen surfaces. These findings imply a stronger coagulation of the fines from the poor processing ore on bitumen in a real flotation system, resulting in a harmful slime coating. Therefore, a low bitumen flotation rate and poor froth quality are anticipated for a poor processing ore.

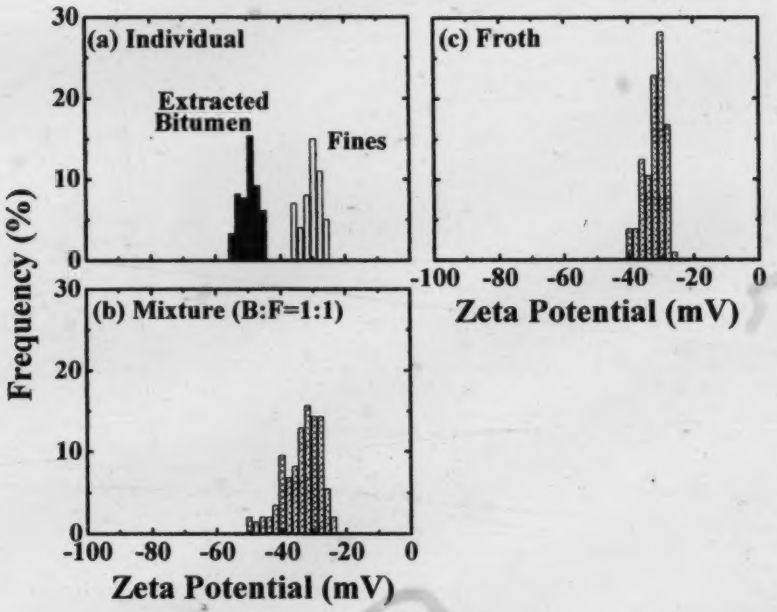

Figure 9.8 Zeta potential distributions in its corresponding process water. (a) Emulsified bitumen and fines suspension measured separately; (b) their mixture at a mass ratio of 1:1; and (c) emulsified froth from a poor processing ore.

9.4 Surface force measurement

To further understand the essence of the colloidal interactions between the bitumen and fines, direct surface force measurements for a number of bitumen-fines pairs were conducted with an atomic force microscope (AFM).

9.4.1 Fines from good processing ore

In 1 mM KCl solutions At pH 8, the measured force profiles between bitumen-fines pairs from the good processing ore are shown in Figure 9.9. The long-range forces are strongly repulsive, while the contacted adhesive forces are distributed mainly at zero with a small extension to 2.5 mN/m. This observation suggests a negligible attachment of the fines on bitumen, which is consistent with the interpretation of the zeta potential distribution measurement (see Figure 9.3). Although the data are scattered for a number of different fines particles, the trend of the force profiles is clear.

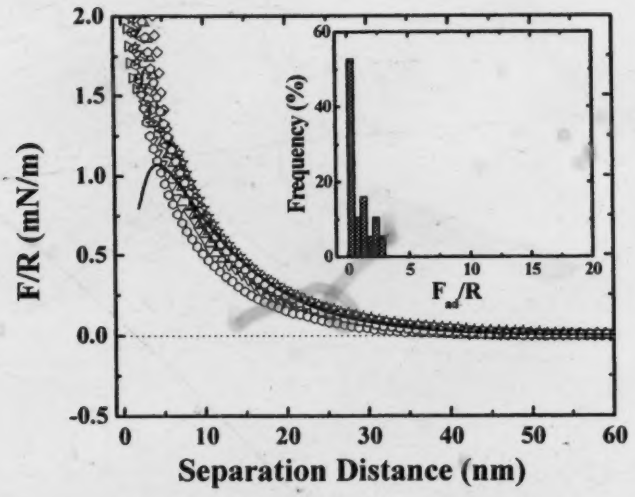

Figure 9.9 Normalized interaction forces (F/R) between bitumen and fines from a good processing ore as a function of separation distance in 1 mM KCl solutions at pH 8. The solid line represents the fitting of the classical DLVO theory using $A_{132}=6.5\times10^{-21}$ J with the best-fitted decay length and Stern potential being: $\kappa^{-1} = 8.6\ nm$, ψ_B=-75 mV, ψ_F=-45 mV. Insert: distribution of normalized adhesive forces (F_{ad}/R) measured at loading forces of 8~10 mN/m.

In 1 mM $CaCl_2$ solutions The measured force profiles between the bitumen and fines when 1 mM calcium ions are added are shown in Figure 9.10. Compared with Figure 9.9, it is evident that the addition of calcium ions significantly depresses the repulsive force profiles, but increases the adhesive force only marginally. This finding implies a weak

interaction between the bitumen and fines, if there is any. This result correlates well with the result from zeta potential distribution measurements (Figure 9.4).

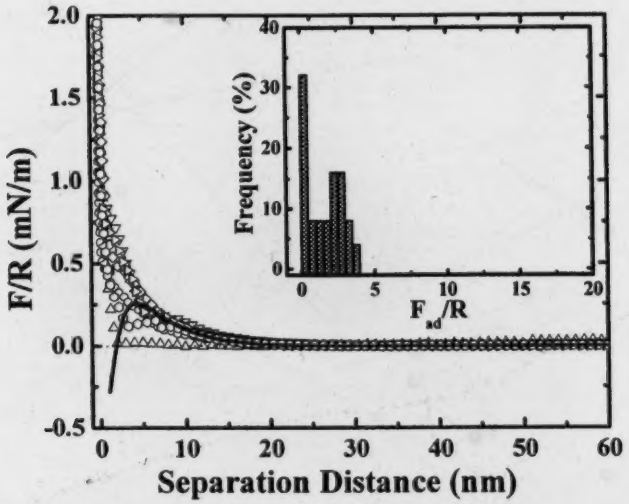

Figure 9.10 Normalized interaction forces (F/R) between bitumen and fines from a good processing ore as a function of separation distance in 1 mM KCl solutions containing 1 mM $CaCl_2$ at pH 8. The solid line represents the fitting of the classical DLVO theory using $A_{132}=6.5x10^{-21}$ J with the best-fitted decay length and Stern potential being: $\kappa^{-1} = 4\ nm$, ψ_B=-38 mV, ψ_F=-18 mV. Insert: distribution of normalized adhesive forces (F_{ad}/R) measured at loading forces of 8~10 mN/m.

In process water The measured force profiles between bitumen-fines pairs in the corresponding process water are shown in Figure 9.11. A finite repulsion with a small adhesion is observed. Compared with Figures 9.12, force profiles in the process water are only moderately depressed due to the presence of a small amount of divalent cations in the process water. From the measured force profiles, a weak attraction between bitumen and fines as interpreted from the zeta potential distribution measurement (Figure 9.5) can be claimed.

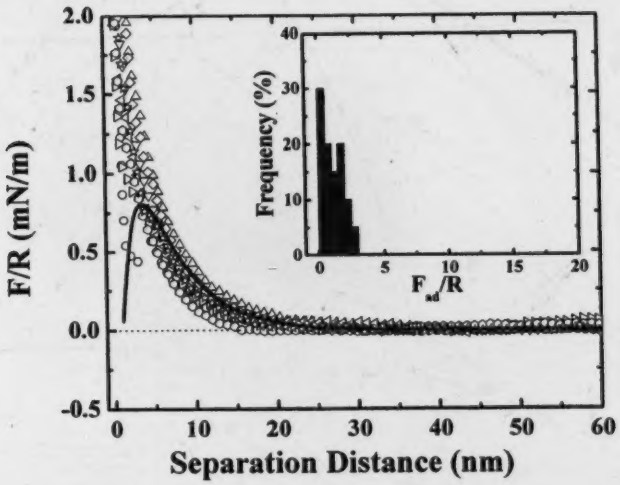

Figure 9.11 Normalized interaction forces (F/R) between bitumen and fines from a good processing ore as a function of separation distance in its corresponding process water. The solid line represents the fitting of the classical DLVO theory using $A_{132}=6.5x10^{-21}$ J with the best-fitted decay length and Stern potential being: $\kappa^{-1} = 4.6\,nm$, ψ_B=-60 mV, ψ_F=-30 mV. Insert: distribution of normalized adhesive forces (F_{ad}/R) measured at loading forces of 8~10 mN/m.

9.4.2 Fines from poor processing ore

In 1mM KCl solutions At pH 8, the measured force profiles for a number of bitumen-fines pairs from the poor processing ore are shown in Figure 9.12. In this system, a repulsive force profile with a finite adhesive force is observed. Compared with Figure 9.9, the repulsion between the bitumen and fines from the poor processing ore is noticeably weaker while the adhesive force is stronger. The results imply that the surface hydrophobicity of the fines from the poor processing ore might induce an additional attractive force, which accounts for a stronger attachment between the bitumen and fines from the poor processing ore than between the bitumen and fines from the good processing ore.

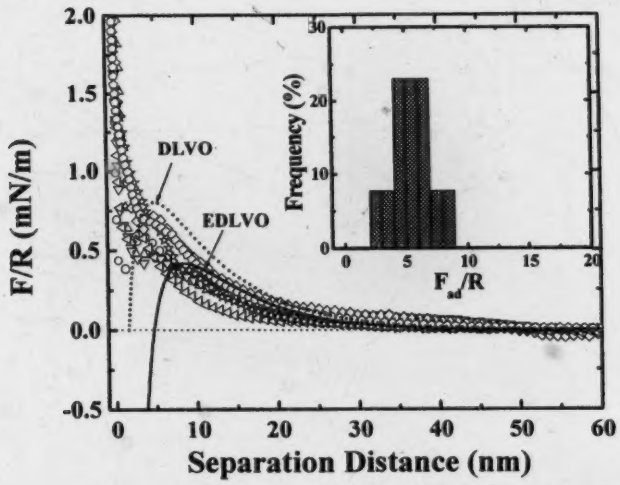

Figure 9.12 Normalized interaction forces (F/R) between bitumen and fines from a poor processing ore as a function of separation distance in 1 mM KCl solutions at pH 8. Dotted line represents the fitting of the classical DLVO theory using $A_{132}=6.5\times10^{-21}$ J with the best-fitted decay length and Stern potential being: $\kappa^{-1}=8.0\,nm$, ψ_B=-70 mV, ψ_F=-36 mV. Solid line represents the fitting of the extended DLVO theory using $A_{132}=6.5\times10^{-21}$ J with the best-fitted decay length, Stern potential, hydrophobic force constant K being: $\kappa^{-1}=8.0\,nm$, ψ_B=-70 mV, ψ_F =-36 mV, $K=8\times10^{-20}$ J. Insert: distribution of normalized adhesive forces (F_{ad}/R) measured at loading forces of 8~10 mN/m.

In 1 mM $CaCl_2$ solutions The interaction force profiles between the bitumen and fines from poor processing ore in the presence of 1 mM calcium ions are shown in Figure 9.10. In this case, the long-range force becomes attractive with a marginal force barrier being observed at a separation of 10 nm. The diminishing electrostatic double layer force by calcium addition is responsible for the observed change of the force profiles. Comparison of Figure 9.10 with Figure 9.12 shows a substantial increase in the adhesive force between the bitumen and fines with the addition of calcium ions. The result implies that the presence of calcium and surface hydrophobicity of the fines induce an attractive long-

range force and a strong adhesive force, which accounts for the strong attachment between the bitumen and fines as observed in the zeta potential distribution measurement.

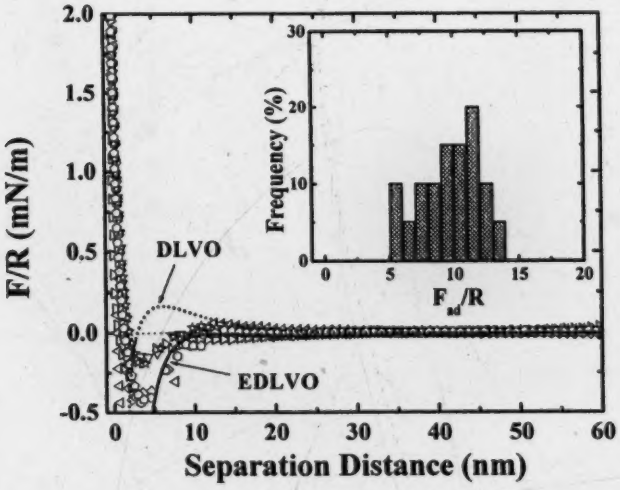

Figure 9.13 Normalized interaction forces (F/R) between bitumen and fines from a poor processing ore as a function of separation distance in 1 mM KCl solution containing 1 mM $CaCl_2$ at pH 8. The dotted line represents the fitting of the classical DLVO theory using A_{132}=6.5x10^{-21} J with the best-fitted decay length and Stern potential being: $\kappa^{-1} = 4.7\ nm$, ψ_B=-40 mV, ψ_F=-15 mV. The solid line represents the fitting of the extended DLVO theory using A_{132}=6.5x10^{-21} J with the best-fitted decay length, Stern potential, hydrophobic force constant K being: $\kappa^{-1} = 4.7\ nm$, ψ_B=-40 mV, ψ_F=-15 mV, K=7x10^{-20} J. Insert: distribution of normalized adhesive forces (F_{ad}/R) measured at loading forces of 8~10 mN/m.

In process water The measured interaction force profiles between the bitumen and fines pairs are shown in Figure 9.14. In this system, an attractive force profile with a strong adhesive force is observed, which is similar to the force profiles with the addition of 1 mM calcium (Figure 9.13). This similarity suggests the presence of divalent cations in the process water. The results imply a strong attachment of fines onto bitumen in the process water, i.e., a severe slime coating in a real flotation system.

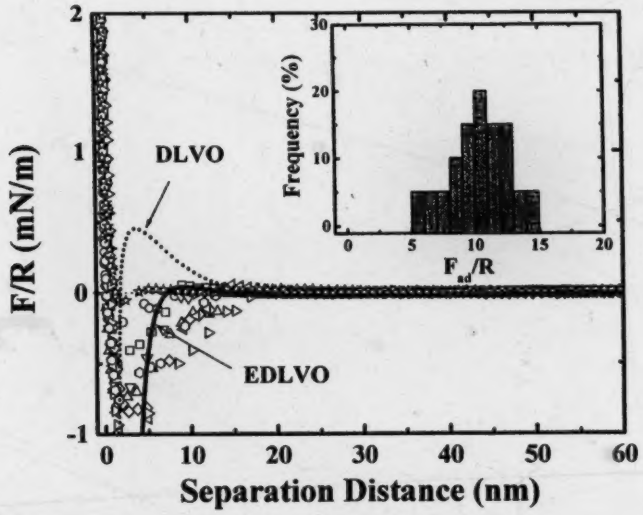

Figure 9.14 Normalized interaction forces (F/R) between bitumen and fines from a poor processing ore as a function of separation distance in its corresponding process water. The dotted line represents the fitting of the classical DLVO theory using A_{132}=6.5x10^{-21} J with the best-fitted decay length and Stern potential being: $\kappa^{-1} = 4.3\ nm$, ψ_B=-40 mV, ψ_F=-25 mV. The solid line represents the fitting of the extended DLVO theory using A_{132}=6.5x10^{-21} J with the best-fitted decay length, Stern potential, hydrophobic force constant K being: $\kappa^{-1} = 4.3\ nm$, ψ_B=-40 mV, ψ_F=-25 mV, K=7x10^{-20} J. Insert: distribution of normalized adhesive forces (F_{ad}/R) measured at loading forces of 8~10 mN/m.

9.4.3 Data fitting and nature of colloidal force

At a separation of greater than 5~6 nm, the scattered force profiles measured between the bitumen and fines from the good processing ore can be reasonably well described with the classical DLVO theory as shown by solid lines in Figures 9.9, 9.10 and 9.11. this indicates that the electrostatic double layer force controls their interactions. On the other hand, the measured force profiles between the bitumen and fines from the poor processing ore as shown by solid lines in Figures 9.12, 9.13 and 9.14 can be described only with the extended DLVO theory by considering a hydrophobic force. This indicates that both the electrostatic double layer force and hydrophobic force control their

interactions. Considering the moderate hydrophobicity of the fines from the poor processing ore, an attractive hydrophobic force between bitumen and fines is not unexpected. The hydrophobic force constant (K) values in this case is smaller than those obtained in the system of bitumen-bitumen, indicating that the surface of the fines from the poor processing ore is less hydrophobic than bitumen surface. The deviation of the measured force profiles at a separation of less than 5~6 nm from the predication with the classical or extended DLVO theory could be of steric origin, as discussed in Chapters 6 and 7. The fitted Debye lengths are in the range of the values calculated from the electrolyte concentration of the medium. The fitted Stern potentials (see figure captions) are slightly smaller than the measured zeta potentials (see zeta potential distribution peaks), as is expected from the roughness of the fines used in the force measurement. The data fitting with the classical or extended DLVO theory allows us to identify the origin of the interaction forces, which in turn allows us to control the interaction behavior of the complex bitumen extraction system by monitoring the factors that affect the interaction forces. The micro-scale colloidal force measurements using AFM provided insights into mega-scale industrial operations of oil sands extraction. The implication here is that to avoid slime coating (attraction between bitumen and fines) and to improve bitumen flotation for a poor processing ore, a change of process variables has to cause a reduction in the hydrophobicity of fines or a significant increase in the electrostatic repulsion. For example, increasing the pulp pH would be one of the options that could decrease the hydrophobicity of fines as well as increase the repulsive double layer forces.

9.5 Implication to bitumen flotation

The results above clearly show that the fines from various types of oil sand ores exhibit significant difference in coagulation with bitumen droplets, although their components (EDX in Table 4.3), structure (XRD in Figure 9.1) and even surface electric properties (Figure 5.7) are similar. In addition to the higher fines content in the poor processing ore than that in the good processing ore (Table 4.1), the surface wettability of the fines is another important difference. As shown in Figure 4.1, the fines from the poor processing ore are darker than the fines from the good processing ore. This visual observation indicates that the fines from the poor processing ore are likely contaminated with organic matters. Similar observation was reported for the fines in froth treatment: the ultra-fine

inorganic solids are found to be coated with toluene insoluble organic materials from both humic acid and asphaltene-like components (polar and aromatic) and the coverage is found to be patchy rather continuous (Kotlyar and Sparks, 1985; Chen et al., 1999; Bensebaa et al., 2000). The results of the chemical analysis shown in Table 9.1 confirm that the carbon and hydrogen content in the fines from the poor processing ore are substantially higher than those from the good processing ore.

Table 9.1 The chemical element (C, H, N) analysis of the fines obtained from oil sands.

Fines from	Good processing ore	Poor processing ore
C (%)	4.05	11.49
H (%)	1.26	1.56
N (%)	0.04	0.12

The adsorption of organic matter on the fines causes them to exhibit some degree of surface hydrophobicity. As shown in Figure 9.5, the surface of the fines from the poor processing ore are much more hydrophobic than that of the fines from the good processing ore. As a result, the fines from the poor processing ore attaches more easily to the hydrophobic bitumen surface than the fines from the good processing ore. As ascertained by the zeta potential distribution measurements (Figures 9.3~8), the stronger attraction is due to the presence of a stronger hydrophobic attraction. However, compared with the bitumen, the surface of the fines is less hydrophobic. The coating of less hydrophobic fines on bitumen accounts for the depression of bitumen flotation and poor froth quality, as in the case of poor processing ores.

In the case of single mineral clays (Chapter 8), the divalent cations are considered to act as a bridge or binder to promote the fines attachment to the bitumen surface. A "fines-cation-bitumen" linkage model is proposed to account for the depression of bitumen flotation by montmorillonite clay addition in the presence of calcium ions (Figure 8.8). However, it should be noted that the origins of the coagulative nature of bitumen with the fines from oil sand ores, especially those from the poor processing ore, are far more complex than what we expect for single mineral clays. The higher content of divalent

ions in the process water of the poor processing ore could drive more cations onto the surface of the fines, and also lead to the adsorption of anionic surfactants onto the surface of the fines. These adsorbed cations and surfactants on he surface of the fines are active sites, readily attaching to bitumen droplets by acting as a bridge (binder) and inducing a moderate hydrophobic attraction between the bitumen and fines. A model showing active sites (cations and surfactants) on fines is shown in Figure 9.15.

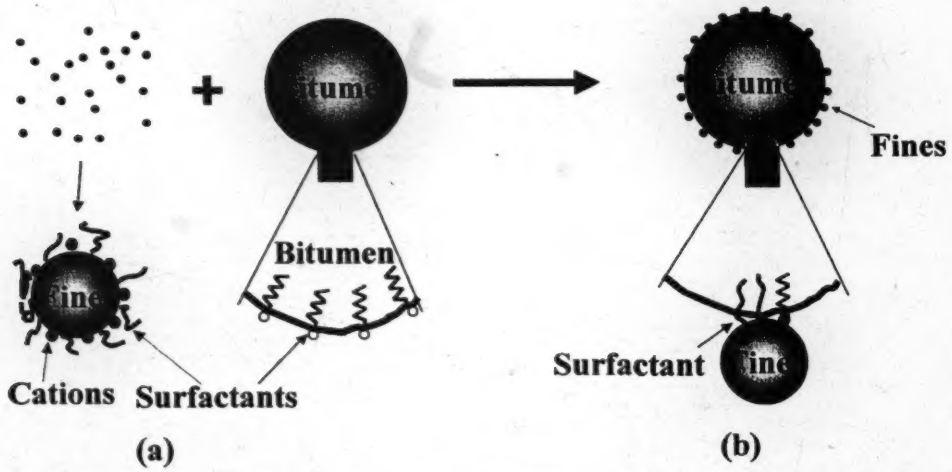

Figure 9.15 Schematics of interactions between bitumen and fines. (a) Active sites (cations and surfactants) on the surface of fines; and (b) surfactants and cations as binders for interactions between bitumen and fines.

More importantly, the current work provides the directions to resolve the difficulties of handling poor processing ores. The key issue is to eliminate the effect of the interfering active sites (both cations and surfactants) in order to prevent the fines from hetero-coagulating with bitumen. A few potential approaches to achieve this objective are: a) remove the active sites by chemicals or mechanical attrition; b) mask or block the active sites with polymers; c) de-activate the active sites through competitive reaction with active sites by chelating or precipitating chemicals such as modified dextrin or bicarbonates; and d) increase electrostatic repulsive force between bitumen and fines by dispersing chemical, such as sodium silicate and polyphosphates.

9.6 Summary of chapter

The current study on the interaction between bitumen and fines, extracted directly from oil sand ores, reveals the coagulative behavior of the fines with bitumen in a real oil sands flotation system. From a practical point of view, it is an important extension of our previous studies on model systems (single minerals) to a real system. The major conclusions derived from the results are:

- The fines from the poor processing ore are more hydrophobic than these from good processing ore, but their electrokinetic characteristics are essentially the same.
- The fines from the good processing ore exhibit marginal attachment to bitumen surfaces and have a negligible effect on zeta potentials of emulsified bitumen. Calcium addition does not significantle enhance little enhancement on the coagulation of the fines with bitumen.
- For the bitumen and fines from the good processing ore in its process water, a strong repulsive force profile with a weak adhesive force is observed. This interaction characteristic is attributed to the hydrophilic nature of the fines and the presence of a very low concentration of divalent cations in the processing water.
- For the fines from the poor processing ore, a strong attachment on the bitumen surface and significant modification on zeta potentials of emulsified bitumen are observed. Calcium addition enhances the coagulation of the fines with bitumen.
- The bitumen and fines from the poor processing ore in its processing water exhibit an attractive force profile with a strong adhesive force due to the surface hydrophobicity of the fines and the presence of divalent cations in the process water.
- The electrostatic double layer force plays a dominant role in the interactions between bitumen and fines from the good processing ore, while both the electrostatic double layer force and the hydrophobic force play a dominant role in the interactions between bitumen and fines from the poor processing ore.

- The low bitumen recovery of poor processing ores with a high fines content and high divalent cation concentration in a mega-scale industrial process can be understood with micro-scale zeta potential distribution measurement and colloidal force measurement.

CHAPTER 10 SUMMARY

10.1 General conclusions

This thesis focused on the colloidal interactions between oil sand components from model systems to a real system with the developed method of zeta potential distribution measurement and surface force measurement. The studies led to the following conclusions.

1. Zeta potential distribution measurement and AFM techniques, incorporating with other techniques such as contact angle measurement and spin-coating technique, allow us to more thoroughly study the colloidal interactions between oil sand components. It was demonstrated that micro-scale fundamental studies from simple model systems to a complex real system could provide insights into mega-scale industrial processes of bitumen extraction from oil sands.

2. The developed novel technique based on the zeta potential distribution measurement makes it possible to qualitatively and directly observe the colloidal interactions between bitumen-silica, bitumen-clays and bitumen-fines in aqueous solutions. It has been proven that the method is a simple, yet informative and powerful tool for studying the colloidal hetero-coagulation.

3. The surface force measurement with the state-of-the-art AFM was successfully adopted to investigate quantitatively the colloidal interactions between bitumen-bitumen bitumen-silica, bitumen-clays and bitumen-fines in aqueous solutions. This technique allows us to identify the essence of the colloidal interactions between oil sand components, and advances our knowledge of bitumen extraction from oil sands from a "know-what" to a "know-why" level. Such knowledge has provided the fundamental basis for further improvement in oil sands processing and exploration.

4. The electrokinetic behaviors of oil sand components are dependent on solution pH, salinity and divalent metal ion concentration. The zeta potentials of bitumen, fines, kaolinite and silica become more negative with increasing solution pH, while the zeta

potentials of montmorillonite clays are not sensitive to the alteration of solution pH. Addition of calcium ions can depress the zeta potentials for all the components.

5. The colloidal interactions between oil sand components are significantly impacted by the alteration of solution pH, salinity and calcium ion level, to different extents. Higher concentration of divalent ions in the medium causes a weaker repulsive force and a stronger adhesive force between bitumen-silica, bitumen-clays, and bitumen-fines.

6. The measured interaction forces between oil sand components can be reasonably described with the classical or extended DLVO theory. The electrostatic double layer force dominates the colloidal interactions for the systems of bitumen-silica, bitumen-clays and bitumen-fines from the good processing ore, while both the electrostatic double layer force and the hydrophobic force dominate the colloidal interactions for the systems of bitumen-bitumen and bitumen-fines form the poor processing ore. At very short range, an additional repulsive force can be described with the steric force theory. These findings provide the guidance to control particle interaction behavior via monitoring the factors that affect the dominant forces.

7. The reasons for variable processibility of different oil sand ores are disclosed. For the good processing ore, the hydrophilic mineral fines with the lower concentration of divalent ions in the ore result in a weak attachment of fines on the bitumen surface, which corresponds to a higher bitumen flotation recovery. For the poor processing ore, the moderately hydrophobic mineral fines coupled with higher concentration of divalent ions in the ore lead to a strong attachment of fines onto bitumen surfaces, which is responsible for the low bitumen recovery and poor froth quality.

8. The interpretation of measured colloidal force profiles agrees well with zeta potential distribution measurements. The findings can provide further insights into bitumen extraction mechanisms in Water-Based Extraction technology, and can provide guidelines for improving bitumen extraction efficiency. The results can advance our current knowledge on bitumen/sands interactions to a more quantitative level.

10.2 Claim for original research

1. A novel method of zeta potential distribution measurement was developed in this thesis to investigate hetero-coagulation of colloidal particles. It was proven by application to a number of other systems to be a powerful tool to study the hetero-coagulation for colloidal systems.

2. Surface force measurements with the state-of-the-art AFM, incooperating with the spin-coating technique, were successfully adopted to quantitatively study surface forces for oil sands systems. The knowledge accumulated from the studies has advanced our understanding of not only "how" but also "why" bitumen can be extracted from oil sands.

3. A Visual basic program to numerically solve non-liner Poisson-Boltzmann equation with different boundary conditions (B.C.) for symmetrical/asymmetrical systems in symmetrical/asymmetrical electrolyte solutions was developed to fit the measured long-range force profiles.

4. The nature of long-range forces between oil sand components and dominant forces for their interactions were identified through fitting with the classical DLVO or extended DLVO theory.

5. The identification of the dominant forces between oil sand components provides guidance for controlling the interaction behavior of the oil sand components via monitoring the factors that could affect the long-range forces.

6. The comparison between the measured long-range force barriers and the contact adhesive forces was used to predict the colloidal interaction for the first time. This comparison provides a theoretical region or boundary between coagulation and dispersion for a given system.

7. Direct evidence on the colloidal interactions between bitumen-clays, and bitumen-fines was obtained with the AFM technique and zeta potential distribution measurement for the first time.

8. The roles of solution pH, salinity and calcium ions in the bitumen extraction system were revealed.

9. The behaviors of fine clays and fines collected from oil sand ores in bitumen extraction systems were characterized.

10. The reasons for variable processibility of different oil sand ores were identified. The hydrophobic nature of the fines and divalent cations in the poor processing ore were found to lead to the slime coating of fines on bitumen and result in low bitumen flotation rate.

11. Some potential approaches to mitigate the slime coating in bitumen flotation were proposed.

10.3 Prospect of future work

It is my hope that this work (the results obtained and the techniques developed) is interesting to the followers in the field of oil sands extraction. Should that be the case, I would like to suggest:

1. The effect of surfactants and other divalent cations such as magnesium on the colloidal interactions between oil sand components be investigated. These chemicals released from oil sand ores into the oil sands extraction system definitely have some impact on bitumen extraction. An investigation on these chemicals could provide more knowledge on the processibility of oil sand ores.

2. A study on mitigating the slime coating of fines on bitumen surface be carried out to find a good avenue for processing of poor processing ores. Some additives such as bicarbonate, sodium silicates or phosphates, sodium sulfur and polymer are recommanded.

3. A systematic study on bitumen/bubble interaction be carried out to provide more information on bitumen extraction from oil sands, in particular on bitumen "aeration". For this purpose, the current techniques should be modified or new methods should be developed.

REFERENCES

Alexander K.L. and D.Q. Li, "Effects of Bitumen Films over Air Bubble Surfaces on Bitumen Drop-Air Bubble Attachment", *Colloid Surf A*, Vol.106, 191-202, 1996.

Almog, Y. and J. Klein, "Interactions between Mica Surfaces in a Polystyrene-Cyclopentane Solution near the Theta-Temperature", *J Colloid Interface Sci,* Vol.106, 33-34, 1985.

Arich Ben- Nain, *Hydrophobic Interactions*, Plenum Press, New York, N.Y. USA, 1980.

Aston, D.E. and J.C. Berg, "Fluid Interfacial Separation for Secondary Fiber Recovery as Probed with Atomic Force Microscopy", *J Pulp Paper Sci*, Vol.24, 121-125, 1998.

Aston, D. E. and J. C. Berg, "Quantitative Analysis of Fluid Interface – Atomic Force Microscopy", *J Colloid Interface Sci*, Vol.235, 162-169, 2001.

Attard, P. and J. L. Parker, "Deformation and Adhesion of Elastic Bodies in Contact", *Phys Rev A*, Vol.46, 7959-7971, 1992.

Attard, P., "Interaction and Deformation of Viscoelastic Particles. 2. Adhesive particles", *Langmuir*, Vol.17, 4322-4328, 2001.

Bachmann, D. J. and S.J. Miklavic, "Deformation of Fluid Interfaces Induced by Electrical Double-Layer Forces and its Effect on Fluid-Solid Interactions", *Langmuir*, Vol.12, 4197-4204, 1996.

Baptista, M. V. and C.W. Bowman, "The Flotation Mechanism of Solids from the Athabasca Oil Sand"' *Preprint, 19th Can Chem Eng Conf,* Edmonton, Alberta, 1969.

Basu S. and K. Nandakumar and J.H. Masliyah, "A Study of Oil Displacement on Model Surfaces", *J Colloid Interface Sci*, Vol.182, 82-94, 1996.

Basu S. and K. Nandakumar and J.H. Masliyah, "On Bitumen Liberation from Oil Sands", *Can J Chem Eng*, Vol.75, 476-479, 1997.

Basu S. and M. M. Sharma, "Measurement of Critical Disjoining Pressure for Dewetting of Solid Surface", *J colloid Interface Sci*, Vol.181, 443-455,1996.

Basu, S., K. Nandakumar and J. Masliyah, "Effect of NaCl and MIBC/kerosene on Bitumen Displacement by Water on a Glass Surface", *Colloid Surf* A, Vol. 136, 71-80, 1998a.

Basu, S., W.C. Kanda, K. Nandakumar and J. Masliyah, "Effect if Hydrophobic and Hydrophilic Clays on Bitumen Displacement by Water on a Glass Surface", *Ind Eng Chem Res*, Vol.37, 253-257, 1998b.

Basu, S., K. Nandakumar and J. Masliyah, "A Visual Study of High Grade Oil Sand Disintegration Process", *J Colloid Interface Sci*, Vol.205, 201-203, 1998c.

Basu, S., K. Nandakumar and J. Masliyah, "A Study on Daughter Formation in Bitumen/Glass/Water Contact Line Displacement due to Instability", *Fuel*, Vol.79, 837-841, 2000.

Bensebaa, F., L.S. Kotlyar, B.D. Sparks and K.H. Chung, "Organic Coated Solids in Athabasca Bitumen: Characterization and Process Implication", *Can J Chem Eng*, Vol. 78, 610-616, 2000.

Besseling, N.A.M., "Theory of Hydration Forces between Surfaces", *Langmuir*, Vol.13, 2133-2122, 1997.

Bhatt, D., J. Newman and C.J. Radke, "Equilibrium Force Isotherms of a Deformable Bubble/Drop Interacting With a Solid Particle Across a Thin Liquid Film", *Langmuir*, Vol. 17, 116-130, 2001.

Boon, J.A., "Fluid-Rock Interactions during Steam Injection", **in** *The Oil Sands of Canada-Venezuela*, D.A. Redford and A.G. Winestock, Eds., Special Volume 1, CIM, Montreal, 133-138,1978.

Boukir, A., E. Aries, M. Cuiliano, L. Asia, P. Doumenq and G. Mike, "Subfractionation, Characterization and Photooxidization of Crude Oil Resins", *Chemsphere*, Vol.43, 279-286, 2001.

Bowman C.W., "Molecular and Interfacial Properties of Athabasca Tar sands", *Progress 7th World Petroleum Congress*, Vol. 3, 1967, 583-604.

Brown, C.E. and E.L. Neustadter "The Wettablity of Oil /Water/Silica Systems with Reference to Oil Recovery", *J Can Petro Technol*, 100-110, July-Sept., 1980.

Brove, K.G.N., J. Sjoblom and P. Stenius, "Water-in-Crude Oil Emulsions from the Norwegian Continental Shelf", *Colloid Surf*, Vol. 63, 241-251, 1992.

Buckley, J.S., K. Takamura and N.R. Morrow, "Influence of Electrical Surface Charges on the Wetting Properties of Crude Oils", *SPE Reservoir Engineering*, 332-340, Aug. 1989.

Burnham, N.A. and A. J. Kulik, in "Handbook of Micro/Nanotribology" (ed. Bhushan, B) 247-271, CRC Press, Boca Raton, 1999.

Butt, H. J., M. Kappl, H. Mueller and R. Raiteri, "Steric Forces Measured with the Atomic Force Microscope at Various Temperatures", *Langmuir*, Vol.15, 2559-2565, 1999.

Camp, F.W., "*The Tar Sands of Alberta, Canada*", Cameron Engineers Inc., Colorado, USA, 1976.

Camp, F.W., "Processing Athabasca Tar Sands – Tailing Disposal", *Can J Chem Eng*, Vol.55, 581-591, 1977.

Chan, D.Y.C., R.R. Dagastine and L.R. White, "Forces Between a Rigid Probe Particle and a Liquid Interface", *J Colloid Interface Sci*, Vol.236, 141-154, 2001.

Chan, D.Y.C. and R.G. Horn, "The Drainage of Thin Liquid Films between Solids", *J Chem Phys*, Vol.8310, 5311-5324, 1985.

Chan, D.Y.C., T.W. Healy and L.R. White, "Electrical Double Layer Interactions under Regulation by Surface Ionization Equilibria – Dissimilar Amphoteric Surfaces", *J Chem Soc Faraday Trans.*, Vol.172, 2844-2854, 1976.

Chen, F., J.A. Finch, Z. Xu, and J. Czarnecki, " Wettability of Fines Solids Extracted from Bitumen Froth", *J Adhesion Sci Technol*, Vol. 13, 1209-1224, 1999.

Chow, R.S. and K. Takamura, "Electrophoretic Mobilities of Bitumen and Conventional Crude-in-Water Emulsions Using the Laser Doppler in the Presence of Multivalent Cations", *J Colloid Interface Sci*, Vol.125, 212-225, 1988.

Clark, K.A. and D.S. Pasternack, "Hot water Separation of Bitumen from Alberta Bituminous Sand", *Ind Eng Chem*, Vol.24, 1410-1416, 1932.

Clark, K.A., "Hot Water Separation of Alberta Bituminous Sand", *Tran Can Inst Min Met*, Vol.47, 257-274, 1944.

Claesson P.M., C.E. Blom, P.C. Herder and B.W. Ninham, "Interactions between Water-stable Hydrophobic Langmuir-Blodgett Monolayers on Mica", *J Colloid Interface Sci*, Vol.114, 234-242, 1986

Cottrell, J.H., "Development of an Andydrous Process for Oil sands Extraction", in *The K.A. Clark Volume, M.A. Carrigy*, Ed., Alberta Research Council, Edmonton, Alberta, 193-206, 1963.

Dagastine, R. R. and L. R. White, "Forces between a Rigid Probe Particle and a Liquid Interface II. The General Case", *J Colloid Interface Sci*, Vol.247, 310–320 2002.

Dai, Q. and K. H. Chung, "Bitumen-Sand Interaction in Oil Sand Processing", *Fuel*, Vol.74, 1858-1864, 1995.

Dai Q. and K. H. Chung, "Hot Water Extraction Process Mechanism using Model Oil Sands", *Fuel*, Vol.75, 220-226, 1996.

de Gennes, P.G., "Polymers at an Interface – A Simplified View", *Adv Colloid Interface*, Vol.27, 189-209, 1987.

Derjaguin, B., V.M. Muller and Y. P. Toporov, "Effect of Contact Deformations on the Adhesion of Particles", *J Colloid Interface Sci*, Vol.53, 314-326, 1975.

Drelich, J. and J.D. Miller, "Surface and interfacial Tension of the Whiterocks Bitumen and its Relationship to Bitumen Release from Tar Sands during Hot Water Processing", *Fuel*, Vol.73, 1504-1510, 1994.

Drelich, J., K. Bukka, J.D. Miller and F.V. Hanson, "Surface Tension of Toluene-extracted Bitumen from Utah Oil Sands as Determined by Welhelmy Plate and Contact Angle Technique", *Energy & Fuels*, Vol.8, 700-707, 1994.

Drelich, J., D. Lelinski, J. Hupka and J.D. Miller, "The Role of Gas Bubbles in Bitumen Release during Oil Sand Digestion", *Fuel*, Vol.74, 1150-1155, 1995.

Drelich, J., D. Lelinski and J.D. Miller, "Bitumen Spreading and Formation of Thin Bitumen Films at a Water Surface", *Colloids Surf A*, Vol. 116, 211-223, 1996.

Ducker, W.A., T.J., Senden and R.M. Pashley, "Direct Measurement of Colloidal Forces Using an Atomic Force Microscope", *Nature*, Vol.353, 239-241, 1991.

Ducker, W.A., T. J. Senden and R.M. Pashley, "Measurement of Forces in Liquids Using a Force Microscope", *Langmuir*, Vol.8, 1831-1836, 1992.

Ducker, W.A., Z. Xu, D.R. Clarker and J.N. Israelachvili, "Forces between Alumina Surfaces in Salt Solutions Non-DLVO Forces and the Implications for Colloidal Processing", *J Am Ceram Sci*, Vo.77, 437-43,1994.

Ducker, W. A. and E.J. Wanless, "Surface-Aggregate Shape Transformation", *Langmuir*, Vol.12, 5915–5920,1996.

Duran, J.D.G., M.M. Ramos-Tejada, F.J. Arroyo and F. Gonzalez-Caballero, "Rheological and Electrokinetic Properties of Sodium Montmorillonite Suspensions - I. Rheological Properties and Interparticle Energy of Interaction", *J Colloid Interface Sci*, Vol.229, 107-117, 2000.

Eskin D, Y. Leonenko, S. Lezhnin and O. Vinogradov, "A Model of Oil Sand Lump Digestion", *Miner Eng*, Vol.15, 469-472, 2002.

Fielden, M. L., R.A. Hayes and J. Ralston, "Surface and Capillary Forces Affecting Air Bubble-Particle Interactions in Aqueous Electrolyte", *Langmuir*, Vol.12, 3721-3727, 1996.

Flynn, M., B. Bara, J. Czarnecki and J. Masliyah, "An Investigation of the Effect of Air Addition during Oil Sand Conditioning, *Can. J Chem Eng*, Vol.79, 468-470 2001.

Forsman, J., C.E. Woodward and B. Jonsson, "The Origins of Hydration Forces: Monte Carlo Simulations and Density Functional Theory", *Langmuir*, Vol.13, 5459-5464, 1997.

FTFC (Fine Tailings Fundamentals Consortium), "Advances in Oil Sands Tailings Research", AOSTRA, Edmonton, 1995.

Grabbe, A and R.G. Horn, "Double-Layer and Hydration Forces Measured between Silica Sheets Subjected to Various Surface Treatments", *J Colloid Interface Sci*, Vol.157, 375-383, 1993.

Graig, V.S.J., B.W. Ninham and R.M. Pashley, "Direct Measurement of Hydrophobic Forces: A Study of Dissolved Gas, Approach Rate, and Neutron Irradiation", *Langmuir*, Vol.15, 1562-1569, 1999.

Gu, G., Z. Xu, K. Nandakumar and J. Masliyah, "Influence of Water-Soluble and Water-insoluble Natural Surface Active Components on the Stability of Water-in-toluene-diluted Bitumen Emulsion", *Fuel*, Vol.81, 1859-1869, 2002.

Gu, G., Z. Xu, K. Nandakumar and J. Masliyah, "Effects of Physical Environment on Induction Time of Air-bitumen Attachment", *Inter J Miner Process*, Vol.69, 235-250, 2003.

Hartley, P. G., F. Grieser, P. Mulvaney and G.W. Stevens, "Surface Forces and Deformation at the Oil-Water Interface Probed Using AFM Force Measurement", *Langmuir*, Vol. 15, 7282-7289, 1999.

Heath, O. and T.E. Tadros, "Influence of pH, Electrolyte, and Polyvinyl-Alcohol Addition on the Rheological Characteristics of Aqueous Dispersions of Sodium Montmorillonite", *J Colloid Interface Sci*, Vol.93, 307-319, 1983.

Hepler, L.G. and C. Hsi, "AOSTRA Technical Handbook on Oil Sands, Bitumen and Heavy Oils", *AOSTRA technical publication series #6*, Alberta Oil Sands Technology and Research Authority: Edmonton, AB, 1989.

Hepler, L.G. and R.G. Smith, "The Alberta Oil Sands: Industrial Procedures for Extraction and Some Recent Fundamental Research", *AOSTRA technical publication series #14*, Alberta Oil Sands Technology and Research Authority: Edmonton, AB, 1994.

Horn, R.G., D. J. Bachmann, J.N. Connor and S.J. Miklavic, "The Effect of Surface and Hydrodynamic Forces on the Shape of a Fluid Drop Approaching a Solid Surface", *J Phys Conden Mat*, Vol.8, 9483-9490, 1996.

Hunter, J.R., *Introduction to Modern Colloid Science*. Oxford Press: New York, NY, 1993.

Ingersent, K., J. Klien and P. Pincus, "Forces between Surfaces with Adsorbed Polymers 3. Theta Solvent Calculations and Comparison with Experiment", *Macromolecules*, Vol.23, 548-560, 1990.

Israelachvili, J.N. and G.E. Adams, "Measurement of Forces between 2 Mica Surfaces in Aqueous-electrolyte Solutions in Range 0-100nm", *J Chem Soc, Faraday Trans*, Vol.74, 975-100, 1978.

Israelachvili, J.N. and R.M. Pashley, "The Hydrophobic Interaction Is Long-range, Decaying Exponentially with Distance", *Nature*, Vol.300, 341-342, 1982.

Israelachvili, J .N. and R.M. Pashley, "Measurement of the Hydrophobic Interaction between 2 Hydrophobic Surfaces in Aqueous-electrolyte Solutions", *J Colloid Interface Sci*, Vol. 98, 500-514, 1984.

Israelachvili, J.N., Tirrel, M., and J. Klein, "Forces between 2 Adsorbed Polyethylene Immersed in Cyclohexane below and above the Theta-temperature", *Macromolecules*, Vol.17, 204-209, 1984.

Israelachvili, J.N., *Intermolecular and surface forces*, 2nd ed. Academic Press, San Diego, 1992.

Jada, A., B. Siffert and M. Salou, "Effects of the Bitumen Polar Fractions in the Stability of Bitumen Aqueous Dispersions", *Petrol Sci Technol*, Vol.19, 119-127, 2001

Johnson, K.L., K. Kendalland and A.D. Roberts, "Surface Energy and the Contact of Elastic Bodies", *Proc R Soc Lond A.*, Vol.324, 301-313, 1971.

Kappl, M and H.J. Butt, "The Colloidal Probe Technique and Its Application to Adhesion Force Measurements", *Part Part Syst Char*, Vol.19, 129-144, 2002

Kasongo, T., Z. Zhou, Z. Xu and J. Masliyah, "Effect of Clays and Calcium Ions on Bitumen Extraction from Athabasca Oil Sands Using Flotation", *Can J Chem Eng*, Vol. 78, 674-681, 2000.

Kent, W. and J. Ralston, "Polymer-Stabilized Emulsions and Fine-Particle Recovery, II. The Chalcopyrite-Quartz System", *Inter J Miner Process*, Vol.14, 1985, 217-232.

King, R. P. *Principles of Flotation*, South Africa Institute Mining Metallurgy: Johannesburg, 1982.

Klein, J., "Forces between Mica Surfaces bearing Layers of Adsorbed Polystyrene in Cycleohexane", *Nature*, Vol.288, 248-250, 1980.

Klein, J. and P.E. Luckham, "Forces between 2 Adsorbed Poly (ethylene oxide) Layer in a Good Aqueous Solvent in the Range 0-150nm", *Macromolecules*, Vol.17, 1041-1048, 1984.

Kotlyar, L.S. and B.D. Sparks, "Isolation of Inorganic Matter-Humic Complexes from Athabasca Oil Sands", *AOSTRA Journal of Research*, Vol. 2, 103-111, 1985.

Laroche, I., X. Wu, J.H. Masliyah, J. Czarnecki and T. Dabros, "Dynamic and Static Interactions between Bitumen Droplets in Water", *J Colloid Interface Sci*, Vol. 250, 316-326, 2002.

Laskowski, J.S. "Weak electrolyte collectors". In *Advances in Flotation Technology*. Barekh, B. K.; Miller, J.D. Eds.; SME Inc.: Littleton, CO, 1999, 58-82.

Liu, J., Z. Zhou and Z. Xu, "Electrokinetic Study of Hexane Droplets in Surfactant Solutions and Process Water of Bitumen Extraction Systems" *Ind Eng Chem Res*, Vol.41, 52-57, 2002.

Luthra, M., Master Thesis: *A visualization technique for estimating bitumen recovery from oil sands*, University of Alberta, 2001.

Mackay, G.D.M., A.Y. Mclean, O.J. Betancourt and, B.D. Jhonson "The Formation of Water-in-Oil Emulsions Subsequent to an Oil Spill", *J Colloid Interface Sci*, Vol.59, 164-173, 1973.

Malysa, K., S. Ng, L. Cymbalisty, J. Czarnecki and J. Masliyah, "A Method of Visualization and Characterization of Aggregate Flow Inside a Separation Vessel, Part I. Size, Shape and Rise Velocity of the Aggregates", *Inter J Miner Process*, Vol.55, 171-188, 1999.

Malysa, K., S. Ng, L. Cymbalisty, J. Czarnecki and J. Masliyah, "A Method of Visualization and Characterization of Aggregate Flow Inside a Separation Vessel, Part II. Composition of the Bitumen-Air Aggregates", *Inter J Miner Process*, Vol.55, 189-202, 1999.

Mankowski, P., S. Ng, R. Siy, J. Spence and P. Stapleton, "Syncrude's Low Energy Extraction Process: Commercial Implementation", *Syncrude Research Report*, 1990.

Marra, J. and M.L. Hair, "Interaction between Adsorbed Polystyrene Layers in Acetone Heptane Solvent Mixtures - Effect of Segment of Surface Adsorption Affinity", *Macromolecules*, Vol.21, 2356-2362, 1988.

Marra, J. and H.K. Christenson, "Effect of Miscible and Immiscible Polar Displacers on the Forces between Adsorbed Polystyrene Layers in Nonpolar-solvents", *J Phys Chem*, Vol.93, 7180-7184, 1989.

Masliyah, J.H., *Electrokinetic Transport Phenomena*, AOSTRA Series #12, University of Alberta, Edmonton, AB, Canada, 1994.

Masliyah, J., "Intensive Short Course: Extraction of Oilsands Bitumen", University of Alberta, Edmonton, AB, Canada, 2000.

Masliyah, J., "Intensive Short Course: Extraction of Oilsands Bitumen", University of Alberta, Edmonton, AB, Canada, 2003.

Masliyah, J., Z. Zhou, Z. Xu, J. Czarnecki and H. Hamza, "Understanding Water-Based Bitumen Extraction from Athabasca Oil Sands", submitted to *Can J Chem Eng* (Aug. 2003).

Meagher, L., "Direct Measurement of Forces between Silica Surfaces in Aqueous $CaCl_2$ Solutions Using an Atomic Force Microscope", *J Colloid Interface Sci*, Vol.152, 293-295, 1992.

Meyer, E., R.M. Overney, K. Dransfeld and T. Gyalog, *Nanscience: Friction and Rheology on the Nonometer Scale*, World Scientific Publishing Co., Singapore, 1998.

Miklavic, S.J., R.G. Hornand D. J. Bachmann, "Colloidal Interaction between a Rigid Solid and a Fluid Drop", *J Phys Chem*, Vol.99, 16357-16364, 1995.

Miklavic, S.J., "Deformation of Fluid Interfaces under Double-layer Forces Stabilizes Bubble Dispersions", *Phys Rev E*, Vol. 54, 6551-6556, 1996.

Moran, K., A. Yeung, J. Czarnecki and J. Masliyah, "Mirco-scale Tensiometry for Studying Density-matched and Highly Viscous Fluids – with Application to Bitumen-in-Water Emulsions", *Colloids Surf A*, Vol.174, 147-157, 2000.

Moran, K., A. Yeung and J. Masliyah, "Factors Affecting the Aeration of Small Bitumen Droplets", *Can J Chem Eng*, Vol.74, 625-634, 2000.

Mossop, G.D., "Geology of the Athabasca Oil Sands", *Science*, Vol.207, 145-152, 1980.

Mulvaney, P., J.M. Perera, S. Biggs, F. Grieser and G.W. Stevens, "The Direct Measurement of the Interaction between a Colloid Particle and an Oil Droplets", *J Colloid Interface Sci*, Vol.183, 614-616, 1996.

Ng, S., P. Warszynski, M. Zembala and K. Malysa, "Bitumen-Air Aggregates Flow to Froth Layer: I. Method of Analysis", Miner Eng, Vol. 13, 1505-1517, 2000a.

Ng, S., P. Warszynski, M. Zembala and K. Malysa, "Bitumen-Air Aggregates Flow to Froth Layer. II. Effect of Ore Grade and Operating Conditions on Aggregate Composition and Bitumen Recovery", *Miner Eng*, Vol. 13, 1519-1532, 2000b.

Nishimura, S., M. Kodama, H. Noma, K. Inoue and H, Tateyama, "The Use of AFM for Direct Force Measurements between Expandable Fluorine Mica", *Colloid Surf A*, Vol.143, 1-16, 1998.

Olphen, H.V., *An Introduction to Clay Colloid Chemistry* (2nd edition), John Wiley & Sons, Inc., New York, USA, 1976.

O'Shea S.J., M.E. Welland and T. Rayment, "An Atomic Force Microscope Study of Grafted Polymers on Mica", *Langmuir*, Vol.9, 1826-1835, 1993.

Outrim, C.P. and R.G. Evan, "Alberta's Oil Sands Reserves and their Evaluation", **in** *The Oil Sands of Canada – Venezuela*, CIM special Issue, Vol.17, D.A. Redford and A.G. Winestock, Eds., 1997.

Parker, J. L. and P. M. Claesson, "Forces between Hydrophobic Silanated Glass Surfaces", *Langmuir*, Vol.10, 635-639, 1994.

Pashley, R.M., "Hydration Force between Mica Surface in Aqueous Electrolyte Solutions", *J Colloid Interface Sci*, Vol.80, 153-162, 1981a.

Pashley, R.M., "DLVO and Hydration Force between Mica Surface in Li^+, Na^+, K^+, and Cs^+ Electrolyte Solutions - A Correlation of Double-layer and Hydration Forces With Surface Cation-Exchange Properties", *J Colloid Interface Sci*, Vol. 83, 531-546, 1981b.

Pincus, P. "Colloid Stabilization with Grafted Polyelectrolytes", *Macromolecules*, Vol.24, 2912-2919, 1991.

Preuss, M. and H.J. Butt, "Direct Measurement of Particle-Bubble Interactions In Aqueous Electrolyte: Dependence on Surfactant", *Langmuir*, Vol.14, 3164-3714, 1998.

Rabinovich, Y.I. and R.H. Yoon, "Use of Atomic Force Microscope for the Measurements of Hydrophobic Forces between Silanated Silica Plate and Glass Sphere"' *Langmuir*, Vol.10, 1903-1909, 1994.

Rabinovich, Y.I., M.S. Esayanur, K.D Johanson, J.J. Adler and B.M. Moudgil "Measurement of Oil-Mediated Particle adhesion to a silica Substrate by Atomic Force Microscope", *J Adhe Sci Tech, Vol.16, 887-904, 2002*.

Ralston, J., Kent, W. and G. Newcombe, "Stabilized-stabilized Emulsions and Fine-particle recovery, I. The Calcite-Quartz system", *Inter J Miner Process*, Vol.13, 1984, 167-186.

Ralston, J., D. Fornasiero and N. Mishchuk, "The Hydrophobic Force in Flotation –a Critigue", *Colloid Surf A*, Vol.192, 39-51, 2001.

Ravishankar S.A. and R.H. Yoon, "Long-Range Hydrophobic Forces in the Amine Flotation of Quartz", *Miner Metall Proc*, Vol.14, 10-17, 1997.

Sader, J.E. I. Larson, P. Mulvancy and L.R. White, "Method for the Calibration of Atomic Force Microscopic Cantilevers", *Rev Sci Instrum*, Vol.66, 3789-3798, 1995.

Salou, M., B. Siffert and A. Jada, "Study of the Stability of Bitumen Emulsions by Application of DLVO Theory", *Colloid Surf A*, Vol.142, 9-16, 1998a.

Salou, M., B. Siffert and A. Jada "Interfacial Characteristic of Petroleum Bitumen in Contact with Acid Water", *Fuel*, Vol. 77, 343-346, 1998b.

Sanford, E.C., "Processibility of Athabasca Oil Sand: Inter-relationship between Oil and Fine Sands", *Can J Chem Eng*, Vol.61, 554-567, 1983.

Sanford, E.C. and F.A. Seyer, "Processibility of Athabasca Tar Sand Using Batch Extraction Unit: the Role of NaOH", *CIM Bulletin*, Vol.72, 164-169, 1979.

Schramm, L. L., R.G. Smith and J.A. Stone, "The Influence of Natural Surfactant Concentration on Hot Water Process For Recovering Bitumen from the Athabasca Oil Sands", *AOSTRA J Res*, Vol.1, 5-13, 1984.

Schramm, L. L., R.G. Smith and J.A. Stone, "A Surface-tension Method for the Determination of Anionic Surfactants in Hot Water Processing of Athabasca Oil Sands", *Colloid Surf*, Vol.11, 247-263, 1984.

Schramm, L. L. and R.G. Smith, "The Influence of Natural Surfactant on Interfacial Charges in the Hot Water Process For Recovering Bitumen from the Athabasca Oil Sands", *Colloid Surf*, Vol. 14, 67-85, 1985.

Schramm, L. L. and R.G. Smith, "Two Classes of Anionic Surfactants and their Significance in Hot Water Processing of Oil Sands", *Can J Chem Eng*, Vol. 65, 799-811, 1987.

Schramm L.L., E.N. Stasuik and D. Turner, "The Influence of Interfacial Tension in the Recovery of Bitumen by Water-Based Conditioning and Flotation of Athabasca Oil Sands", *Fuel Proc Technol*, Vol. 80, 101-118, 2003.

Sheeran, D.E. "Volume Reduction of Clark Hot Water Extraction Fine Tailings". In *Advancing in oil sands tailings research.* Alberta Department of Energy (Oil Sands Research Division): Edmonton, AB, Vol. III, 1-56, 1995.

Smith R.G. and L. L. Schramm, "The Influence of Mineral Components on the Generation of Natural Surfactants From Athabasca Oil Sands in the Alkaline Hot Water Process", *Fuel Proc Technol*, Vol.30, 1-14, 1992.

Somasundaran, P. and A. Luo, "Oxide Mineral Flotation Fundamentals", In: *Advances in Flotation Technology*, B.K.Parekh and J.D. Miller eds., Society for Mining, Metallurgy, and Exploration, Inc., Denver, CO, 23-43, 1999.

Sondi, I., J. Biscan and V. Pravdic, "Electrokinetics of Pure Clay Minerals Revisited", *J Colloid Interface Sci*, Vol.178, 514-522, 1996.

Sondi, I., O. Milat and V. Pravdic, "Electrokinetic Potentials of Clay Surfaces Modified by Polymers", *J Colloid Interface Sci*, Vol.189, 66-73, 1997.

Spence, J., R. Siy, K. Sury, K. McDowell and S. Ng, "Aurora Extraction Process: 1995 OSLO Cold Water Extraction Research Pilot Test Program", *Syncrude Research Report 96-3*, June 1996.

Sury, K.N., "Low Temperature Bitumen Recovery Process", US patent 4 946 597, August 7, 1990.

Sury, K.N., "Low Temperature Bitumen Recovery Process", Canadian Patent 1,302,327, June 2, 1992.

Synder B. A., D.E. Aston and J.C. Berg, "Particle-Drop Interactions Examined with an Atomic Force Microscope", *Langmuir,* Vol.13, 590-593, 1997.

Takamura K., "Microscopic Structure of Ahtabasca Oil Sands", *Can J Chem Eng*, Vol.60, 538-545, 1982.

Takamura, K. and R.S. Chow, "A Mechanism for Initiation of Bitumen Displacement from Oil Sands", *J Can Petrol Technol*, Vol.22, 22-30, 1983.

Takamura, K. and R.S. Chow, "The Electric Properties of the Bitumen/Water Interface Part II: Application of the Ionizable Surface-group Model", *Colloid Surf*, Vol.15, 35-48, 1985.

Takamura, K. and D.Wallace, "The Physical-Chemistry of the Hot Water Process", *J Can Petrol Technol,* Vol. 27, 98-106, 1988.

Vakarelski, I.U., A. Toritani, M. Nakayama and K. Higashitani, "Effects of Particle Deformability on Interaction between Surfaces in Solutions", *Langmuir*, Vol.19, 110-117, 2003.

Vanoss, C.J., M.K. Chaudhury and R.J. Good, "Interfacial Lifshitz-van der Waals and Polar Interactions in Macroscopic Systems", *Chem Rev*, Vol.88, 927-941, 1988.

Veeramasuneni, S., M.R. Yalamanchili and J.D. Miller, "Measurement of Interaction Force between Silica and Alumina by Atomic Force Microscope", *J Colloid Interface Sci*, Vol.184, 594-600, 1996.

Vincent, B., "The van der Waals Attraction between Colloidal Particles Having Adsorbed layers: II. Calculation of Interaction Curves", *J Colloid Interface Sci*, Vol.42, 270-285, 1973.

Wallwork, V., Z. Xu and J. Masliyah, "Processibilty of Athabasca Oil Sand Using a Laboratory Hydrotransport Extraction System (LHES)", Can J Chem Eng, (2003, in press).

Wang, C. X., S.Z. Wan, Z.X. Xiang and Y.Y. Shi, "Incorporation Hydration force Determined by Boundary Element Method into Stochastic Dynamics", *J Phys Chem B*, Vol.101, 230-235, 1997.

Wang, W., Z. A. Zhou, K. Nandakumar, Z. Xu and J. Masliyah, "Attachment of Individual Particles to a Stationary Air Bubble", *Inter J Miner Process*, Vol. 68, 47-69, 2003a.

Wang, W., Z. A. Zhou, K. Nandakumar, Z. Xu and J. Masliyah, "Effect of Surface Mobility on the Sliding of Glass Beads around a Bubble or Glass Sphere", *J Colloid Interface Sci*, Vol.259, 81-88, 2003b.

Wang, W., Zhou, Z. A., Nandakumar, K., Xu, Z. and Masliyah, J., "An Induction Time Model for the Attachment of an Air Bubble on a Hydrophobic Sphere in Aqueous Solutions", *Inter J Miner Process*, (2003c, submitted).

Warszynski, P and Z. Adamczyk, "Calculation of Double Layer Electrostatic Interaction for the Sphere/plane Geometry", *J Colloid Interface Sci*, Vol.187, 283-295, 1997.

Wen, W.W. and S.C. Sun, "An Electrokinetic Study on the Oil Flotation of Oxidized Coal", *Separation Sci Technol*, Vol.16, 1491-1521, 1981.

White, L.R., "On the Derjaguin Approximation for the Interaction of Macro-bodies", *J Colloid Interface Sci*, Vol.95, 286-288, 1983.

Wiacek, A. and E. Chibowski, "Zeta Potential, Effective Diameter and Multimodal Size Distribution in Oil/Water Emulsion", *Colloid Surf A*, Vol.159, 253-261, 1999.

Williams M.C. and D.W. Fuerstenau, "A Simple Flotation for Rapidly Assessing the Hydrophobicity of Coal Particles", *Inter J Miner Process*, Vol.20, 153-157, 1987

Wu, X., J. Czarnecki, N. Hamza and J.H. Masliyah "Interaction Forces between Bitumen Droplets in Water", *Langmuir*, Vol.15, 5244-5250, 1999a.

Wu, X., T. Dabros and J. Czarnecki, "Determining the Colloidal Forces between Bitumen Droplets in Water Using the Hydrodynamic Force Balance Technique", *Langmuir*, Vol.15, 7806-8713, 1999b.

Wu, X., I. Laroche, J.H. Masliyah, J. Czarnecki and T. Dabros, "Applications of Colloidal Force Measurements Using a Microcollider Apparatus to Oil Sand Studies", *Colloid Surf A*, Vol.174, 133-146, 2000.

Yang, C., T. Dabros, D.Q. Li, J. Czarnecki and J.H. Masliyah, "A Visualization Method for Study of Micron Bubble Attachment onto a Solid Surface under Varying Physicochemistry Conditions", *Ind Eng Chem Res*, Vol.39, 4949-4955, 2000.

Yang, C., Ph. D. thesis: *Attachment of fine gas bubbles onto a solid surface and electrokinetics of gas bubbles*, University of Alberta, 2000.

Yoon, R.H, D. Guzonas, B.S Aksoy, J. Czarnecki and A. Leung, "Role of Surface Forces in Tar Sand Processing", *Processing of Hydrophobic Minerals and Fine Coal. Proceeding of the 1st UBC-McGill Bit-Annual International Symposium*, 277-289, 1995.

Yoon, R.H., D.H. Flinn and Y.I. Rabinovich, "Hydrophobic Interactions between Dissimilar Surfaces", *J Colloid Interface Sci*, Vol.185, 363-370, 1997.

Yoon, R.H. and Y.I Rabinocich, "Role of Asphaltene in the Processing of Tar Sand", *Polymers in Mineral Processing: Proceeding of the 3rd UBC-McGill Bi-Annual International Symposium*, CIM, Montreal, Quebec 1999.

Zhang, L.Y., S. Lawrence, Z. Xu and J. Masliyah, "Studies of Athabasca Asphaltene Langmuir Films at Air–Water Interface", *J Colloid Interface Sci*, Vol. 264, 128-140, 2003a.

Zhang, L.Y., Z. Xu and J. Masliyah, "Langmuir and Langmuir-Blodgett Films of Mixed Asphaltene and a Demulsifier", *Langmuir*, Accepted (2003b)

Zhou, Z.A., H. Hussein, Z. Xu, J. Czarnecki and J. H. Masliyah, "Interaction of Ionic Species and Fine Solids with a Low Energy Hydrophobic Surface from Contact Angle Measurement", *J Colloid Interface Sci*, Vol.204, 342-349,1998.

Zhou, Z.A., Z. Xu, J.H. Masliyah and J. Czarnecki, "Coagulation of Bitumen with Fine Silica in Model Systems", *Colloid Surf A*, Vol.148, 199-211, 1999.

Zhou, Z., Z. Xu and J. Masliyah, "Effect of Natural Surfactants Released from Athabasca Oil Sands on Air Holdup in a Water Column", *Can J Chem Eng*, Vol.78, 617-624, 2000a.

Zhou, Z. A., Z. Xu, J. Masliyah, T. Kasongo, T. Kizior and D. Cox, "Application of On-Line Visualization to Flotation Systems", Proceedings, *32nd Annual Meeting of Canadian Mineral Processors*, Ottawa, Canada, 119-137, 2000b.

APPENDIX

A: Fundamental principle of AFM

In 1982, Binnig et al. (1982) developed a scanning tunneling microscope (STM), which is capable of imaging conductors at the Angstrom resolution. This landmark contribution was recognized with a Noble price in physics in 1986. In the same year, Binnig with his colleagues (Binnig et al., 1986) reported a STM's next of kin-AFM device, which can be used not only to image the surfaces of both conductor and non-conductor materials, but also to measure molecular or colloidal forces at nN level.

In AFM, the elastic deformation of the spring caused by the force between tip and surface is monitored. Well-developed devices such as a laser beam can measure such displacement as small as 10^{-4}~10^{-6} Angstroms. The force produced by such a small displacement can be as small as 10^{-18} N by choice of delicate spring (with spring constant 0.01 N/m). This level of sensitivity certainly penetrates the region of inter-atomic force between single atoms, and opens the doors to a variety of applications to the micro-world! As shown in Figure A.1, a typical AFM consists mainly of a piezo scanner, a cantilever substrate with four cantilevers (springs), a laser source and a split photodiode. The piezo scanner is used to position and scan the sample substrate fixed on the piezo stage, relative to the tip or the probe particle on a cantilever spring, at a nanometer resolution in three-dimensions. The force between the sample substrate and probe particle then causes the cantilever spring to deflect upward or downward, depending on the nature of the force between them. The deflection of cantilever spring is detected with a position-sensitive laser beam that is focused on the upper surface of the cantilever spring right above the tip position and reflected to the split photodiodes through a mirror. A relationship between cantilever deflection and sample position can be obtained via a computer data acquisition system by employing various feedback options. A thorough discussion of AFM is given in a monograph by D. Sarid (1991). Today, a whole family of Scanning Probe Microscope (SPM) is commercially available, specializing in imagining topography, measuring colloidal force, determining chemical, magnetic, viscoelastic, frictional, electrical, and thermal features of surfaces at a resolution ranging from atomic to macroscopic scale (Erlandsson et al., 1988; Nonnenmacher et al., 1991; Frisble et al.,

1994; Bohm, 1996; Noy et al., 1997; Bottomley, 1998; Takano and Porter, 2001; Burgi et al., 2002; Roseman and Grutter, 2002; Hodges, 2002; Carcia and Perez, 2002; Kappl and Butt, 2002; Best et al., 2003).

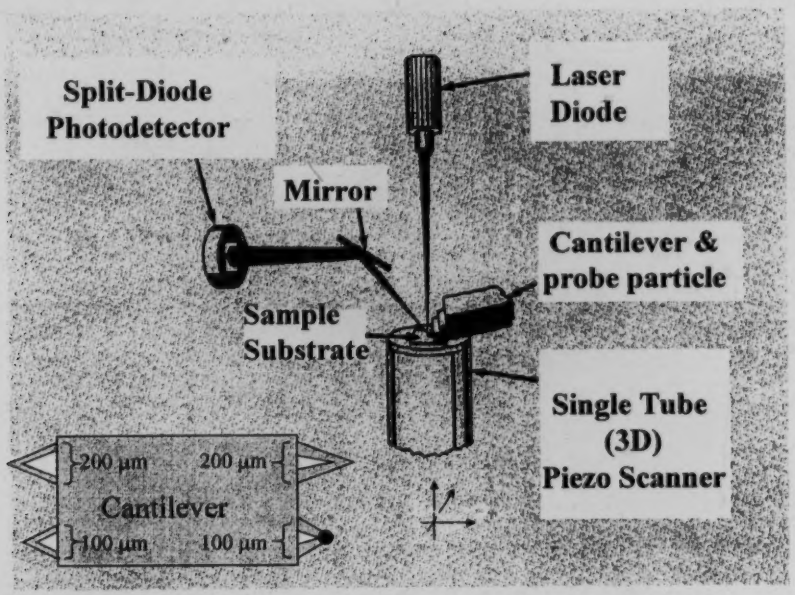

Figure A.1 Schematic of an atomic force microscope (AFM technique).

B. AFM imaging technique

A Nanoscope J AFM is used for imagining. The AFM has been successfully used to image both conducting and non-conducting materials at atomic resolution. Images are obtained by measurement of the force on a sharp tip created by the proximity to the surface of the sample. This force is kept small at a constant level with a feedback mechanism. When the tip scans over the surface in a raster pattern, it will follow the surface counters to keep the force (i.e. the distance) between the tip and surface constant. In general, there are two operation modes.

In the contact mode (imaging), the force (normally10^{-9}~10^{-7}N) between the tip and sample surface is kept constant by the feedback loop while the tip maps the surface (XY) plane. To complete this action, the piezo continuously adjusts its extension to maintain a constant deflection of the cantilever since the applied force to the tip depends on the deflection of the cantilever, which otherwise would vary as the tip scans across a featured surface. By monitoring the voltage applied to control the piezo extension, a three-

dimensional topographic image is yielded. In the tapping model (imaging), the cantilever oscillates at its resonant frequency, excited by a piezo stack. As the cantilever oscillates vertically, the reflected laser beam is defected in a regular pattern over a photodiode array, generating a sinusoidal electric signal. During imaging process, the piezo stack continues to excite the cantilever substrate with the fixed energy, while the tip is deflected in its encounter with the surface. The deflected laser beam reveals the information about the characteristics of the sample surface. Tapping mode imaging is particularly useful for imaging soft surfaces at high resolution with minimal surface damage.

The surface topography is visualized using computer graphics capabilities. Surface-related features such as average roughness, size of particles, distance and angles between nano or micro objects can be calculated easily.

C. AFM force profile and data analysis

The raw data from AFM measurement are only in the form of "Tip deflection (voltage)-Piezo displacement (nm)". To fully utilize this information, the data analysis is critical, especially in cases involving a deformable surface/probe. In the current study, the data processing procedure is shown in Figure A.2. The specific description for each step is given below.

- Baseline correction

Theoretically, the baseline where the cantilever deflection or the interaction force is zero at far away separation should be a horizontal line. However, the signal drift or laser scattering often cause the baseline to incline slightly. Therefore, baseline correction is needed. To accomplish this, the zero force region is fitted by a liner function, as shown by a solid line in Figure A.2a. The raw data is then corrected by subtracting this linear function to correct instrument drift. After this correction, a horizontal line of zero over the zero force regions is obtained (Figure A.2b).

- "Constant compliance region" assumption

As mentioned early, AFM records the data as "tip deflection (voltage) vs. piezo displacement (nm)". The recorded tip deflection in voltage needs to be converted into tip deflection in nm to calculate the force. To accomplish this conversion, a "constant compliance region" or "hard wall contact" (where the piezo and cantilever move together at the same rate) needs to be identified (shown by a solid line in Figure A.2b). The conversion of the cantilever deflection from voltage to nm is achieved by dividing the cantilever deflection in voltage by the slope of the "constant compliance region", as shown in Figure A.2c.

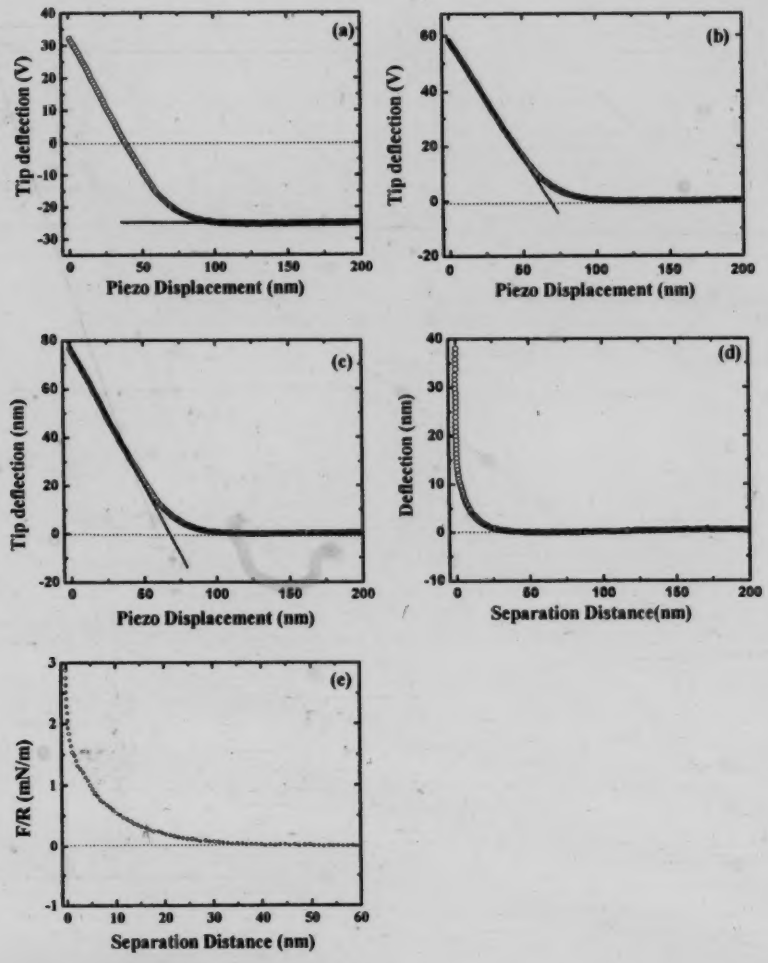

Figure A.2 Data processing procedure of surface force measurement with AFM.

- Zero distance assumption

Over the "constant compliance region", the separation between tip and substrate is assumed to be zero. The separation can then be obtained by subtracting the cantilever deflection from the piezo displacement. To accomplish this, the "constant compliance region" is fitted by a linear function, as shown by the line in Figure A.2c. The data of tip deflection vs. Piezo displacement is then subtracted by this linear function to get the separation between tip and substrate, as shown by Figure A.2d.

- Force profile

The interaction force as a function of separation distance is simply determined by multiplying the cantilever deflection by the cantilever spring constant. The obtained force profiles are further normalized by the radius of probe particle and the resultant force profiles is shown in Figure A.2e.

- Surface deformation

For a deformable surface, accurate separation cannot be obtained by the procedure described above. Both the attractive and repulsive forces might cause surface to deform before, at and after contact. The deformation can be modeled by three different approaches based on contact mechanics, elastic model or exact analytical solution of Laplace equation.

Contact mechanics theory incorporated in Hertz (Meyer et al., 1998), JKR (Johnson et al., 1971) and DTM (Derjaguin et al., 1975) models can be used to predict the central displacement when two surfaces are in contact. However, it cannot predict the deformation of surfaces before their contact.

Elastic model is based on the assumption that the bubble/drop behave as a purely elastic solid and the change in shape of the deformable object is negligible during interaction. The deformable object in this case can be characterized simply by an elastic parameter – spring constant, which remains constant throughout the interaction between a deformable object and a solid across a thin liquid film (Ducker et al., 1994; Fielden et al., 1996;

Preuss and Butt, 1998; Hartley et al., 1999, Dagastine and White, 2002; Vakarelski, 2003). However, not all the fluid interfacial deformation is a linear function of the applied force. Therefore, treating a deformable surface such as an oil droplet or an air bubble as an elastic object (Hookean spring) would incur a significant deviation.

To avoid any assumptions, a more rigorous method for interpreting the experimental force-distance profile is developed. Equilibrium shapes of the deformable surfaces such as oil drops or air bubbles are calculated with the augmented Young-Laplace equation given below (Miklavic et al., 1995; Bachmann and Miklavic, 1996; Miklavic, 1996; Horn et al., 1996; Aston and Berg, 2001; Bhatt et al., 2001; Chan et al., 2001 and Attard, 2001).

$$\gamma\left(\frac{z''(r)}{(1+z'(r)^2)^{3/2}}+\frac{z'(r)}{r\sqrt{1+z'(r)^2}}\right)=g\Delta\rho z(r)-[P_0-\Pi(D(r))] \qquad \text{(A-1)}$$

where γ is the interfacial energy, $g\Delta\rho z$ is the net gravity force, P_0 is the internal pressure of the drop, Π is disjoining pressure (sum of surface forces). This method can rigorously describe the deformation of deformable interface, but the assumption of a parameterized $\Pi(D)$ must be made first.

To simplify the concern of deformation in current study, the deformation of bitumen surface was minimized by coating silica wafers or spheres with a diluted bitumen solution. Using this method, a thin bitumen film in the order of 100 nm can be obtained. With such a thin bitumen film, the deformation can be negligible as confirmed experimentally in Chapters 6 and 7.

- Hydrodynamic force and scan rate

When particles move in a fluid, hydrodynamic forces have to be considered. For a sphere-plate system in a medium of viscosity η, the hydrodynamic force F_H at separation D is given by (Chan and Horn, 1985).

$$F_H = -\frac{6\pi\eta R^2}{D}\frac{dD}{dt} \quad \text{where} \quad R = \frac{R_1 R_2}{R_1 + R_2} \tag{A-2}$$

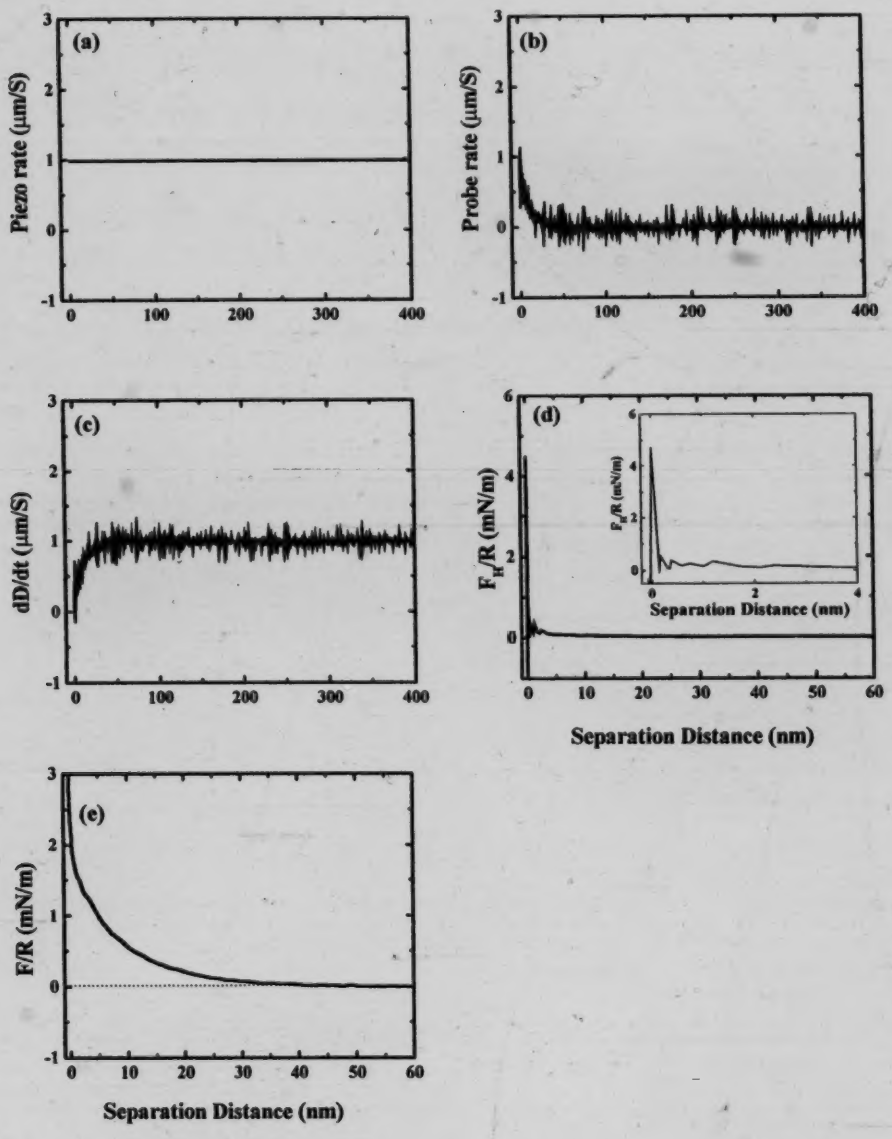

Figure A.3 Calculation of hydrodynamic force in an AFM surface force measurement. (a) Piezo moving rate; (b) probe moving rate; (c) local approach rate (dD/dt); (d) hydrodynamic force (F_H / R); and (e) interaction force (F/R).

The piezo approach rate is typically in the order of 1μm/s. To calculate hydrodynamic force on the probe, the local approach velocity of piezo has to be determined, which can be accomplished by considering the distance traveled between neighboring data points. For a typical force measurement with probe particle radius R=4μm at a piezo approach rate 1.97Hz, the calculated local approach rate and hydrodynamic force are shown in Figure A.3. As shown in Figure A.3d, the hydrodynamic force is negligible at separation greater than 0.2nm. Therefore, the hydrodynamic forces are not considered in the current study.

D: Numerical solution to DLVO theory-constant Stern potential as B.C.

Step 1: Numerical solution to non-linear Poisson-Boltzmann equation. The Poisson-Boltzmann equation can be re-arranged as:

$$\frac{d^2\psi}{dx^2} = f(\psi), \text{ With } f(\psi) = -\frac{e}{\varepsilon\varepsilon_0}\sum_j z_j n_{j\infty} e^{-z_j e\psi/kT} \tag{D-1}$$

$$\text{B.C.} \quad \begin{cases} \psi_0 \equiv \psi_a \\ \psi_n \equiv \psi_b \end{cases}$$

where n_j is the number density of ions j with valence z_j, $n_{j\infty}$ is the number density of ion j in the bulk, ψ is the electric potential in the double layer, e and k are the electron charge and Boltzmann constant, respectively, T is the temperature, ψ_a and ψ_b are the surface potentials of two surfaces a and b.

Assuming that the separation between two plates a and b is evenly divided into n steps with step size h, the differential equation can be expanded numerically with a step size h given by

$$h = \frac{x_n - x_0}{n}$$

Using central difference theorem with even space to expand left side of equation (D-1), one obtain:

$$\frac{d^2\psi(x_i)}{dx^2} = \frac{\psi_{i+1} - 2\psi_i + \psi_{i-1}}{h^2}, \text{ i=0,1, 2...n} \qquad \text{(D-2)}$$

Using Newton method to expand right side of equation (D-1):

$$f(x_i,\psi_i) = f(x_i,\psi_i^m) + f'_\psi(x_i,\psi_i^m)(\psi_i - \psi_i^m), \text{ i=0,1, 2...n} \qquad \text{(D-3)}$$

Combining equation (D-2) and (D-3) leads to a set of linear equations:

$$\begin{bmatrix} d_1 & 1 & & & & & \\ 1 & d_2 & 1 & & & & \\ & \ddots & \ddots & \ddots & & & \\ & & 1 & d_i & 1 & & \\ & & & \ddots & \ddots & \ddots & \\ & & & & 1 & d_{n-2} & 1 \\ & & & & & 1 & d_{n-1} \end{bmatrix} \begin{bmatrix} \psi_1 \\ \psi_2 \\ \vdots \\ \psi_i \\ \vdots \\ \psi_{n-2} \\ \psi_{n-1} \end{bmatrix} = \begin{bmatrix} b_1 \\ b_2 \\ \vdots \\ b_i \\ \vdots \\ b_{n-2} \\ b_{n-1} \end{bmatrix} \qquad \text{(D-4)}$$

in which :

$$d_i = -2 - h^2 f'_\psi(x_i,\psi_i^m), \quad \text{i=1,2,---, n-1}$$

$$b_i = h^2 f(x_i,\psi_i^m) - h^2 f'_\psi(x_i,\psi_i^m)\psi_i^m, \qquad \text{i=2, 3 --, n-2}$$

$$b_1 = -\psi_0 + h^2 f(x_1,\psi_1^m) - h^2 f'_\psi(x_1,\psi_1^m)\psi_1^m$$

$$b_{n-1} = -\psi_n + h^2 f(x_{n-1},\psi_{n-1}^m) - h^2 f'_\psi(x_{n-1},\psi_{n-1}^m)\psi_{n-1}^m$$

Boundary condition: $\begin{cases} \psi_0 = \psi_a \\ \psi_n = \psi_b \end{cases}$

Numerically, with initial guess $\underline{\psi^m}$, this matrix equation can be solved using Thomas Algorithm until the convergence is OK. Using this procedure, the surface potential distribution $\psi(x)$ between two plates can be obtained.

Step2: Numerical solution to osmotic pressure. First, the central difference theorem is used to calculate the differential of surface potentials:

$$\frac{d\psi(x_i)}{dx} = \frac{\psi(x_{i+1}) - \psi(x_{i-1})}{2h} \quad \text{i=2, 3, ...n-1.}$$

Then the pressure at separation D can be calculated at middle plane:

$$P(D) = kT\sum_i (n_i - n_{i\infty}) - \frac{\varepsilon\varepsilon_0}{2}\left(\frac{d\psi(x_{n/2})}{dx}\right)^2 = kT\sum_i n_{i\infty}(e^{-z_i e\psi(x_{n/2})/kT} - 1) - \frac{\varepsilon\varepsilon_0}{2}\left(\frac{d\psi(x_{n/2})}{dx}\right)^2$$

Step 3: Numerical solution to electrostatic double layer energy. The interaction energy between two plates can be calculated by Trapezoidal rule:

$$U_E = -\int_{\infty}^{D} P(x)dx = \int_{D}^{\infty} P(h)dh = \frac{1}{2h}\sum_{j=i}^{\infty}(P_j + P_{j+1}) = \frac{1}{2h}(P_i + 2\sum_{j=i+1}^{\infty} P_j + P_n) \quad \text{per unit area}$$

Step 4: Numerical solution to van der Waals energy.

Step 5: Convert interaction energy to interaction force using equation (3-16).

The full Visual Basic code for DLVO theory is developed as shown below. The information about boundary condition, electrolyte (concentration and valence) and Hamaker constant has to be provided as the inputs. The other parameters including the temperature and the number of steps are optional. If these optional parameters are not specified, the default values of room temperature 22^0C and 101 points will be used in the calculation. The number of steps is only related to the accuracy of this method itself, and has nothing to with data fitting. Usually 100 to 400 points are used, with the larger number of steps resulting in a more precise result. Other parameters such as electrolyte concentration and surface potential are the adjustable parameters for data fitting. First,

the electrolyte concentration is changed to obtain the best fit of the decay length to the interaction force at larger separation (20 ~100 nm). Then the surface potentials are altered to fit the force profile.

```
Option Base 1
Option Explicit
'This code is designed to calculate the DLVO theory

---------------------------------------------------------------------

Function DLVO(Potentialbound, C, Z, Ha, Optional n As Integer = 11, Optional xbound
As Double = 110, Optional T As Double = 25, Optional tol As Double = 0.000000001)
Dim Ve() As Double, Vtotal() As Double, h As Double, i As Integer, j As Integer, tem()
As Double
ReDim Ve(n, 4), Vtotal(n, 11), tem(n)
h = xbound / 1000000000# / (n - 1)  ' stepsize

'Claculate the separation Vtotal(i,1), nm

For i = 1 To n
Vtotal(i, 1) = (i - 1) * h * 1000000000#
Next i
' calculate the electric force Vtotal(i, 2) for plate-plate

For i = 2 To n
Call Velect(Ve, Vtotal(i, 1), Potentialbound, C, Z, n, T, tol)
Vtotal(i, 2) = Ve(n / 2, 4)
Next i
'calculate the electric energy Vtotal(i, 3) for plate-plate

For i = 1 To n
tem(i) = 0#
For j = i + 1 To n - 1
tem(i) = tem(i) + Vtotal(j, 2)
Next j
Vtotal(i, 3) = (h / 2# * (Vtotal(i, 2) + 2# * tem(i) + Vtotal(n, 2))) * 1000#
Next i
'calculate Van der Waals energy Vtotal(i, 4)
Dim Ham As Double
Ham = (Ha(1) ^ 0.5 - Ha(3) ^ 0.5) * (Ha(2) ^ 0.5 - Ha(3) ^ 0.5)
Vtotal(1, 4) = (-Ham / 12# / 3.14159 / 0.000000000001 ^ 2) * 1000#
For i = 2 To n
Vtotal(i, 4) = (-Ham / 12# / 3.14159 / (Vtotal(i, 1) / 1000000000#) ^ 2) * 1000#  'for
plate-plate
Next i
'calculate the total force

For i = 1 To n
Vtotal(i, 5) = 2# * 3.14159 * (Vtotal(i, 3) + Vtotal(i, 4))
```

```
Next i

Dim tep() As Double
ReDim tep(n, 4)
For i = 1 To n
tep(i, 1) = Vtotal(i, 1)
tep(i, 2) = Vtotal(i, 5)
Next I
DLVO = tep
End Function
```

```
' calculate the surface potential distribution, surface potential differential & interaction
force between two plates

Sub Velect(Ve, xbound As Double, Potentialbound, C, Z, n As Integer, T As Double, tol
As Double)
Dim Ve0() As Double, A() As Double, b() As Double, h As Double
Dim i As Integer, sum1 As Double, sum2 As Double

ReDim Ve0(n - 2), A(n - 2, n - 2), b(n - 2), d(n - 2)
h = xbound / 1000000000# / (n - 1)
'calculate the zeta potential Ve(i,2), mV

Ve(1, 2) = Potentialbound(1)
Ve(n, 2) = Potentialbound(2)
For i = 1 To n - 2 ' initial guess
Ve0(i) = 0
Next i
Do
Call MatrixD(d, h, Ve0, n - 2, C, Z, T)   ' calculate the diagonal di
Call Martixb(b, h, Ve0, Potentialbound, n - 2, C, Z, T)  'calculate bi
Call Thomas(d, b, n - 2)    ' use Thomas method to solve the matrix equation
For i = 2 To n - 1
Ve(i, 2) = b(i - 1) * 1000
Next i
sum1 = 0#
sum2 = 0#
For i = 1 To n - 2
sum1 = sum1 + Abs(b(i) - Ve0(i))
sum2 = sum2 + Abs(b(i))
Next i
If (sum1 / sum2 < tol) Then Exit Do    ' check the convergence
For i = 1 To n - 2
Ve0(i) = b(i)
Next I
Loop
'calculate the potential differential Ve(i,3), v/m
```

```
Ve(1, 3) = (Ve(2, 2) - Ve(1, 2)) / 1000# / h
Ve(n, 3) = (Ve(n, 2) - Ve(n - 1, 2)) / 1000# / h
For i = 2 To n - 1
Ve(i, 3) = (Ve(i + 1, 2) - Ve(i - 1, 2)) / 2000# / h
Next i
'calculate force Ve(i,4) @ middle plane
Dim m As Integer, F As Double, j As Integer
m = C.Count
For j = 1 To n
F = 0
For i = 1 To m
F = F + C(i) * (Exp(-Z(i) * 1.602E-19 * Ve(n / 2, 2) / 1000# / 1.38E-23 / (T + 273)) - 1#)
Next i
Ve(j, 4) = 1.38E-23 * (T + 273) * 1000 * 6.03E+23 * F - 0.5 * 78.5 * 0.00000000000885
* Ve(n / 2, 3) ^ 2
Next j
End Sub
```

```
Sub MatrixD(d, h, y0, n As Integer, C, Z, T As Double)

Dim i As Integer
For i = 1 To n
d(i) = -2# - h ^ 2 * Jac(y0(i), C, Z, T)
Next i
End Sub
```

```
Private Function Jac (Y, C, Z, T) As Double
Dim n As Integer, i As Integer, F As Double
n = C.Count
F = 0
For i = 1 To n
F = F + C(i) * Z(i) ^ 2 * Exp(-Z(i) * 1.602E-19 * Y / 1.38E-23 / (T + 273))
Next i
Jac = F * (1000 * 6.03E+23) * (1.602E-19) ^ 2 / (1.38E-23 * (T + 273) * 78.5 *
0.00000000000885)
End Function
```

```
Sub Martixb(b, h, y0, Potenialbound, n, C, Z, T As Double)
Dim F() As Double, fy() As Double
ReDim F(n), fy(n)
Dim i As Integer
For i = 1 To n
F(i) = Fun(y0(i), C, Z, T)
fy(i) = Jac(y0(i), C, Z, T)
b(i) = h ^ 2 * F(i) - h ^ 2 * fy(i) * y0(i)
Next i
```

```
b(1) = -Potenialbound(1) / 1000# + b(1)
b(n) = -Potenialbound(2) / 1000# + b(n)
End Sub
```

```
Private Function Fun(Y, C, Z, T) As Double
Dim n As Integer, i As Integer
n = C.Count
For i = 1 To n
Fun = Fun - (1000 * 6.02E+23) * 1.602E-19 / (78.5 * 0.00000000000885) * (C(i) * Z(i) *
Exp(-Z(i) * 1.602E-19 * Y / 1.38E-23 / (T + 273)))
Next i
End Function
```

```
Sub Thomas(d, r, ByVal n As Integer, Optional ByVal ist As Integer = 1)
'This subroutine solves a set of tridiagonal linear equations using Thomas Algorithm
'd contains the diangular terms

'Forward substitution
Dim i As Integer
For i = ist + 1 To n

  d(i) = d(i) - 1# / d(i - 1)
  r(i) = r(i) - 1# * r(i - 1) / d(i - 1)
Next i

'Backward substitution
r(n) = r(n) / d(n)
For i = n - 1 To ist Step -1
 r(i) = (r(i) - 1# * r(i + 1)) / d(i)
Next i
'Solution obtained successfully!
End Sub
```

E: Numerical solution to DLVO theory-constant surface charge density as B.C.

Poisson-Boltzmann equation can be re-arranged as:

$$\frac{d^2\psi}{dx^2} = f(\psi), \text{ with } \quad f(\psi) = -\frac{e}{\varepsilon\varepsilon_0}\sum_j z_j n_{j\infty} e^{-z_j e\psi/kT}$$

$$\text{B.C.} \quad \begin{cases} \dfrac{d\psi(x_0)}{dx} \equiv a, & \psi(x_0) = \psi_a \\ \dfrac{d\psi(x_n)}{dx} \equiv b, & \psi(x_n) = \psi_b \end{cases}$$

Step 1: Calculation of surface charge density:

Transfer the non-linear Poisson-Boltzmann equation into form of equation

$$\frac{d^2\psi}{dx^2} = \frac{1}{2}d(\frac{d\psi}{dx})^2 = -\frac{e}{\varepsilon\varepsilon_0}\sum_j z_j n_{j\infty} e^{-z_j e\psi/kT}$$

for a single particle, we can get the values of a and b from given surface potential ψ_0 by equation

$$\frac{d\psi}{dx} = \pm\sqrt{\frac{2000NkT}{\varepsilon\varepsilon_0}\sum_j C_{j\infty}(e^{-\frac{z_j e\psi_0}{kT}} - 1)}$$

Step 2: calculate the zeta potential distribution:

By guessing the initial values: $\begin{cases}\psi_0 = \psi_a \\ \psi_n = \psi_b\end{cases}$, the routine described in Appendix A is used to calculate the potential distribution $\psi(x_i)$ and differential potential distribution $\frac{d\psi(x_i)}{dx}$.

Then check the convergence of $\left(|a| - \left|\frac{d\psi(x_o)}{dx}\right| + |b| - \left|\frac{d\psi(x_n)}{dx}\right|\right)$. If it is not converged, use new guess $\begin{cases}\psi_0 = \psi_a + ah \\ \psi_n = \psi_b + bh\end{cases}$ until it is converged.

The other steps are the same as Appendix D.

References

Attard, P., "Interaction and Deformation of Viscoelastic Particles. 2. Adhesive particles", *Langmuir*, Vol.17, 4322-4328, 2001.

Aston, D. E. and J. C. Berg, "Quantitative Analysis of Fluid Interface – Atomic Force Microscopy", *J Colloid Interface Sci*, Vol.235, 162-169, 2001.

Bachmann, D. J. and S.J. Miklavic, "Deformation of Fluid Interfaces Induced by Electrical Double-Layer Forces and its Effect on Fluid-Solid Interactions", *Langmuir*, Vol.12, 4197-4204, 1996.

Best, R.B. D.J. Brockwell, J.L. Toca-Herrera, A.W. Blake, D.A. Smith, S.E. Radford and J. Clarke, "Force mode atomic force microscopy as a tool for protein folding studies", *Analytical Chimica Acta*, Vol.479, 87-105, 2003

Binnig, G., H. Rohere, C. Gerber and E. Weibei, "Tunneling Through a Controllable Vacuum Gap", *Appl Phys Lett*, Vol.40, 178-180, 1982.

Binnig, G., C.F. Quate, and C. Gerber, "Atomic Force Microscope", *Phys Rev Lett*, Vol.56, 930-933,1986.

Bhatt, D., J. Newman and C.J. Radke, "Equilibrium Force Isotherms of a Deformable Bubble/Drop Interacting With a Solid Particle Across a Thin Liquid Film", *Langmuir*, Vol. 17, 116-130, 2001.

Bohm, C., "Electric force microscopy: Gigahertz and Nanometer Measurement Tool", *Microelectronic Eng*, Vol.31, 171-179, 1996.

Bottomley, L.A., "Scanning Probe Microscope", *Anal Chem*. Vol.70, 425R-475R, 1998.

Burgi, L., H. Sirringhaus and R.H. Friend, "Noncontact Potentiometry of Polymer Field-Effect Transistors", *Phys Rev Lett*, Vol.80, 2913-2915, 2002.

Chan, D.Y.C., R.R. Dagastine and L.R. White, "Forces Between a Rigid Probe Particle and a Liquid Interface", *J Colloid Interface Sci*, Vol.236, 141-154, 2001.

Chan, D.Y.C. and R.G. Horn, "The Drainage of Thin Liquid Films between Solids", *J. Chem. Phys.*, Vol.8310, 5311-5324, 1985

Dagastine, R. R. and L. R. White, "Forces between a Rigid Probe Particle and a Liquid Interface II. The General Case", *J Colloid Interface Sci*, Vol.247, 310–320 2002.

Derjaguin, B., V.M. Muller and Y. P. Toporov, "Effect of Contact Deformations on the Adhesion of Particles", *J Colloid Interface Sci*, Vol.53, 314-326, 1975.

Ducker, W.A., Z. Xu, D.R. Clarker and J.N. Israelachvili, "Forces between Alumina Surfaces in Salt Solutions Non-DLVO Forces and the Implications for Colloidal Processing", *J Am Ceram Sci*, Vo.77, 437-43,1994.

Erlandsson, R.; G. Hadziioannou, C. M. Mate, G. M. McClelland and S. Chiange, "Atomic Scale Frication between the Muscovite Mica Cleavage Plane and a Tungsten", *J Phys Chem*, Vol. 89, 5190-5193, 1988.

Fielden, M. L., R.A. Hayes and J. Ralston, "Surface and Capillary Forces Affecting Air Bubble-Particle Interactions in Aqueous Electrolyte", *Langmuir*, Vol.12, 3721-3727, 1996.

Frisble, C.D., L.F. Rozsnyai, A. Noy, M.S. Wrighton and C.M. Lieber, "Functional-Group Imaging by Chemical Force Microscope", *Science*, Vol.265, 2071-2074, 1994.

Garcia, R. and R. Perez, "Dynamic Atomic Force Microscopy Methods", *Surface Science Reports*, Vol.47, 197-301, 2002.

Hartley, P. G., F. Grieser, P. Mulvaney and G.W. Stevens, "Surface Forces and Deformation at the Oil-Water Interface Probed Using AFM Force Measurement", *Langmuir*, Vol. 15, 7282-7289, 1999.

Hodges, C.S., "Measuring Forces with the AFM: Polymeric Surfaces in Liquids", *Adv Colloid Interface*, Vol.99, 13-75, 2002.

Horn, R.G., D. J. Bachmann, J.N. Connor and S.J. Miklavic, "The Effect of Surface and Hydrodynamic Forces on the Shape of a Fluid Drop Approaching a Solid Surface", *J Phys Conden Mat*, Vol.8, 9483-9490, 1996.

Johnson, K.L., K. Kendalland and A.D. Roberts, "Surface Energy and the Contact of Elastic Bodies", *Proc R Soc Lond A.*, Vol.324, 301-313, 1971

Kappl, M. and H.J. Butt, "The Colloidal Probe Technique and its Application to Adhesive force Measurements", *Particle & Particle Systems Characterization*, Vol.19, 129-143, 2002.

Meyer, E., R.M. Overney, K. Dransfeld and T. Gyalog, *Nanscience: Friction and Rheology on the Nonometer Scale*, World Scientific Publishing Co., Singapore, 1998.

Miklavic, S.J., "Deformation of Fluid Interfaces under Double-layer Forces Stabilizes Bubble Dispersions", *Phys Rev E*, Vol. 54, 6551-6556, 1996.

Miklavic, S.J., R.G. Hornand D. J. Bachmann, "Colloidal Interaction between a Rigid Solid and a Fluid Drop", *J Phys Chem*, Vol.99, 16357-16364, 1995.

Nonnenmacher, M., M.P. Aboyle and H.K. Wickramasinghe, "Kelvin Probe Force Microscopy", *Phys Rev Lett*, Vol. 58, 2921-2923, 1991.

Noy, A., D.V. Vezenov and C.M. Lieber, "Chemical Force Microscopy", *Annu Rev Mater Sci*, Vol.27, 381-421, 1997.

Preuss, M. and H.J. Butt, "Direct Measurement of Particle-Bubble Interactions In Aqueous Electrolyte: Dependence on Surfactant", *Langmuir*, Vol.14, 3164-3714, 1998.

Roseman, M. and P. Grutter" Determination of T-c, Vortex Creation and Vortex Imaging of a Superconducting Nb Film Using Low-Temperature Magnetic Force Microscopy", *J Appl Phys*, Vol.91, 8840-8842, 2002.

Sarid, D., *Scanning Force Microscopy*, New York, N.Y. USA, 1991.

Takano, H. and M.D. Porter, "Monitoring Chemical Transformations at Buried Organic Interfaces by Electric Force Microscopy", *J Am Chem Soc*, Vol.123, 8412-8413, 2001.

Vakarelski, I.U., A. Toritani, M. Nakayama and K. Higashitani, "Effects of Particle Deformability on Interaction between Surfaces in Solutions", *Langmuir*, Vol.19, 110-117, 2003.